12-15-2022 2:00 PM

Design and Evaluation of Fabric Cooling Channels for Twisted Coiled Actuators

Alex Lizotte, *The University of Western Ontario*

Supervisor: Trejos, Ana Luisa, *The University of Western Ontario*

A thesis submitted in partial fulfillment of the requirements for the Master of Engineering Science degree in Electrical and Computer Engineering

Design and Evaluation of Fabric Cooling Channels for Twisted Coiled Actuators

Alex Lizotte

M.E.Sc. Thesis, 2022

Electrical and Computer Engineering

The University of Western Ontario

Abstract

Twisted coiled actuators (TCAs) are biomimetic and inexpensive artificial muscles. To enable their integration into soft robotics, a novel cooling apparatus was designed, consisting of a fabric channel to house the TCA and a miniature air pump for forced convection. The channel was designed to be lightweight, flexible, and easy to integrate into a soft wearable robotic device. The effect that the channel dimensions had on TCA performance (cooling time, heating time, and stroke) was investigated by testing combinations of three widths (6, 8, and 10 mm) and three heights (4, 6, and 8 mm). In general, as the channel dimensions increased, the cooling time and heating time decreased, however the stroke was unaffected (provided that the channel height was above 4 mm). The largest channel, 10 mm width and 8 mm height, resulted in the best combination of cooling time, heating time, and stroke, and thus it was used in a secondary experiment to compare the performance of the TCA with and without the cooling apparatus. When compared to passive cooling without a channel, the cooling apparatus resulted in a 42% decrease in cooling time (21.71 $\pm$ 1.24 s vs. 12.54 $\pm$ 2.31 s), 9% increase in the heating time (3.46 $\pm$ 0.71 s vs. 3.76 $\pm$ 0.71 s), and a 28% decrease in stroke (5.40 $\pm$ 0.44 mm vs. 3.89 $\pm$ 0.77 mm). This work demonstrates that fabric cooling channels are a viable option for cooling TCAs. Future work can continue to improve the channel design and investigate alternative means of air flow to further improve the performance of the TCA.

Index terms— Fabric cooling channels, twisted coiled actuators, wearable robotic systems.

Lay Summary

Wearable devices have the potential to improve the quality of life for many individuals, either as assistive devices or as rehabilitation aids. These devices are not common, because the motors used are often heavy, bulky, and expensive. Twisted Coiled Actuators (TCAs) are a type of artificial muscle made from nylon thread. They are a promising alternative because they are lightweight, slim, and inexpensive. They contract when heated and extend when cooled. Unfortunately, their natural cooling speed is too slow for many applications in healthcare and rehabilitation.

Therefore, a new cooling method was developed. It consists of a fabric channel to house the TCA and a miniature air pump to move air through the channel. This system has been specifically designed for soft wearable robotics, as it was designed to be lightweight, low-profile, and flexible, to help with user comfort. Additionally, since the channel is made from fabric, it can easily be sewn onto other materials for assembly into a robotic device.

The effect of channel size on TCA performance was evaluated by testing nine channel sizes, which were combinations of three widths (6, 8, and 10 mm) and three heights (4, 6, and 8 mm). TCA performance was evaluated by comparing the cooling time, heating time, and displacement of TCAs in each channel size. In general, the cooling and heating times of the TCA decreased as the channel size increased, however, there was no change in the displacement when the height was above 4 mm. The channel with a 10 mm width and 8 mm height had the best combination of heating time, cooling time, and displacement. Using this channel, a second experiment was completed to compare TCA performance with and without the cooling system. With the cooling system, the average TCA cooling time decreased by approximately 42%, however there was a 9% increase in heating time and a 28% decrease in displacement. This work shows that fabric cooling channels a promising way to improve the cooling time of TCAs.

Dedicated to: Gingi

Thank you for the constant companionship, cuddles, and smiles.

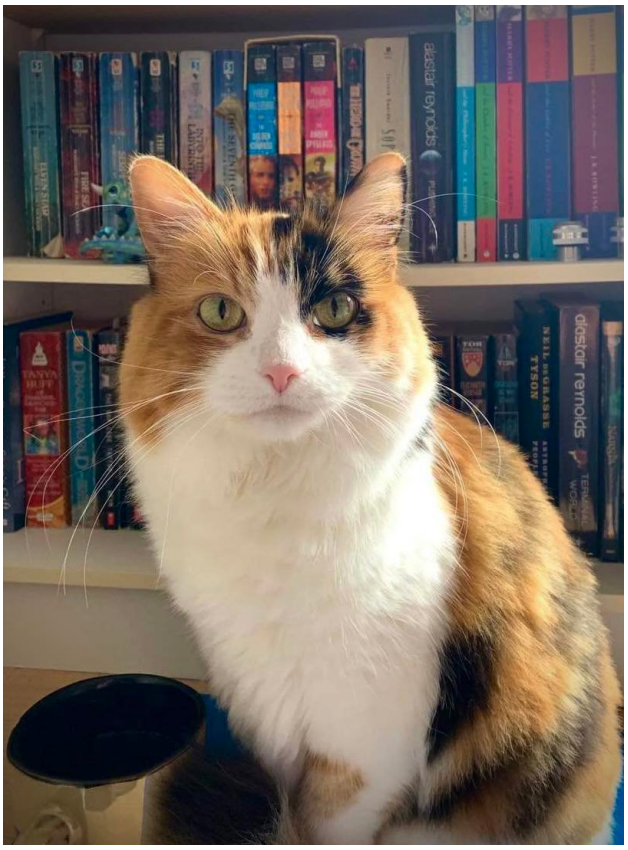

Acknowledgments

First and foremost, I would like to express my sincere gratitude to my supervisor, Dr. Ana Luisa Trejos. Thank you for your constant support and guidance throughout this degree. You are an incredible mentor and person, and it has been an honour to work with you. I could not have asked for a better supervisor.

I would also like to acknowledge Dr. Brandon Edmonds for his contributions to the hardware used in the experiments described in this work. Thank you for taking the time to teach me about TCAs; your help has been invaluable.

It has been a privilege to be part of the WearME lab, and to get to know all of the incredible humans there. Thank you for your help and encouragement. I have enjoyed working with each of you. I would especially like to thank Memo for his help with LaTeX, Eagle, and statistics. My sincere thanks go to my friends who supported me throughout this degree, especially to Katie, Ashton, and Mahshad; I would not have made it without you.

Finally, I would like to thank my mother, Janice, and my sister, Sarina, for their support throughout my degree. I appreciate and love you both.

This work was funded in part by the Natural Sciences and Engineering Research Council (NSERC) of Canada under grant RGPIN-2020-05648; by the Canadian Foundation for Innovation (CFI), and the Ontario Research Fund (ORF), by the Canada Research Chairs Program, and by scholarships awarded to A. Lizotte from NSERC, the Ontario Graduate Scholarship, the Transdisciplinary Training Award from the Bone and Joint Institute at Western, and the Canadian MSK Rehab Research Network (CIHR FRN: CFI-148081). I would also like to thank InsulTech and Trident Textiles for providing the insulation and nylon fabric used in this work.

Contents

List of Figures

List of Tables

Nomenclature and Acronyms

Latin Letters

A	Cross-sectional area
A_{TCA}	Surface area of a TCA
b	Damping coefficient
c	Thermal coefficient
C_{th}	Thermal capacitance
D	Diameter of the precursor fiber
D_H	Hydraulic Diameter
D_ω	Cross-diffusion term
E	Modulus of the material
f	Frequency
F	Load applied to a TCA during use
$F_{Payload}$	Optimal load for a TCA
$F_{Training}$	Load applied to a TCA during the training phase
$F_{Twisting}$	Load applied to a TCA during the twisting and coiling phase of fabrication
G	Shear modulus of the material
G_k	Generation of k_t
G_ω	Generation of ω

h	Convective heat transfer coefficient
h_e	Enthalpy
I	Current
J	Diffusion flux
k	Stiffness of the TCA
k_{eff}	Effective thermal conductivity
k_t	Turbulent kinetic energy
l	Length
n	Required sample size
p	p value
P	Pressure
P_{in}	Input power
Q	Fluid flow
r	Radius
R	Electrical resistance
Re	Reynolds number
R_{conv}	Convection thermal resistance
R_{flow}	Fluid flow resistance
R_{th}	Thermal resistance
s	Sample standard deviation
S	Heat source energy input
t	Time
T	Temperature
T_0	Initial temperature of the TCA
T_{amb}	Ambient temperature

T_c	Number of twisted to insert into precursor fiber to reach critical twist
u_i	Magnitude of the x, y, or z component of velocity
u_j	Magnitude of the x, y, or z component of velocity
v	Velocity magnitude
V	Voltage
$\vec{V}$	Velocity vector
V_{in}	Input air velocity
x	Position
x_0	Initial position
x_i	Magnitude of the x, y, or z component of position
x_j	Magnitude of the x, y, or z component of position
$\dot{x}$	Velocity
Y_k	Dissipation of k_t due to turbulence
Y_ω	Dissipation of ω due to turbulence
Z_α	Z-score for acceptable Type I error
Z_β	Z-score for acceptable Type II error

Greek Letters

Γ_k	Effective diffusivity of k_t
Γ_ω	Effective diffusivity of ω
Δ	Minimally discernible effect size
η	Dynamic fluid viscosity
ρ	Density
σ	Stress applied to precursor fiber
τ	Time constant

τ_{req}	Required time constant
$\bar{\bar{\tau}}$	Stress-strain tensor
ω	Specific turbulent dissipation rate

Acronyms

2D	Two-Dimensional
3D	Three-Dimensional
ADL	Activities of Daily Living
BP	Bianca Pumps
CNT	Carbon Nanotube Muscles
CSA	Cross-Sectional Area
DIP	Distal Interphalangeal Joint
PAM	Pneumatic Artificial Muscle
PIP	Proximal Interphalangeal Joint
MCP	Metacarpophalangeal Joint
SMA	Shape Memory Alloy
SP	Schwarzer Precision
TCA	Twisted Coiled Actuator
TPU	Thermoplastic Polyurethane

Chapter 1

Introduction

1.1 Motivation

Musculoskeletal disorders impact a significant portion of the population. Studies have shown that they are the most common cause of disability in Canada, and each year over 50,000 Canadians suffer from upper limb workplace injuries that require them to take time off work [1–3]. Severe injuries frequently take weeks or months of time-consuming physiotherapy, requiring the patient to perform repetitive exercises to regain mobility and strength. Patients often lose interest and stop treatment due to the tedious tasks and difficulty in tracking progress. Fortunately, the repetitive nature of these exercises allows them to be a great candidate for robotic involvement. Robotic therapy has been proven to be effective with stroke rehabilitation and can be expanded to other injuries [4–6]. Its advantages include increased patient engagement, the ability to quantify progress, and lower workloads for the physiotherapists [7, 8]. To expand their usefulness, robotic rehabilitation devices should be portable and wearable, so that they can be used at home and in settings outside of the clinic.

Current rehabilitation robots are often bulky, heavy, and expensive, leading them to be stationary devices. These limitations occur in part due to their actuation systems, which are most often motors or pneumatics [9–11]. One method to reduce the cost and increase the portability of wearable robotic devices is to use alternative actuators, such as artificial muscles. Artificial muscles have the additional advantages of being biomimetic and compliant, which reduce the chance

of injury to the user.

A promising artificial muscle, called the Twisted Coiled Actuator (TCA), was proposed in 2014 [12]. These artificial muscles are created by super-coiling polymer thread, and can contract up to 21% of their length when heated. They are most often created with silver-coated nylon to enable electric heating. TCAs meet the desired requirements of a slim, lightweight, and inexpensive actuator, allowing them to be a viable option for portable robotic devices. They also have the advantages of a high power-to-mass ratio, and low hysteresis, when compared to other artificial muscles [12]. Unfortunately, their low bandwidth with passive cooling (0.03 Hz) limits their applications in devices for rehabilitation purposes [13]. To increase the potential for TCAs to be used in wearable robotic devices, their cooling time needs to be decreased in a manner suited for portable soft robotics.

1.2 Existing Solutions

Previous work has demonstrated that changing the environment of the TCA significantly changes its cooling time. TCAs have been tested with forced air, still water, forced water, and hydrogel. Liquid coolants are effective at decreasing the cooling time of the TCA, however, they come with the cost of significant power increases for heating the TCA [14]. Liquid coolants have other disadvantages for wearable robotic devices, including a higher mass when compared to forced air, the potential to leak, and the change in TCA behavior as it absorbs the liquid. Hydrogel coatings can produce cooling times similar to still water, however they only last for approximately 30 actuation cycles, and thus are not capable of long-term use [14].

Conversely, forced air cooling does not have a limited life cycle and it does not impact the power requirements for the heating phase. Depending on the rate of airflow, forced air can produce cooling rates comparable to standing water [15]. This method of cooling has been implemented with fans and compressed air, generally with the TCA still exposed to the environment. While this has been effective, it is not practical to have exposed TCAs on a wearable device, as they can be heated up to 120°C, and the user must be protected. In light of this constraint, there has been some success in cooling TCAs by placing them in rigid tubes to direct the air flow and shield the user from the

heat [13], however these rigid tubes would be difficult to embed in fabric for wearable devices.

1.3 General Problem Statement

Portable robotic devices have the potential to help individuals with rehabilitation and activities of daily living at home and in other settings outside of the clinic. The ideal device would be lightweight, low-profile, and unobtrusive, to ensure user comfort, and affordable, to ensure that the technology can be adopted by the target population. Whether or not a design meets these objectives is affected by the actuators used in the device. TCAs meet these requirements, however, few designs have chosen to employ TCAs due to their limitations of slow natural cooling rates, low efficiency, and high operating temperatures. Therefore, the purpose of this work is to address the main challenge involved in implementing TCAs in soft wearable robotic devices—their slow cooling rate. If TCAs can be cooled in a manner that meets the above objectives, it would allow them to be used in soft wearable robotic devices for rehabilitation purposes.

1.4 Research Objectives and Scope

This thesis consists of the design and assessment of a cooling mechanism for TCAs that can easily be incorporated into soft wearable devices. The designed cooling mechanism consists of a fabric channel to house a TCA and guide airflow over it, as well as a miniature air pump to provide the airflow. The scope of this work is limited to the design and improvement of the fabric channel, and does not include a detailed investigation of alternative means of airflow.

The primary objectives of this thesis are as follows:

1. To investigate the design of a mechanism to house and cool a twisted coiled actuator that meets the requirements for soft wearable robotic devices.

2. To assess the feasibility of the system and determine if it can be supported by commercially available miniature air pumps.

3. To evaluate the effect that the channel dimensions have on the performance of the TCA.

4. To compare the performance of the TCA with and without the novel cooling channel.

1.5 Overview of the Thesis

The structure of this thesis is summarized in the outline below:

Chapter 1 Introduction: This introductory chapter.

Chapter 2 Literature Review: Presents a review on robotic devices for rehabilitation purposes, focusing on their effectiveness and the actuators used. After comparing the actuators, a detailed description of twisted coiled actuators is provided.

Chapter 3 Computational Fluid Dynamics Study to Assess Solution Feasibility: Describes simulations completed with the channel design to assess the feasibility of cooling twisted coiled actuators with miniature air pumps and a preliminary version of the channel design.

Chapter 4 Active Cooling of Twisted Coiled Actuators via Fabric Air Channels: Describes the design of a novel cooling apparatus for twisted coiled actuators, an evaluation of the size of the channel on TCA performance, and a comparison of TCA performance with and without the channel.

Chapter 5 Conclusion and Future Work: Summarizes the contributions and limitations of the studies presented in previous chapters, as well as directions for future work.

Appendix A Pilot Study: Describes the pilot study and results that were completed prior to Chapter 4.

Appendix B Additional Experimental Analysis: Presents an additional discussion of the results from Chapter 4.

Appendix C Copyright Permissions

Chapter 2

Literature Review

This chapter presents a review of the literature of wearable robotic systems (Section 2.1) and TCAs (Section 2.2). First, a brief summary about the effectiveness of robotic systems for rehabilitation is presented, followed by a comparison between the actuators used in these devices. After selecting which actuator to focus on for this work (TCAs), the operational mechanism and fabrication process for TCAs is explained. Finally, the factors that effect the performance of TCAs and wearable devices that have employed TCAs are discussed. To create this chapter, a literature search was conducted between May 2020 and October 2022 using keywords such as robotic stroke rehabilitation, robot-aided rehabilitation, robotic physiotherapy, upper limb exoskeleton overview, twisted coiled actuator, twisted coiled polymer, twisted coiled muscle, and cooling twisted coiled actuators.

2.1 Robotic Devices

2.1.1 Introduction to Robotic Rehabilitation Devices

The concept of exoskeletons has existed since the late 1800s, however, the first robotic exoskeletons did not appear until the late 1900s [11]. Exoskeletons have been developed to increase the performance (either strength or endurance) of healthy individuals for military and industrial applications, aid with rehabilitation of individuals with temporary musculoskeletal disorders, and assist those with permanent musculoskeletal disorders [16]. Recently, there has been a focus on devices

for assistance with activities of daily living (ADLs) and rehabilitation, for applications such as Parkinson's disease, spinal cord injury, and arthritis [10, 16]. These devices could supplement the user's strength or suppress tremor to help them complete ADLs with more independence. Another developing application is when robotic devices are used to aid with rehabilitation for individuals with stroke or traumatic brain injuries, as rehabilitation requires many hours of repetitive motions. For these applications, there are three categories of devices in development: end effector devices, exoskeletons, and exosuits.

End effector devices are purely for rehabilitation purposes, and the only contact between the user and the robot is through the end effector of the robot, which is usually held by the user's hand. These devices move the user through an exercise, however, there is no control over the user's individual joints or how the user is completing the exercise due to the limited contact [9]. The user could easily compensate for the injured body part by engaging or moving other joints or muscles, which can be undesirable if the goal is to regain their range of motion or strength in a certain area. These devices are simpler than exosuits and exoskeletons, although the nature of these devices requires them to be stationary.

By contrast, exoskeletons mimic the user's skeletal structure using rigid links that are parallel to the human skeleton. They can control individual joints, either independently or synchronously. The main advantage of exoskeletons is their rigid nature, as the links are capable of delivering high forces to the user, carrying the weight of the actuators (reducing the load on the user), and maintaining high accuracy due to the structural integrity of the links [17]. However, these rigid links and joints contribute to one of the main disadvantages of exoskeletons—difficulty in obtaining and maintaining joint alignment [17]. It is important that the axes of rotation of the wearable device align with the axes of rotation of the user's joints, as misalignment can result in excess forces and moments applied to the user's body that cause discomfort and risk injury or damage to the joint [18]. Maintaining joint alignment is difficult, as the center of rotation of the user's joint will change throughout an exercise, and there is the possibility of the device sliding on the user's limb [18]. Some exoskeleton designs circumvent this problem by adding additional degrees of freedom to ensure that the joints are aligned; however, this adds to the bulk, complexity, and mass of the system.

Exosuits solve this problem by being made from soft, compliant materials and often using actuators or transmission systems without additional or external axes of rotation that must be aligned with the user's joints. Similar to exoskeletons, they are worn by the user and can control individual joints. They generally have a lower profile than exoskeletons and they are usually intrinsically compliant, allowing for increased user safety [17]. However, the lack of rigid links often reduces the amount of force that they can apply to a user, when compared to exoskeletons. Recent reviews have shown that there is a recent trend in wearable devices and soft robotics (exosuits) to increase the portability and safety of the devices [10, 19].

2.1.2 Effectiveness of Rehabilitation Robots

All three types of devices have the potential to help individuals with rehabilitation exercises or activities of daily living for a wide range of conditions. Some of the applications for these systems include arthritis, Parkinson's disease, spinal cord injuries, and stroke [10]. To date, end effector devices and exoskeletons have been assessed for rehabilitation exercises, primarily with stroke patients. Review papers conclude that the robotic therapy results in improved patient-reported outcomes, as users find robotic therapy more engaging, and encouraging [4, 8]. In terms of clinical measures, one review paper concluded that there is no difference between conventional and robotic therapy if the intensity and duration of the rehabilitation sessions are the same [20]. Conversely, another review paper determined that there was increased improvement in upper limb functioning for chronic stroke patients who participated in robotic therapy, though there was no significant difference for acute stroke patents [21]. While clinical scales for robotic devices only report a mild positive effect, improved patient reported outcomes are still a desirable result. Increased patient engagement and motivation results in higher therapy success rates, and thus patients may obtain higher benefits by utilizing robotic devices for therapy [7, 8].

Other advantages of robotic rehabilitation include the real-time feedback it can provide and the quantitative measurements on patient progress, such as range of motion or strength [6, 7]. Robotic rehabilitation would allow the therapist to quantitatively analyze the kinematics and/or dynamics of their patient's motions, which could assist in developing new physiotherapy techniques [6]. Active motion tracking could allow for more consistent repetitions and exercises throughout

each physiotherapy session, between sessions, and between patients [22].

Another potential advantage of robotic rehabilitation is that it could increase access to physiotherapy. Robotic devices could allow intensive rehabilitation without high labor hours for a therapist [7]. This decrease in labor hours with a specific patient could allow physiotherapists to support more individuals. Portable robotic devices could also allow easier access to therapy for those with mobility difficulties.

Overall, while there are positive effects of robotic therapy, they are not significant enough to justify the high cost of existing systems. Additionally, the studies that have been completed to date are small scale and at risk of bias. Conclusive statements on the efficacy of robotic therapy cannot be made until larger studies are completed [4, 7, 23]. To facilitate those studies, the costs of these devices need to be reduced [17]. Additionally, low cost robotic rehabilitation systems could be employed in home, community, or other low resource settings [24]. Portable devices that allow home rehabilitation and assistance would be especially beneficial since the patient population in Canada is increasing in age and there is a shortage of therapists and caregivers, especially for at home care [9].

2.1.3 Requirements for Portable, Wearable Robotic Devices

To help create portable wearable devices, there are several challenges that need to be addressed, in addition to the overall cost of the system. Primarily, systems need to be developed so that they are safe and appealing for the user. They should be designed to have a slim profile so they remain unobtrusive, both for user comfort and aesthetics, especially if the goal of the device is to be worn for extended periods of time [11]. Similarly, the mass of the device needs to be minimized to improve wearability and portability; particularly if the intended user is already injured or not at full strength [10]. To help protect the user, the actuators used should be compliant or backdrivable. Compliant actuators have low stiffness and are more capable of mimicking biological motion. Similarily, backdrivability ensures that the user can move the actuators by applying a force to the output. These qualities would help to ensure user comfort and to protect the user during interactions with the device. To aid with adoption of wearable devices, they should be designed to be intuitive, fast to set up, and affordable [9]. Additionally, assistive and rehabilitative

devices must be able to adjust for different individuals, or be custom designed, as every person has different anatomical measurements. The device must adequately fit each user to prevent discomfort and excess strain on their joints [25]. Finally, exoskeletons and exosuits would ideally allow the user to have full range of motion. Especially for rehabilitation, it is essential that the device can support all of the required degrees of freedom over the required ranges of motion for the exercises [18]. If the user cannot properly perform the motions due to restrictions, there would be changes in the muscle activation patterns, impacting the effectiveness of the therapy [26]. At minimum, the device should be able to support ADLs, as studies have shown that patients perform better on motions that were part of the rehabilitation exercises, in comparison to motions that were not integrated into the exercises [27].

Overall, the mechanical design of wearable devices should be compliant, slim, lightweight, and portable. However, a consistent conclusion across review papers is that current devices are heavy, bulky, and have limited portability, which occurs in part due to the actuators that are being selected [9–11]. Additionally, the high cost of electric motors, the most popular actuator, is a contributing factor to the cost of the devices. For wearable robotic devices to become a feasible, economic solution, alternative actuators need to be employed to address the cost, weight, and portability concerns.

2.1.4 Actuators for Wearable Robotics Devices

This need has been captured in recent reviews of wearable robotic systems, upper limb exoskeletons, and robotic devices for upper limb rehabilitation [9–11, 25]. These papers show that the majority of devices designed use DC motors for actuation (62–72% of devices), with more recent reviews having a lower percentage of devices utilizing motors. The second most common actuator are pneumatics (13–28% of devices), and the remaining devices utilize a wide variety of actuators such as hydraulics, shape memory alloys, and twisted coiled actuators. The following sections will discuss the advantages and disadvantages of actuator options for wearable devices, as well as provide examples of devices with each of the actuators.

2.1.4.1 Motors

As mentioned previously, motors have become one of the most common actuation methods for any robotic system. They operate by passing a current through a coil of wire that is surrounded by a permanent magnet. This results in the generation of a force (electromagnetic induction) that causes the coil to rotate. Since they are well researched and easily available, they have several advantages. There are many models of motors and controllers, making motors easy to use and integrate into new designs. Additionally, motors are efficient, especially in comparison to thermal-based actuators, and they can deliver high speeds.

Since motors are the most popular actuator, there are numerous examples of devices that employ them. They have been used to control all joints in the upper extremities (fingers/hand, wrist, elbow, and shoulder), both independently and in groups of 2–3 serial joints. When the focus of the system is to control distal joints, some portable systems have been developed, such as the system developed by Stein *et al.*, that controls the elbow in flexion–extension [28]. However, when the focus of the system is the shoulder, or when multiple adjacent joints are actuated simultaneously, the designed systems become stationary [9].

Of the existing devices, very few have been commercialized. Some of the existing commercialized systems include the Hand of Hope, which controls individual finger motion for stroke rehabilitation [29], and the PowerGrip Robotic Glove[1], a hand orthosis developed to help C4 or C5 quadriplegics. The Hand of Hope is a portable system that employs linear motors attached to the hand to move the fingers in extension and flexion for rehabilitation exercises, whereas the PowerGrip Glove simultaneously flexes or extends the thumb, index, and middle fingers to allow the user to grasp objects. Since these commercialized systems are expensive (*e.g.* the PowerGrip Robotic Glove costs $7,602.00–9,254.00 CAD), there has been some exploration into 3D printed devices for the hand and wrist to help lower the cost. For example, Yoo *et al.* designed a wrist orthosis that can be constructed for approximately $315 CAD, except for the cost of the 3D printer [30]. Their device is similar to the PowerGrip, in that it uses a motor and EMG signals to simultaneously flex the thumb, index, and ring fingers to enable the user to pick up objects. In this design, the motor is still the most expensive component, and thus there would be a significant

[1]Inclusive Inc. `https://inclusiveinc.org/en-ca/products/powergrip`

increase in cost for each additional degree of freedom added to the design.

In addition to the high cost of motors, they have other disadvantages for wearable robotic devices. They are often bulky and heavy, require high power, and have high impedance. Their axis of rotation is generally parallel to the longest side of the motor, meaning that to control a joint, the motor either has to be fixed to the body in such a way that there is a large protrusion, or a coupling system needs to be implemented. Coupling systems such as gears and cable systems are effective at separating the motor from the joint axis, although they introduce efficiency losses and can complicate the control system. They also add to the mass and physical complexity of the system. However, the main disadvantage of motors for a wearable application lies in their lack of compliance. As discussed above, compliance and flexibility in wearable devices are important to ensure the user's safety and comfort. One method that is used to improve the compliance of motors is to add an elastic element in series with the load, turning it into a series elastic actuator, however this often complicates the design and requires an additional degree of freedom to control the compliance of the system.

2.1.4.2 Pneumatic Actuators

Unlike motors, pneumatics are inherently compliant due to the compressibility of air. They have other advantages such as their high power-to-weight ratio (provided the air compressor is neglected), and no fixed axis of rotation [10]. The main disadvantage of pneumatics for wearable devices is that they require an air compressor to power the muscles. This often leaves the user either carrying a large load or tethered to one spot. Additionally, the air compressor can be very noisy, potentially decreasing the user's comfort.

There are several types of pneumatics that can be employed in wearable devices, such as pneumatic bending actuators, pneumatic cylinders, and pneumatic artificial muscles (PAMs). PAMs are composed of an internal air bladder to store the air, and an external woven mesh to control the displacement of the actuator. The mesh of the PAM is designed such that when the air bladder is full, the muscle will contract longitudinally from the circumferential pressure and expansion [31]. Recently, a variation on PAMs were developed that allow pneumatic actuators to be embedded in fabric [32–34]. This novel implementation uses anisotropic fabrics to obtain bending actuation,

as well as two internal air bladders to allow both flexion and extension with the same actuator. These actuators were successfully implemented in a glove that improved the power and pinch grasp forces of individuals with a spinal cord injury [35].

Another example of a pneumatic device is the Gloreha, which uses five double effect cylinders to move a user's fingers both in flexion and extension [36]. The cylinders are attached to user's forearm, and a flexible rod transmits the force from the cylinder to the fingers. This device has been developed for stroke rehabilitation, and while wearable, the device is not fully portable as it employs an industrial air compressor to actuate the cylinders.

Apart from the hand, pneumatic actuators have been used in devices to actuate the wrist, elbow and shoulder, as well as combinations of joints [9, 10]. Similar to motors, pneumatic systems lose their wearability when the proximal joints are being actuated.

2.1.4.3 Hydraulic Actuators

Some research groups have used hydraulic actuators to move the hand, elbow, or shoulder, also in a stationary manner [9, 10]. Hydraulics use a liquid (generally oil) to transmit pressures, and are rarely used in wearable devices [9]. They involve more complicated hardware, such as pumps, valves, and reservoirs, are heavier than pneumatics, and have the potential to leak [16]. A few teams have worked to tackle these limitations, such as Pylatiuk *et al.*, who developed custom pumps, valves, and flexible fluidic actuators to construct a portable hydraulic elbow brace [37]. The main advantages of hydraulics are their high power density and high efficiency.

2.1.4.4 Shape Memory Alloys

On the opposite end of the efficiency spectrum, shape memory alloys (SMAs) have very low efficiency (0.15–2%), which is partially due to the fact that they are a thermal actuator. SMAs are unique actuators that return to a set shape when heated, despite any deformation that occurred when they were cool. SMAs most commonly are made from a nickel–titanium alloy that is commonly referred to as Nitinol. Nitinol, and other alloys with SMA properties, alternate between a martensite state when cool and an austinite state when heated. SMAs can be categorized as one-way or two-way SMAs. One-way SMAs require an external force to deform them when they

are cool, otherwise they will maintain their shape from the last austinite cycle. Two-way SMAs are fabricated with thermomechanical conditioning cycles and can alternate between two shapes—one for martensite state and one for austinite state [38, 39].

SMAs have been used to actuate the hand by placing SMA cables along the forearm, and using tendons to connect the actuators to the fingers, resulting in a low-profile glove [40]. They have also been knit into the fabric of a glove on the dorsal side of the fingers, to help flex the fingers [41].

These actuators have numerous advantages, including a high power-to-mass ratio, low voltage requirements, biocompatibility, and silent actuation. However, they also have many disadvantages, including low efficiency, slow cooling rates, and limited strain (5–8%) [38]. Additionally, they have non-linear responses with large amounts of hysteresis that can make them challenging to control.

2.1.4.5 Twisted Coiled Actuators

Twisted coiled actuators (TCAs) are a type of artificial muscle that overcome some of the main disadvantages of SMAs—they have significantly less hysteresis and can repeatedly obtain displacements up to 34% of their length. As the displacement is temperature dependent, a maximum strain of approximately 20% is more commonly reported, as 20% strain can occur between 100–150°C, as opposed to 34%, which requires the temperature to be above 225°C.

TCAs are made by supercoiling polymer threads whose radial thermal expansion coefficient is larger than its axial thermal expansion coefficient. When heat is applied to the supercoiled structure, the radial expansion of the polymer creates an untwisting torque that causes the TCA to contract. TCAs are simple and inexpensive to fabricate and are significantly slimmer and lighter than other actuation methods, such as DC motors. They are inherently compliant due to their structure and can easily be actuated through the use of electric heating (provided a resistance wire or silver-coated nylon is used). However, since they are actuated by heat, their efficiency is low, and their actuation speed is limited by the cooling rate, similar to SMAs.

Silver-coated nylon 6,6 is the most popular material for making TCAs as its silver coating enables electrical heating and its axial thermal expansion coefficient is negative, increasing the obtainable displacement. Nylon TCAs have been implemented in wearable devices designed to

actuate the wrist or the fingers [42–44]. In these cases, the TCAs have been placed along the forearm in order for longer TCAs to be used to obtain larger displacements. The forces from the TCAs were transmitted to the target joints using cables as artificial tendons. These devices were designed to help users complete activities of daily living independently. In addition to wearable devices, TCAs have been employed as actuators in artificial hands, fingers, and elbows [15, 45–48]. They have also been used for applications outside of healthcare, such as creating artificial jellyfish [49].

2.1.4.6 Artificial Muscles Similar to TCAs

Other artificial muscles have been developed with TCAs, to try to improve their performance. In an attempt to obtain the best of both TCAs and SMAs, Xiang *et al.* twisted nylon with an SMA [50]. Their actuator achieved up to 7.53% contraction under 4 V and 3 N, which is almost twice what a nylon TCA could obtain under similar circumstances (4% contraction). However, the actuator had significant hysteresis in the displacement–voltage curve compared to the TCA counterpart.

Another hybrid artificial muscle was developed by Aziz *et al.*, by combining nylon and spandex threads. As opposed to twisting the threads together, the threads were twisted separately (stopping before they started to coil), and then joined serially. The ends of the combined fiber were fixed, however the junction was free to rotate. When heated, the nylon would untwist, forcing the spandex to twist more. As the spandex was twisted, it formed coils, causing the overall structure to contract. They achieved a maximum contraction of 12% at 120°C with a 0.02 N load, independent of the diameter of the spandex fiber. Unfortunately, as the load increased, the contraction decreased to 1.5% at 0.1 N.

Finally, carbon nanotube muscles (CNTs) are similar to TCAs, except that they are made from carbon sheets that are rolled to form threads, which are then twisted and coiled to form CNTs. While similar to TCAs, if thermally actuated they require extremely high temperatures (approximately 2560°C to obtain 7.3% contraction), causing thermally activated CNTs to be impractical for wearable robotic devices [51]. However, alternative forms of CNTs that can be actuated by absorbing different solvents are currently being developed. For example, Lee *et al.*

present a CNT with electrochemical actuation that can achieve 16.5% strain at 0.02 Hz and a 5.4% efficiency [52]. Their CNT is surrounded by an electrolyte fluid, and when a voltage is applied, the ions in the fluid migrate into the carbon threads. The influx of ions causes the volume of the thread to increase, resulting in either tensile or torsional actuation, depending on the configuration. This actuator surpasses TCAs in terms of efficiency, however the requirement of an electrolyte environment could be challenging to implement in a wearable device.

2.1.4.7 Summary and Comparison of the Actuators

Overall, many types of actuators have been explored for use in wearable robotic devices. There is continuing development in the field of artificial muscles with the goal of creating an actuator that is biomimetic, slim, lightweight, and inexpensive, to meet the needs of wearable robotic devices. While each actuator has its own advantages and disadvantages, the focus of the remainder of this work will be on TCAs, due to their biomimetic properties, inherent compliance, and slim profile. Their flexible, lightweight, and inexpensive characteristics allow them to be a promising actuator for soft wearable robotic devices.

When compared to the other actuators discussed above, TCAs are significantly slimmer, lighter, and less expensive than motors, pneumatics, or hydraulics. A more detailed comparison of TCAs and SMAs is presented in Table 2.1, which provides some of the mechanical properties of the two actuators. The same properties are provided for biological muscle, to demonstrate how TCAs can operate as an artificial muscle. TCAs can obtain larger strains than SMAs, with similar efficiencies and specific powers. While their maximum static stress (the maximum force produced under isometric conditions, normalized to the cross-sectional area) is less than SMAs, they have significantly less hysteresis. In comparison to biological muscle, there is overlap between the achievable strain and similar densities. TCAs have a larger modulus, as well as a higher specific power. The main shortcomings of TCAs in comparison to biological muscle are their low efficiency and slow natural cooling time.

While Table 2.1 presents ranges found in the literature, it is important to recognize that many of these properties depend on the way the specific actuator was fabricated (*e.g.*, the material), its geometry (*e.g.*, the actuator diameter), what state the actuator is in (*e.g.*, martensite or austinite

Table 2.1: Comparison of actuator properties for SMAs [38, 53–56], TCAs [12, 15, 57–60], and biological muscle [38, 56].

Property	SMA	TCA (Nylon)	Biological Muscle
Strain [%]	5–8	10–34	20–40
Maximum Static Stress [MPa]	> 200	20–55	0.35
Lifetime [Number of Cycles]	300–10^7	1,000–1.2×10^6	10^9
Elastic Modulus [MPa]	20,000–83,000	35–155	10–60
Efficiency [%]	1–2	0.71–1.08	35–40
Specific Power [kW/kg]	10–50	5.3–27.1	0.05–0.284
Density [kg/m^3]	6,400–6,600	1,150	1,037

for SMAs), and how the actuator is activated (*e.g.*, the temperature to which the TCA is heated). These variations lead to a wide range of values reported in the literature, and cause it to be challenging to directly compare the actuators.

2.2 Twisted Coiled Actuators

2.2.1 Fabrication Methods and Operating Principles

There are a wide range of factors that will impact the performance of TCAs, such as maximum strain, load, and cooling time. In general, they can be grouped into fabrication parameters (*e.g.*, the material) and operational parameters (*e.g.*, input power). These factors and their effect on TCA behavior will be discussed in detail, however, to understand what these factors are and why they affect TCA performance, the discussion will begin with an explanation of how TCAs are made and how they operate.

The first step in TCA fabrication is to twist polymer threads, which is generally accomplished with a motor. Nylon 6,6 and other materials with polymer chains that are highly orientated in the fiber direction are suitable candidates for making TCAs. The distinguishing material property for successful TCAs is a highly anisotropic thermal expansion coefficient. For TCAs to actuate upon heating, the thermal expansion coefficient in the radial direction must be significantly larger than the thermal expansion coefficient in the axial direction. It is even better if the axial coefficient is negative, such as is the case with nylon 6,6 [12]. The effect of radial expansion when heated

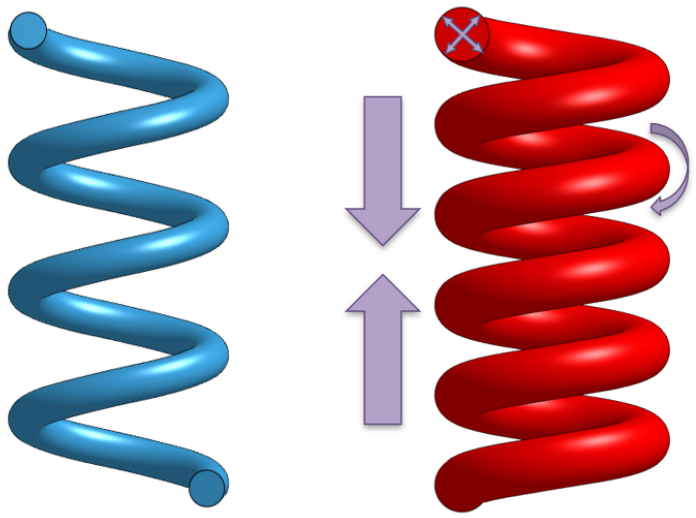

Figure 2.1: When heated, TCAs will radially expand, which causes an untwisting torque. This torque causes the coils to rotate, drawing them closer together, and resulting in contraction of the overall structure.

allows an untwisting torque to be generated due to the twisting of the thread, and this effect is amplified as the difference between the axial and radial thermal expansion coefficients increases. The untwisting torque causes the coils of the TCA to be pulled together, resulting in an overall muscle contraction, as illustrated in Figure 2.1.

This phenomenon can be explained using knot theory [61]. Knot theory states that twist and writhe (coils) are linked by a number that must remain constant while neither end of the material can rotate. When the TCA is heated, the untwisting torque causes the amount of twist in the fibers to decrease, which is then converted to writhe, and forms tighter coils. There is a limited amount of contraction that can occur, as when the coils encounter one another, further contraction will be blocked.

During the twisting process, there must be a load on the thread to ensure that the threads twist consistently. The twisting load applied during this stage is critical for the quality of the TCA—if the load is too high, the TCA will break, however insufficient load results in the fibers curling and snarling instead of twisting and coiling. The fiber is twisted until it is saturated with twist, which is known as the critical twist point. This point can be estimated using Equation 2.1, where T_c is the number of twists required to achieve critical twist, σ is the stress applied to the

precursor fiber, E is the modulus of the material, D is the diameter of the fiber, and G is the shear modulus of the material [61].

$$T_c = \frac{\sqrt{2\sigma E}}{\pi D G} \tag{2.1}$$

The next step is to coil the twisted thread. Coiling can be accomplished in one of two manners: either the thread can continue being twisted under the twisting load, forming a self-coiling TCA, or the twisted thread can be wrapped around a mandrel, forming mandrel-coiled TCA. Mandrel-coiled TCAs can obtain significantly larger strains (over 49%) than self-coiled TCAs (up to 34%), however self-coiled TCAs can carry much larger loads [12, 60].

For the fabrication of mandrel-coiled TCAs, when the fiber is saturated with twists, it is removed from the twisting apparatus and wrapped around a mandrel. This method allows the diameter of the coil and the space between the coils to be controlled, allowing for a wide range of achievable strains. Interestingly, two types of mandrel-coiled TCAs can be made, depending on which direction the twisted thread is wrapped around the mandrel. If it is wrapped such that the chirality of twists and coils are the same, the TCA will contract upon heating (homochiral TCA). Alternatively, the fiber can be wrapped around the mandrel such that the chirality of the twists and coils are opposite, to form a TCA that will expand upon heating (heterochiral TCA), as the untwisting torque will be in the opposite direction.

Unlike mandrel-coiled TCAs, self-coiling TCAs are always homochiral and will always contract upon heating. For self-coiling TCAs, the thread is left on the twisting apparatus after the critical twist point, and twists continue to be inserted into the fiber. Since the fiber is already saturated with twists, the additional twists are converted to coils. Twisting is continued until the entire fiber has coiled, as shown in Figure 2.2A–C.

At this stage, all the coils are tight against one another, leaving little room for actuation. For TCAs to contract, there must be space between the coils. This can be accomplished by slightly untwisting the fiber after complete coiling while maintaining the same load. This cause the coils to increase in diameter and adds space between the coils, resulting in a larger spring index (the ratio between the coil diameter and fiber diameter). Conversely, if additional twists are added,

the coils will continue to tighten, decreasing the spring index until the fiber breaks [12].

Space can also be added between the coils during the annealing process. Annealing is the next step in creating TCAs, and involves heating the TCA under a constant load to allow the polymer chains in the fiber to re-orient themselves and maintain the coiled form. This step is important, as the twisting and coiling processes are cold drawing the fibers, creating stress [62]. This stress can be released by annealing the TCAs at a temperature that is above the selected maximum operating temperature, yet below the melting temperature [12]. To add space between the coils in this step, the annealing load can be increased from the twisting load, or the TCA can be stretched prior to heating.

In the literature, annealing has been performed through Joule heating silver-coated TCAs, placing the TCAs in an oven, or by blowing hot air over them for a given time. This step is required for mandrel-coiled TCAs, as otherwise they will untwist, however self-coiled TCAs can be plied together (Figure 2.2D), allowing them to maintain their shape without annealing. This concept can be expanded to create 3-ply (or more) TCAs by twisting multiple self-coiled TCAs together. The multi-ply muscles can withstand higher loads than their single-ply counterparts, however they require more power to heat [62].

The final step in fabricating TCAs is to train the muscle, so that the performance of the TCA is consistent. This step is often combined with annealing, as both steps involve heating the TCA. Training the TCA involves heating and cooling cycles similar to those that would occur during use. During training, the length of the muscle will increase as the material plastically deforms. According to literature 4–15 cycles must be completed for the TCA to produce repeatable results. There are two methods commonly employed for training TCAs. First, the maximum load that the TCA will encounter in use is placed on the TCA and alternating heating and cooling periods are applied until the length of the TCA converges. If the mass used is too large, the length of the TCA will not converge, and the TCA will eventually break. Alternatively, the TCA can be stretched 5–10 mm and heated, until approximately 30% strain is achieved. This method results in more consistent final lengths compared to the first method [13].

To summarize, TCAs are created from polymer threads that are twisted and coiled. Provided that the polymer has anisotropic thermal expansion coefficients, the coiled structure will contract

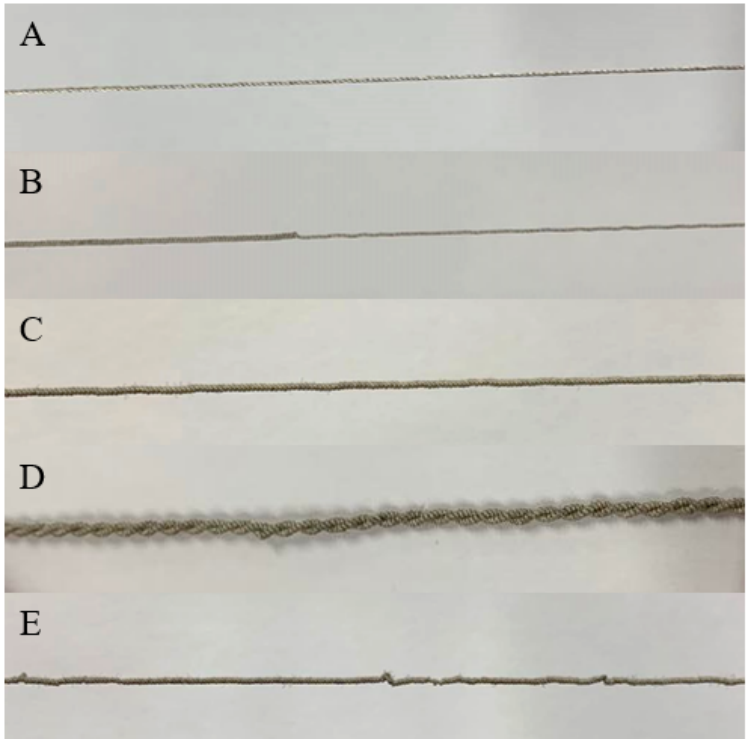

Figure 2.2: Fabrication process for self-coiling TCAs. First the precursor fiber is twisted (A). After the critical twist point, additional twists will be converted to coils (B). Twists are inserted until the entire fiber has coiled (C), at which point it can be plied to prevent untwisting (D). If the applied load during twisting is too low, the fiber will snarl instead of coil (E).

upon heating due to the untwisting torque that the thermal expansion generates. Thus, since the operating principle of TCAs is that radial thermal expansion causes linear contraction by decreasing the space between coils, any factor that effects the thermal expansion, rate of heat transfer, or the space between the coils will impact TCA behavior. While many factors have been investigated, there have been very few statistical analyses performed. Additionally, most of the papers either do not report a sample size, or have a sample size lower than five. Thus, while the trends seen in literature are discussed below, it is unclear if the same trends would be found with larger sample sizes. Table 2.2 summarizes some of the key contributing factors. The wide variety of fabrication parameters causes it to be challenging to directly compare the performance of TCAs seen in the literature. There has yet to be a TCA fabrication method or performance evaluation criteria that is adopted by the majority of researchers.

Table 2.2: The effects that some of the fabrication and operational parameters have on the performance of self-coiling TCAs. While these are the trends observed in the literature, it is worth noting that the majority of these studies were completed with small sample sizes, and without a statistical analysis, it is difficult to determine whether the same patterns would be observed with a larger sample size. The effects that were reported with an unknown sample size are marked by ‡, fewer than five samples are marked with †, and more than five samples are marked with ◇. Additionally, the interactions between these factors are unknown.

Category	Factor	Property that is affected	Effect of factor increasing
Material	Difference between thermal expansion coefficients [12, 63, 64]	Achievable strain	Increases‡
	Elastic modulus [12]	Maximum load	Increases‡
	Fiber diameter [12, 61]	Maximum load	Increases‡
		Achievable strain	No effect‡
	Strands/ply of precursor fiber [44, 61]	Fabrication success rate	Increases†
		Cooling time	Increases‡
Twisting and Coiling	Load applied to the TCA [12, 63]	Optimal and maximum load	Increases‡
		Achievable strain	Decreases‡
	Consistency of twisting speed [65]	Fabrication success rate	Increases◇
	Amount of twist [12, 66]	Achievable strain	Decreases‡
Annealing and Training	Load applied to the TCA [63, 67]	Achievable strain	Increases◇
		TCA modulus	Decreases◇
	Consistency of heating method [44]	General Performance	Increases†
TCA Configuration	Ply of coiled TCA [62, 66]	Achievable strain	Decreases†
		Maximum load	Increases†
Operational Factors	Applied load [12]	Achievable strain	Increases to a maximum‡
	Applied power (electric heating) [15, 68, 69]	Heating time	Decreases◇
Environmental Factors	Thermal resistance between TCA and environment [14, 15, 69, 70]	Cooling time	Increases◇
	Moisture content (Nylon 6,6) [71]	Elastic modulus (Precursor fiber)	Decreases†

2.2.2 Factors That Impact TCA Performance

2.2.2.1 Material

First, the material used will impact the achievable strain of the TCAs, since different materials have different thermal expansion coefficients. As mentioned previously, the material requires anisotropic thermal expansion coefficients for the fiber to produce an untwisting torque upon coiling [12]. The most popular material is silver-coated nylon 6,6 due to its highly anisotropic thermal expansion coefficients, relatively high melting temperature, commercial availability, and the ease of actuation through electric heating.

Other materials such as Kevlar, polyethylene, and spandex have been tested. Compared to nylon, polyethylene and Kevlar have lower strains (up to 16%, instead of 34%) due to the smaller difference in radial and axial thermal expansion coefficients, however their higher elastic moduli allow them to withstand higher loads [12]. Park *et al.* investigated TCAs made out of polyethylene terephthalate (PET) yarns and achieved 12% strain through electric heating after covering the yarns in silver [63]. When spandex was used, large displacements were obtained (up to 45%), however the load carrying capabilities of the TCA decreased significantly—the spandex TCA held 80 g/strand, compared to 1000 g/strand for the nylon TCA [64, 72].

In addition to the material used, the quality and type of the fiber impacts the quality of the muscle. For example, when two different conductive nylon 6,6 fibers were tested, Shieldex 117/17 and 235/34, it was found that the 117/17 fiber frequently broke during fabrication and actuation [44]. Additionally, the 117/17 TCAs only achieved 7% strain, whereas the 235/34 fiber could produce up to 16% strain; however, the coiling loads were different. In this case, the 235/34 fiber was made with more filaments (35 vs. 17), thus indicating that more filaments allow the fiber to carry larger loads. The fiber diameter also influences the load-carrying capabilities of the TCA, as it was shown that the amount of untwisting torque produced by the TCAs increases as the fiber diameter increases [61]. Interestingly, the fiber diameter does not affect the strain of the TCA, provided that the coiling load and payload are the same [12].

Similar to the amount of filaments in the fiber, twisting multiple strands of the precursor fiber together will result in a higher fabrication success rate and larger load carrying capabilities [59].

This has lead to TCAs commonly being created by twisting 4-ply precursor thread, and then plying the coiled fibers by folding the structure in half, known as a 2–4-ply TCA, where the first number represents how many coiled fibers are plied together, and the second number is how many precursor threads are twisted together [13, 66]. The ply of the precursor fiber also impacts the cooling time—higher ply TCAs result in longer cooling times than their lower-ply counterparts, due to the additional material.

2.2.2.2 Twisting and Coiling

After the material and the ply of the precursor fiber are selected, there are a number of factors during the fabrication procedure that impact the outcome of the muscle. These factors include the twisting/coiling mass, the speed and consistency of the rotations during twisting, and the coil density. When creating mandrel-coiled TCAs, there is additional control over the coil density and overall TCA diameter, as the mandrel and coil spacing are selected during fabrication. While the operating principles for mandrel- and self-coiled TCAs are the same, the focus of this discussion will be self-coiling TCAs, as they are more suitable for wearable robotic devices due to their higher load-carrying capabilities and slimmer shape.

First, the mass used during twisting has a drastic impact on the resulting TCA [12, 63]. It is important to use an appropriate mass—if the mass is too light, the fiber will snarl and curl during twisting (Figure 2.2E), however if the mass too heavy, the fiber will break [12]. Each material and thread diameter have their own range of acceptable loads. For example, 0.127 mm diameter nylon 6,6 thread requires 10–35 MPa, and 0.2 mm diameter conductive nylon 6,6 thread has been coiled with approximately 31.4–94.9 MPa [12, 59]. Heavier loads during coiling will cause the coils to form more tightly together, resulting in less space for actuation and lower strains. The tightness of the coils also influences the optimal load under which the TCA can operate, where the optimal load is defined as the lowest load that prevents the coils from contacting one another. For example, a 0.127 mm diameter nylon 6,6 thread coiled with 10 MPa, 16 MPa, and 35 MPa, results in maximum strains of 21%, 14%, and 9.3%, with optimal loads of 22 MPa, 30 MPa, and 50 MPa [12]. Additionally, if multiple fibers are twisted together, the load should be increased to maintain the pressure range [59].

The next factor that influences TCA behavior is the twisting speed. Preliminary work investigating this relationship has been completed; however, future work is required to solidify the effect that twisting speed has on TCA performance. The results of the preliminary study indicate that as the RPM of the twisting motor increased, the achievable strain decreased, however, this trend was different for 1-, 2-, and 3-ply TCAs, where the ply is the number of coiled fibers twisted together [62]. There has also been some investigation into the consistency of the coiling speed, where a stable twisting speed can produce TCAs more reliably [65]. When TCAs were coiled with a motor at constant speed and a drill, the fabrication success rates were 50% using the motor, and 41% with the drill. It is thought that the variations in the drill speed resulted in the coils forming inconsistently, reducing the success rate.

The final twisting parameter to discuss is how much the thread is twisted during the coiling process, as this will also impact the coil density [12]. After the TCA has been fully coiled, removing a few twists will increase the space between coils, and thus the achievable strain. For example, Cho *et al.* found that untwisting the fully-coiled TCA by approximately 3% of the number of twists resulted in the largest strain [66]. Alternatively, if more twists are added, the coils will be forced closer together, decreasing the maximum strain.

2.2.2.3 Annealing and Training

The tightness of the coils after twisting can also be modified by changing the load that is used during annealing relative to the load used during twisting. If the annealing load is larger than the twisting load, the maximum strain of the TCA will increase, as the larger load will separate the coils further [67]. The larger the difference between these two loads (provided the fiber does not fail), the larger the increase in strain. For example, when TCAs were fabricated with 0.234 mm diameter nylon thread with a 22.8 MPa twisting load, the maximum strain was increased from approximately 6% to 18% by increasing the annealing stress from 22.8 MPa to 45.6 MPa [67]. The increase in annealing load also caused a decrease in the modulus of the TCA.

In addition to the annealing load, the method of heat transfer during annealing has been shown to potentially affect the achievable strain of the TCA [44]. Bahrami and Dumond fabricated several TCAs with the same twisting and training procedure, except that they varied the annealing

procedure. Some TCAs were only annealed through a heat gun at 480°C for 10 s, and these produced an average strain of 12.96%. Other fibers were baked in an oven at 260°C for 45 min in addition to the heat gun and they produced an average strain of 25.32%. While there were not enough samples to claim a statistically significant result (only 3 samples were baked), the doubling of the strain due to annealing in an oven vs. heat gun warrants further investigation. A possible explanation is that the oven would heat the fiber more evenly, and the lower temperature reduced the chance of a particular section of the TCA getting singed.

Park *et al.* investigated the relationship between twisting load, training load, payload, and strain. They found a complex relationship between the four variables. To help simplify the selection of the loads, they suggest that the payload that will result in the maximum tensile actuation can be found with Equation 2.2. They achieved good experimental validation when they tested PET TCAs with twisting loads of 300 g, 400 g, and 500 g and training loads of 500 g, 600 g, and 700 g.

$$F_{Payload} = \frac{F_{Twisting} + F_{Training}}{2} \tag{2.2}$$

2.2.2.4 TCA Configuration

The final fabrication parameter that will impact the performance of the artificial muscles is their configuration. It is simple to twist multiple TCAs together to form 2-, 3-, or more ply TCAs to increase their load-carrying capabilities, although this depends on how many precursor threads are used. When 2–4-, 4–2-, and 8–1-ply TCAs were compared, the 2–4-ply structure obtained larger displacements under the same load [66]. Other configurations such as weaves, 2D braids and 3D braids have been investigated using 2-ply TCAs [73]. For both weaves and braids, as the number of TCAs in the bundle increases, the force it is capable of producing increases, the overall electrical resistance decreases, and the actuation speed decreases. When comparing braided and woven TCA configurations, the braids required less power, produced more force and obtained larger strains. When the TCAs were bundled together, there was some hysteresis in the strain–power curve, which is likely due to friction between the TCAs in the bundle. The amount of hysteresis was comparable between braids and weaves.

2.2.2.5 Operational Factors

Once the TCA is ready for use, there are two main operational parameters that will influence the performance of the TCA. The first is the amount of load that is applied to the TCA. As the applied load increases, there will be additional space between the coils due to the applied force. The maximum strain for a given TCA will occur at the smallest load (during use) that prevents the coils from touching over the actuating temperature range—the optimal load [12]. For loads below this, the coils will contact earlier, limiting the strain, and for loads larger than the optimal load, the TCA will be unable to coil completely.

The second operational parameter is how the TCA will be heated. There are several different methods that have been commonly employed to actuate the TCAs including hot water, hot air, and electric heating. Electric heating has been accomplished by using silver-coated nylon 6,6 fibers, coating the resulting TCA in CNT sheets, or adding a resistance wire to be twisted with the precursor fiber. Li *et al.* suggested coating the TCAs in silicone with two resistance wires to take advantage of the ease of Joule heating, and remove the disadvantage of the shorter lifetime of TCAs with a silver coating [67]. Regardless of how electric heating is achieved, as the input power to the TCA increases, it will heat faster, and the heating time will be reduced.

2.2.2.6 Cooling Methods

The cooling time for TCAs is more complex, as it relies on the environment that surrounds the TCA. Changing the environment the TCA is in allows the thermal resistance between the TCA and the surrounding environment to change, which either increases or decreases the heat flow (and therefore cooling time) of the TCA. Common TCA environments include the following: still water, forced water, still air, forced air, and hydrogel.

In a study that compared still water, hydrogel, still air, and forced air, it was shown that the cooling rate of the TCA increased the most in the liquid environments of still water and hydrogel due to the higher thermal conductivity [14]. Unfortunately, the hydrogel coating only lasted for approximately 30 actuation cycles, and the still water required approximately twice the input power to achieve a 10% stroke compared to the air environments. For nylon TCAs,

water environments require the additional consideration that nylon absorbs water, decreasing its modulus and changing the performance of the TCA [12, 71]. Another study found that similar cooling rates can be obtained in still water and forced air, indicating that forced air convection can be an effective method of cooling TCAs without a significant increase in power requirements [15]. In that work, the TCAs were cooled by constantly running a computer fan near the artificial muscles, and other research groups have followed suit.

As an alternative to the TCA being directly exposed to the environment, TCAs have been placed in plastic tubes to direct water or airflow over the artificial muscle in a compact manner [68, 74]. While forced air through rigid plastic tubes has been shown to be an effective way of cooling TCAs [74], rigid plastic tubes are difficult to embed in soft wearable robotic devices. The use of compliant plastic tubes to direct fluid flow over artificial muscles has been done for other artificial muscles, such as SMAs [75–77]. In these papers, SMAs are placed in a tube and hot or cold water is pumped over the SMA to control its temperature.

There are several disadvantages for cooling artificial muscles with water when the application is a wearable robotic device. First, since the water must circulate in a closed system, the water has to be cooled somehow to maintain the effectiveness of the cooling apparatus, which increases the energy usage of the system. Second, water is significantly denser than air, leading to an increase in the weight of the device. This is especially undesirable for physiotherapy applications where the user is injured. Finally, if there are any leaks in a system that uses water, it would prevent the cooling system from operating as intended, would be uncomfortable for the user, and there is the risk of the fluid coming in contact with the electronics.

Other means of modifying TCAs to increase their cooling speed have been attempted by Piao *et al.* [78]. They coated the TCAs in graphene due to the high thermal conductivity and low thermal mass of the material. They tested three different types of graphene coatings—large area monolayer graphene, porous graphene foam, and high-quality muli-layer graphene flakes. They found that the graphene flakes were the most effective, reducing the cycle time by 30.1% and could increase the maximum strain achieved by a pulsed current input from 0.45% to 1.2% when using a 0.1 Hz 40% duty cycle current input. However, the lifetime of the coating is unknown.

Other coatings to decrease cooling time were investigated for SMAs, though they have yet

to be tested with TCAs. First, carbon nanotube fins were applied to the SMA to increase the convective heat transfer coefficient [79]. Oh *et al.* accelerated the cooling of SMAs by growing a copper nanowire forest on the surface of the SMA [80]. Finally, SMAs have been embedded in materials with high conduction coefficients, such as silicone or conductive paste [81, 82].

Despite the need for alternative actuators for wearable robotic devices, none of the cooling methods described above have been designed specifically for wearable robotics. Portable, wearable robotic systems have several design constraints unique to their applications. The systems must be lightweight and have minimal components, as the user must be able to carry all the apparatus on their body. The system should be flexible and compliant to ensure user comfort and decrease risk of injury. Finally, the apparatus should be cost-effective, to help enable user adoption.

2.2.3 Simple Model for TCAs

In addition to a cooling system, models of TCAs and their behavior are required for wearable devices to improve the control system. There have been many models proposed to represent TCA behavior and relate the temperature of the TCA to its force and displacement. A simple thermomechanical and thermoelectrical model for electrically heated TCAs has been proposed by Yip and Niemeyer [15, 69], which has been implemented by several research groups [42, 43, 78, 83–85].

First, in the thermomechanical model, the temperature, position, and force of the TCA are related by modeling the TCA as a spring–damper system, as seen in Equation 2.3. Here, F is the force applied to the TCA, k is the stiffness of the TCA, x is the current position of the TCA, x_0 is the initial position of the TCA, b is the damping coefficient, $\dot{x}$ is the velocity of the TCA, c is the thermal coefficient, T is the temperature of the TCA, and T_0 is the initial temperature of the TCA. The stiffness and the thermal coefficient were obtained experimentally by plotting the force–strain curve at various temperatures. The stiffness is found by fitting a linear curve to the force–strain profile, and the thermal coefficient is found by measuring how much the force–strain curve translates with an increase in temperature. Alternatively, the thermal coefficient can be measured by finding the slope of the force–temperature curve. Finally, the damping coefficient was obtained by attaching a mass to the TCA, dropping it from a height, and fitting the model

to the measured response.

$$F = k(x - x_0) + b\dot{x} + c(T - T_0) \tag{2.3}$$

The coefficients for the thermoelectric model can also be found with simple experiments. The thermoelectric model is presented in Equation 2.4, where C_{th} is the thermal capacitance of the TCA, T is the temperature of the TCA, P_{in} is the power applied to the TCA, R_{th} is the thermal resistance of the TCA, and T_{amb} is the ambient temperature. This equation is a first order system, whose time-domain solution is presented in Equation 2.5, where τ is the time constant of the system and $\tau = R_{th}C_{th}$ [86]. The thermal resistance and thermal capacitance of the TCA can easily be found by heating the TCA at a constant input power and analyzing the transient response [69, 74].

$$C_{th}\frac{dT(t)}{dt} = P_{in}(t) - \frac{1}{R_{th}}(T(t) - T_{amb}) \tag{2.4}$$

$$T(t) = T_{amb} + P_{in}(t)R_{th}(1 - e^{t/\tau}) \tag{2.5}$$

2.2.4 Wearable Devices Actuated by TCAs

The model shown above was implemented in a wrist brace designed to actuate the wrist in flexion [42]. By anchoring 16 TCAs 2 cm away from the center of rotation of the wrist, the brace was capable of producing up to 0.32 Nm, which was deemed sufficient to support most activities of daily living. The TCAs ran parallel to the length of the forearm, however they were placed beside the arm in such a manner that they protruded on the lateral and medial sides of the forearm (eight TCAs per side). While the brace could successfully track the rising edge of a sinusoidal reference signal, there was difficulty in tracking the falling edges due to the cooling limitations of the TCAs. There was no active cooling implemented in this design, however the TCAs were exposed to the environment. This would not be practical for a commercialized product, as the user could be burned if they came in contact with the TCAs.

Some user safety was considered in the design of another glove that was actuated with TCAs

[43]. Again, the TCAs were placed along the forearm, however, they were placed in contact with the anterior side of the forearm. Insulation was placed beneath the TCAs to ensure that the user would be protected from the heat of the TCAs. Unfortunately, the TCAs were still exposed to the environment, as nothing was placed above the TCAs. This device utilized six TCAs to actuate the user's fingers in flexion, with one TCA for each finger and two for the thumb. The TCAs were attached to the fingers using artificial tendons that were routed across the palm. Extension of the fingers was achieved through elastic bands that were attached on the dorsal side of the hand. The glove was tested on an artificial hand and was able to achieve angles of approximately 85°, 35°, and 30° for the MCP, PIP, and DIP joints, respectively, with 2.7 N of force. The artificial hand was successfully able to grasp a variety of objects such as a tennis ball and a marble.

As opposed to the previous example, another exosuit was developed where the TCAs actuate the fingers in extension [44]. TCAs were placed along the posterior side of the forearm, and they were coupled to the fingers with artificial tendons. The goal of this device was to help overcome hand spasticity from cerebral palsy. Unfortunately, the TCAs used (nylon 6,6 conductive fibers, Sheildex 235/34 4-ply, twisted with a drill and 623 g, annealed with a heat gun for 10 s at 480°C, single ply) were deemed unable to produce enough force to overcome the spasticity in the hand, yet no details as to the testing method or evaluation criteria were provided.

2.3 Conclusion

To conclude, wearable robotic devices have the potential to aid individuals with rehabilitation exercises or activities of daily living. Unfortunately, most of the developed devices are not portable or affordable, which is driving researchers to investigate alternative means of actuation to address these challenges. TCAs are a potential alternative actuator, however for them to be used in wearable devices, their natural cooling rate must be increased. The following chapters will present a novel cooling apparatus for TCAs to address this need.

Chapter 3

Evaluation of a fabric channel cooling apparatus for twisted coiled actuators

As established in Chapter 2, new actuators need to be developed to increase the portability and biocompatibility of wearable devices. A promising option are TCAs, as they are biomimetic, inexpensive, slim, and lightweight. However, a system needs to be developed to allow active cooling in a portable, wearable manner.

This chapter briefly describes the design of a novel cooling apparatus that consists of a flexible fabric channel to house the TCA and guide airflow over it. It then explains the computational fluid dynamics study used to assess if commercially available miniature air pumps are capable of providing the air flow required for the design. This chapter was published by A. Lizotte and A.L. Trejos in the *Canadian Conference for Electrical and Computer Engineering*, Halifax, Canada, September 18–20, 2022,

3.1 Abstract

Wearable robotic systems have the potential to help many individuals with rehabilitation and to support activities of daily living. Unfortunately, these systems are not widespread due to their cost, limited portability, and size. Twisted Coiled Actuators (TCA), novel artificial muscles made from nylon thread, are inexpensive, lightweight, and slim. However, the natural cooling time of these thermally activated muscles is too slow to support rehabilitation or voluntary motions. This paper presents and assesses the feasibility of a novel cooling apparatus for the TCA. The cooling method involves a flexible fabric channel and a miniature air pump to cool the TCA with forced convection. The channel is lightweight, flexible, and can easily be sewn onto other materials to allow easy fabrication of wearable devices. ANSYS Fluent simulations were performed to determine the relationship between the input air velocity and the cooling time constant of the system. The results indicate that the miniature air pumps currently available are not powerful enough to cool the TCA at the required frequencies. There was a 13.2% difference between the cooling time constant predicted by the model and the time constant found experimentally for an input of 1 m/s.

3.2 Introduction

Musculoskeletal disorders are the leading cause of disability in Canada, and each year over 50,000 Canadians must take time off work to recover from upper extremity workplace injuries [1, 3]. Recovery often requires weeks or months of physiotherapy, which can be very tedious, repetitive, and time consuming. Difficulties in quantifying progress can lead to patients becoming disengaged with the treatment and not obtain the full benefits of the exercises.

Recent review papers show that many researchers are developing robotic devices to assist with physiotherapy, support activities of daily living, and suppress tremor in Parkinson's Disease [9, 10]. Robotic rehabilitation was demonstrated to be effective for stroke rehabilitation and patient reported outcomes state that robotic therapy is more encouraging and engaging [4, 5]. This type of therapy has several advantages, including real-time feedback, quantitative measurements, and progress tracking [7].

Unfortunately, the high cost of robotic systems makes it challenging to provide robotic therapy at a large scale [4]. Additionally, most of the developed systems are large, bulky, and stationary, which is caused, in part, by using electric motors as the primary actuator [9, 10]. Thus, there is a need for less expensive, lighter, and slimmer actuators for wearable robotic devices. The transition to an inexpensive, portable system would allow rehabilitation systems to be used at home, in the community, and in other low-resource settings.

A novel artificial muscle, called a Twisted Coiled Actuator (TCA), was proposed by Haines *et al.* [12]. TCAs are created by super-coiling nylon threads. When thermally activated, the expansion in the radial direction allows the actuator to contract up to 21% in length and carry loads up to 80 MPa [12]. An accepted fabrication method involves using silver-coated nylon 6,6 to allow for electrical heating and plying two strands together to create a double helix, as seen in Fig. 3.1 [13, 59].

TCAs are significantly slimmer, lighter, and less expensive than DC motors, the most common actuators for wearable systems [10]. TCAs also have inherent biomimetic and compliant properties that can only be integrated with motors by adding additional elastic components, such as springs. Another compliant actuator, shape memory alloys (SMAs), have been used in wearable devices for the elbow and hand [10]. SMAs are similar to TCAs in that they are thermally actuated and have comparable efficiencies and specific powers. However, SMAs have significantly more hysteresis than TCAs and thus are harder to control. The main disadvantage of TCAs is their low bandwidth, approximately 0.03 Hz, which stems from their slow natural cooling rate.

Fortunately, the cooling rate of TCAs can be improved by changing their environment. It has been shown that enclosing the TCA in a rigid plastic tube to direct the air flow is an effective method of cooling the TCAs, and displacements of up to 7% at 1 Hz were obtained with an input pressure of 50 psi [88]. Active motions occur between 1–5 Hz, however, rehabilitation exercises can occur at as little as 0.05 Hz to promote muscle growth [13, 89–91]. Thus, TCAs could be incorporated in applications with lower frequency requirements, such as stroke rehabilitation, or to provide a load to joints for tremor suppression.

Since rigid plastic tubes are challenging to integrate into soft robotic systems, this paper presents a novel cooling apparatus for TCAs that is specifically designed for wearable devices.

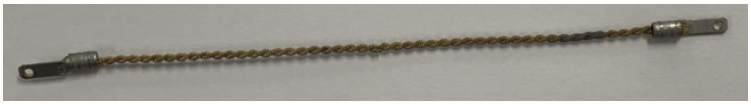

Figure 3.1: A TCA that is 100 mm in length.

The apparatus consists of a lightweight, flexible fabric channel to house the TCA enable forced convection. This paper also presents a feasibility study that was completed in ANSYS Fluent to assess the design of the cooling system.

3.3 Cooling Channel Design

When designing for wearable robotic systems, there are several factors that must be considered. The design should be lightweight, durable, safe for the user, and comfortable.

The novel cooling system involves a flexible fabric channel to guide the air over the TCA and a miniature pump to circulate the air, as seen in Fig. 3.2. A fabric channel can move with the user and it can easily be sewn onto underlying garments to create wearable devices and fix the TCA in place. The fabric channels can be made of any length, but they should be approximately the same length as the TCA at its fully extended position to ensure that the entire TCA is covered.

Air was chosen for the forced convection medium, as when compared to a liquid, it involves less hardware, leaks do not matter, and it is lighter. The material for the channel had to be air impermeable, lightweight, flexible, easy to sew, and withstand the operating temperatures of the TCA (up to 130°C). Thus, tightly woven nylon pack cloth with an ether-based thermoplastic polyurethane film was selected.

Through trial and error, it was found that a semi-circular shape for the cross section of the channel returned to its original shape best when deformed, and was the easiest to fabricate. The outside of the channel can be surrounded with insulation to protect the user from the temperatures that the TCA reaches.

3.4 Feasibility Study Methods

To assess if the channel design will allow the TCA to cool rapidly enough to support either rehabilitation or voluntary motion, it was modeled in ANSYS Fluent (Fig. 3.3A) and the relationship between the cooling time and input air velocity was determined.

3.4.1 Assumptions and Simplifications

First, the size of the channel was set to 6 mm in width, 4 mm in height, and 10 mm in length. The height and width parameters were determined by the size of the TCA crimp and pump outlet, whereas the length was reduced to a tenth of the TCA length to decrease computational time.

As seen in Fig. 3.1, the shape of a TCA is a complex double helix. To reduce the complexity of the geometry, the TCA was simplified to a cylindrical pipe. The diameter of the pipe was calculated by matching the volume of the pipe to the volume of the TCA. The volume of the TCA was obtained through a CAD model (Fig. 3.3B) where the diameter of each TCA strand was 0.8 mm and the pitch was 4 mm to match the physical TCA. This results in a volume of 10.3 mm^3

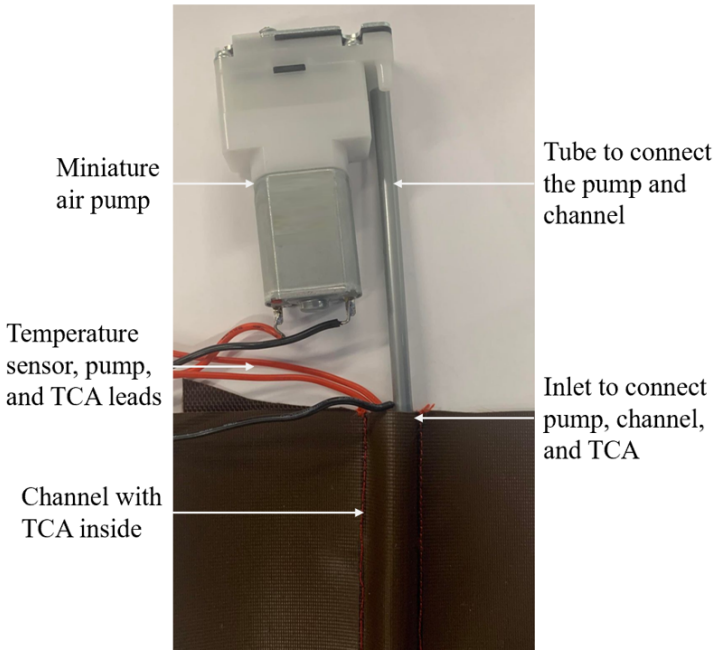

Figure 3.2: The fabric channel to cool the TCA. The TCA sits inside the channel and the miniature air pump will blow air through the channel to have active cooling with forced convection.

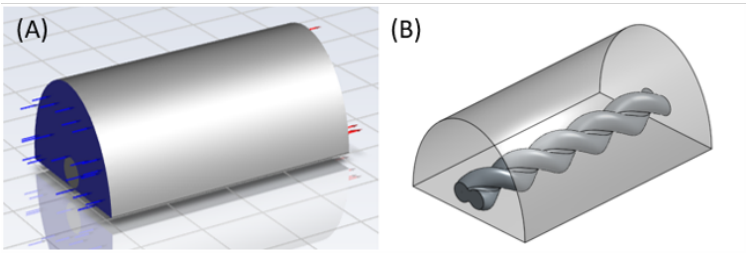

Figure 3.3: Model of the TCA and fabric channel in (A) Fluent and (B) CAD.

and a model TCA diameter of 1.15 mm.

It was assumed that the primary method of heat transfer is the forced convection through the channel and that radiation is negligible. Since the exterior of the channel would be insulated to protect the user, it was assumed that there is no heat transfer through the walls of the channel. It was also assumed that the material of the channel contributes a negligible thermal resistance as the material is only 0.3 mm thick.

To determine if the flow in the channel is laminar or turbulent, the Reynolds number was estimated. The Reynolds number can be computed according to (3.1), where ρ is the density of the fluid, v is the velocity, D_H is the hydraulic diameter, and η is the dynamic fluid viscosity. For air at 22.5°C, $\rho = 1.194$ kg/m^3 and $\eta = 18.6 \times 10^{-6}$ Pas. From the CAD model, the cross sectional area for the air flow is 17.8 mm^2 and the wetted perimeter is 20.65 mm, resulting in a hydraulic diameter of 3.45 mm, according to (3.2). Any input velocity with a Reynolds number below 2300 was simulated with the laminar model, and those with Reynolds numbers above 2300 used a turbulence model.

$$Re = \frac{\rho v D_H}{\eta} \tag{3.1}$$

$$D_H = \frac{4 * cross\ sectional\ area}{wetted\ perimeter} \tag{3.2}$$

ANSYS Fluent uses turbulence models in the Reynolds Averaging Navier Stokes family, which means that only the mean flow quantities (e.g., velocity) are solved, as opposed to solving for the flow eddies. The impact of the eddies is accounted for by estimating the energy loss due to the turbulence in the flow. For this situation, the SST k-omega turbulence model was employed, as

it can be used when the turbulent flow is not fully developed, as is the case with low Reynolds numbers [92]. This model adds two additional transport equations to find the turbulent kinetic energy, k, and the specific turbulent dissipation rate, ω, to estimate the impact of the turbulence on the flow [93].

The input velocities selected were 1 m/s, 5 m/s, 10 m/s, 20 m/s, 30 m/s, 40 m/s, 50 m/s, and 60 m/s. The mach number can be found by dividing the input velocity by the speed of sound. The largest mach number, for the input velocity of 60 m/s, is 0.175. Since the mach number is below 0.3, the flow can be assumed to be incompressible [94].

To further simplify the model, both the motion of the TCA in the channel and gravity will be neglected. The material properties of the TCA were assumed to be the same as those reported by Sun *et al.*, and are displayed in Table 3.1 [95].

Finally, since the heating and cooling curves for TCAs have been modeled as linear first order systems, it was assumed that the simulation results would also follow a first order system [69, 70]. This allows the cooling time to be approximated with the time constant, so the simulations were run until the temperature of the TCA reached below 58.4°C (36.8% of the steady state temperature).

3.4.2 Mathematical Models

To solve this simulation, Fluent will have to solve the conservation of energy (3.3) to find the temperatures of the air and TCA, and the conservation of mass (3.4) and momentum (3.5) equations to find the flow velocities and pressure [96–98]. For the laminar flows, no additional models or equations are required, however for the turbulent flows, two additional transport equations, (3.6) and (3.7), are required to find the turbulent kinetic energy, k_t, and the specific turbulent dissipation rate, ω [93].

In these equations, t is time, ρ is density, $\vec{V}$ is the fluid velocity vector, P is the pressure, k_{eff} is the effective thermal conductivity, T is temperature, h_e is the enthalpy, J is the diffusion flux,

Table 3.1: Material properties of the TCA for the thermal model [95].

Density	**Specific Heat Capacitance**	**Thermal Conductivity**
1300 kg/m^3	1267 J/kgK	4.6 W/mK

$\bar{\bar{\tau}}$ is the stress-strain tensor, and S is the heat source. E is defined as $E = h_e - P/\rho + v^2/2$, where v is the velocity magnitude. For (3.6) and (3.7), x is the position, i and j represent 1, 2, and 3 for the x, y, and z directions, and u is the magnitude of the i component of the velocity. Additionally, G_k and G_ω are the generation of k_t and ω, Γ_k and Γ_ω are the effective diffusivity of k_t, Y_k and Y_ω represent the dissipation of k_t and ω due to turbulence, and ω, and D_ω is the cross-diffusion term.

$$\frac{\delta}{\delta t}(\rho E) + \nabla \cdot (\vec{V}(\rho E + P)) = \nabla \cdot (k_{eff} \nabla T - h_e J + (\bar{\bar{\tau}} \cdot \vec{V})) + S \tag{3.3}$$

$$\frac{\delta \rho}{\delta t} + \nabla \cdot \rho \vec{V} = 0 \tag{3.4}$$

$$\frac{d}{dt}(\rho \vec{V}) + \nabla \cdot (\rho \vec{V} \vec{V}) = -\nabla P + \nabla \cdot \bar{\bar{\tau}} \tag{3.5}$$

$$\frac{\partial}{\partial t}(\rho k_t) + \frac{\partial}{\partial x_i}(\rho k_t u_i) = \frac{\partial}{\partial x_j}(\Gamma_k \frac{\partial k_t}{\partial x_j}) + G_k - Y_k \tag{3.6}$$

$$\frac{\partial}{\partial t}(\rho \omega) + \frac{\partial}{\partial x_i}(\rho \omega u_i) = \frac{\partial}{\partial x_j}(\Gamma_\omega \frac{\partial \omega}{\partial x_j}) + G_\omega - Y_\omega + D_\omega \tag{3.7}$$

3.4.3 Boundary Conditions and Initial Conditions

To solve the differential equations, boundary conditions and initial conditions must be set. For the boundaries of the channel, the inlet was set to a velocity inlet, the outlet was set to a pressure outlet with zero gauge pressure, and the sides of the channel were set to stationary walls with no slip conditions and zero heat flux. The outer surface of the TCA was set to a coupled thermal condition, to allow heat transfer between the TCA and the air, with an additional no slip condition. The faces of the TCA at the inlet and outlet were set with zero heat flux, which assumes that the section of the TCA that is being simulated is not influenced by the material on either side of it.

The system was initialized to 120°C to mimic the end of a TCA heating cycle. The input air was set to 22.5°C as room temperature air will be blown through the channel.

3.4.4 Numerical Methods

When setting up the simulations, several settings must be determined and the model must be divided up into many small segments, called elements. The simulation determines the velocity, pressure, and temperature of the flow by iteratively solving (3.3)–(3.7) for a system of equations with one degree of freedom for each element in the model. The non-linear convergence of these solutions are assessed using the residuals, which are the imbalances in the conservation equations that occur due to the discretization and linearization of these equations. The software repeatedly solves (iterates) through the conservation and transport equations to improve the approximation of the solution to the non-linear system by re-calculating the variables in the equations based on values from the previous iteration.

Relaxation factors can be set to improve the stability of the solution by decreasing the amount of change that occurs between iterations. For this model, relaxation factors were set to 0.75 to ensure that the solution converged, and in each time step iterations were performed until all residuals were below 1×10^{-5}, or until 20 iterations were completed. The mass flow rates at the inlet and outlet were observed to ensure that the solution was physically meaningful, and the temperature of the TCA was monitored by recording the average temperature over the outer surface of the TCA.

To solve the conservation equations, (3.3)–(3.5), the software can use either a segregated or a coupled approach for the pressure–velocity scheme. For the segregated scheme, the flow velocities and pressure are solved by iterating with (3.4) and (3.5), then the result is applied to (3.3) to solve for the temperatures. Alternatively, the coupled scheme solves all three equations each iteration. The coupled scheme was used to improve the solution convergence time [100].

Spacial discretization schemes have to be selected to tell the software how to solve for the values of variables (pressure, momentum, energy, etc.) at the surfaces of the model elements. Second order schemes were selected for all variables to increase solution accuracy.

Finally, since the flow is assumed to be incompressible, the pressure based solver was selected, as it is traditionally better for low-speed incompressible flows [101]. This assumes that the pressure of the fluid is a weak function of density and temperature, which occurs with low mach flows.

3.4.5 Grid and Time Step Independence Tests

Meshing is the process by which the model is split into the small elements. To ensure that the results do not depend on the mesh that is used, a grid independence test must be conducted. Two meshes were created and can be seen in Fig. 3.4. The parameters used to create them and the resulting properties are summarized in Table 3.2. The simulations were run for 0.25 s with a time step of 1 ms. The maximum percent difference between the surface temperature of the TCA was 0.0042%, indicating the results do not depend on the mesh. Mesh 1 was selected to reduce computational time.

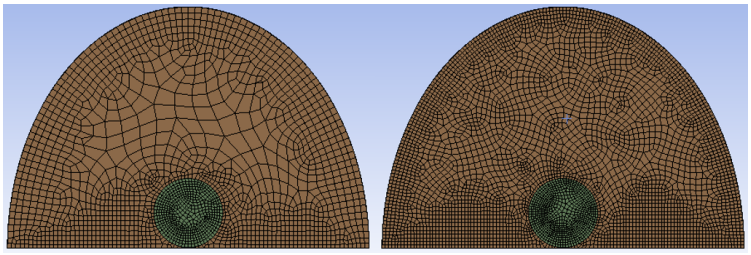

Figure 3.4: Meshes tested in the grid independence test; left is Mesh 1 and right is Mesh 2.

Similarily, a time step independence test must be conducted. Simulations were run for 0.25 s with time steps of 1 ms and 5 ms. Since the maximum percent difference in TCA surface temperature was 0.025%, the results are not dependent on the time step. A time step of 5 ms was selected to reduce computational time.

3.5 Results and Discussion

3.5.1 Air Velocity vs. Cooling Time Constant

Fig. 3.5 displays the TCA temperature vs. time curves for all input velocities and the dashed horizontal line marks 58.4°C, where the time constant was measured. As expected, the time constant decreases as the input velocity increases, as shown in Fig. 3.6. The line of best fit was found to be $\tau = 11.02V_{in}^{-0.58}$ with an R^2 value of 0.98, where τ is the cooling time constant and V_{in} is the input air velocity.

The estimated input velocities for rehabilitation and voluntary motion can be found by using

Table 3.2: Parameters used in mesh fabrication and resulting mesh properties.

Parameter	**Mesh 1**	**Mesh 2**
Divisions Along Upper Wall	120	200
Divisions Along Bottom Wall	100	120
Divisions Around the TCA	70	90
Maximum Element Size [m]	6×10^{-4}	1×10^{-4}
Minimum Orthogonal Quality	2.48×10^{-3}	9.47×10^{-2}
Maximum Aspect Ratio	2660	29.40
Minimum Element Volume [m^3]	3.25×10^{-14}	5.41×10^{-14}
Maximum Element Volume [m^3]	2.56×10^{-11}	3.46×10^{-12}
Number of Elements	87,150	221,850
Number of Nodes	95,674	236,949

the line of best fit, as seen in Table 3.3. To obtain the required time constant from the frequency, it was assumed that half of the period would be allocated to heating the TCA and half of the period would be allocated to cooling the TCA. Then, the required time constant is a fifth of the cooling time, as it takes approximately five time constants for a system to reach steady state. To summarize, $\tau_{req} = 0.1/f$, where f is the desired frequency. Next, the estimated flow rate can be computed from the estimated input velocity using the following relationship: $Q = V_{in}A$, where V_{in} is the input velocity and A is the cross sectional area of the channel obtained from the CAD model (17.8×10^{-6} m^2).

When selecting a pump for a wearable robotic device, it is important to minimize the amount the pump would protrude (its height), the overall size of the pump, and its mass. Some miniature air pumps that would be suitable for use in wearable devices are listed in Table 3.4. It can be seen that these pumps are incapable of providing the flow rates required to support rehabilitation or voluntary motion.

While the predicted input air velocities and flow rates required to support voluntary motion are impractical for a wearable device, the flow rate for the largest air pump (BP SX-8) is close

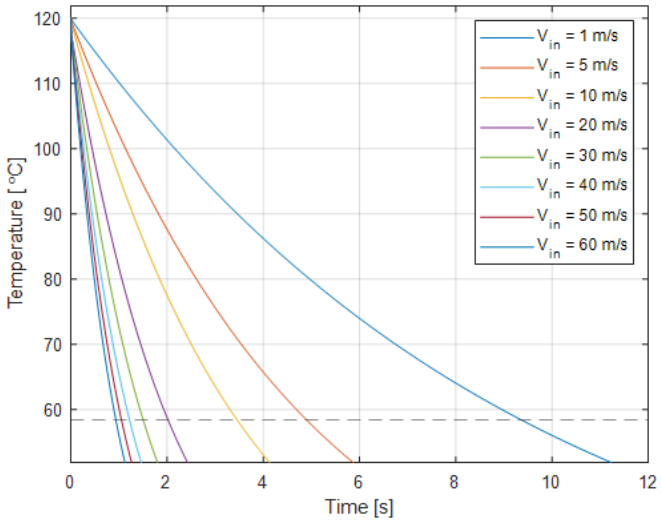

Figure 3.5: Temperature vs. time plots for all inputs velocities. The grey horizontal line marks the temperature at which the time constant was measured (58.4°C).

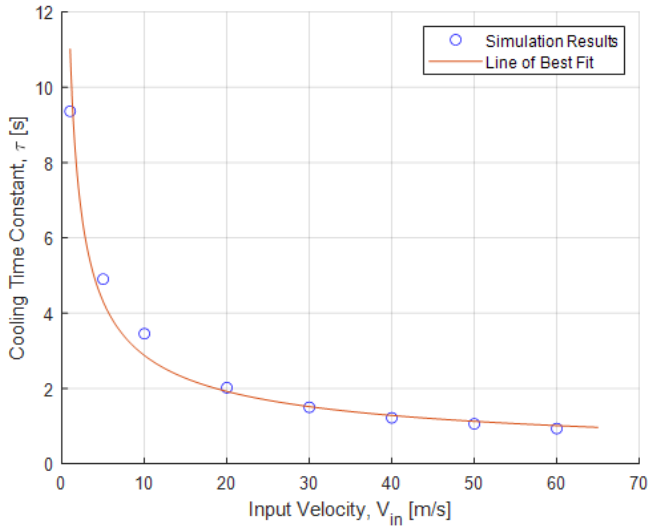

Figure 3.6: TCA cooling time constant vs. input velocity with a line of best fit of $\tau = 11.02V_{in}^{-0.58}$.

to that predicted to support rehabilitation exercises. Previous work has shown that increasing the size of the tube the TCA is in resulted in lower cooling times, thus increasing the size of the channel may allow the fabric channels and miniature air pumps to achieve frequencies required for rehabilitation [74].

Table 3.3: Estimation of input air velocity to obtain the required actuation frequencies.

Frequency [Hz]	**Required τ [s]**	**Estimated V_{in} [m/s]**	**Estimated Flow Rate [m^3/min]**
0.05	2	18.2	0.019
1	0.1	3,182.4	3.403
5	0.02	50,311.7	53.793

Table 3.4: Miniature air pump specifications.

Company/ Part Number	**Air Flow [m^3/min]**	**Height [mm]**	**Length [mm]**	**Width [mm]**	**Mass [g]**
BP SX-1	0.0004	8	32	18	8
SP 16A RO-DV	0.0015	16	56	36	38.5
SP 18A RO-D	0.0025	18	62	32	44
BP SX-4	0.0035	27	58	27	68
BP GX-3-D	0.0080	31	80	78	225
BP SX-7	0.0100	40	86	65	295
BP SX-8	0.0150	60	112	60	295

BP: Bianca Pumps

SP: Schwarzer Precision

3.5.2 Comparison with Experimental Results

To validate the simulation data, a preliminary experiment was performed. Three channels of 6 mm width and 4 mm height were fabricated with nylon pack cloth from Trident Textiles Corp. and were insulated with 8 mm of foil-backed insulation from InsulTech. A TCA was made with silver plated nylon 6,6 thread (Shieldex^{TM}, Part #: 260151023534) and its temperature was monitored using the temperature sensor design proposed by Edmonds [13]. The TCA was loaded with 100 g and was heated to 120°C five times in each channel. It was cooled with the Schwarzer Precision 16A RO-DV pump running at 100% duty cycle and the room temperature was 22.7°C. The air flow was measured with a Renesas FS2012-1020-NG air flow sensor to be between 0.0011 m^3/min to 0.0012 m^3/min, which equates to between 1.0 m/s and 1.1 m/s when divided by the cross-sectional area of the channel (17.8×10^{-6} m^2). The time constants for the experimental results ranged between 9.58 s to 11.67 s with an average of 10.8 s. The simulation predicted a time constant of 9.37 s for an input of 1 m/s, resulting in a percent difference of 13.2% when compared to the mean experimental value. The comparison between the simulation and experimental data is shown in Fig. 3.7.

The variation in the experimental results likely comes from the positioning of the TCA in the channel and differences in the channels due to the fabrication method. The main sources of error between the simulation and experimental results are likely the differences in the geometry of the TCA, the impact of the TCA on either side of the simulated portion, and the variation of the cross-sectional area of the physical channel, which could impact fluid flow. Other sources of error and variation in the results would include the positioning of the TCA in the channel (the model assumes it is perfectly centered), the neglect of the motion and deformation of the TCA in the model, the air input being slightly off-center in the experiment, and slight differences in material properties and room temperature.

3.6 Conclusion

In this study, the relationship between the input air velocity and the cooling time was determined for a novel cooling apparatus for TCAs. This was completed to determine if the cooling apparatus

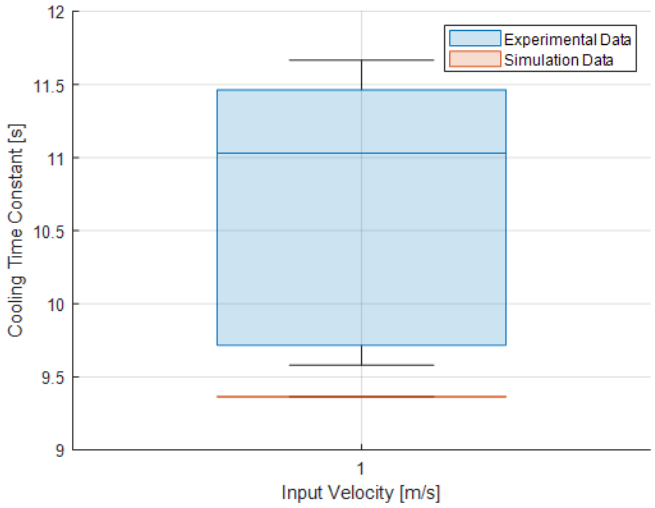

Figure 3.7: Comparison of simulation results with experimental data.

could cool the TCA quickly enough to support slow rehabilitation or voluntary movements with the miniature air pumps that are currently available. The cooling apparatus consists of a flexible, fabric channel to house the TCA and guide the air flow over it. The channel was simulated in ANSYS Fluent where the input air velocity was varied between 1 m/s and 60 m/s.

The relationship between the input air velocity and cooling time constant predicted that air flow velocities over 18.2 m/s were required to support slow rehabilitation motion and velocities over 3,182.4 m/s were required to support active motion. With the selected channel dimensions, this correlated to air flow rates of 0.019 m^3/min and 53.793 m^3/min, which are above the capabilities of the miniature air pumps currently available.

The simulation result for an input velocity of 1 m/s was compared with experimental data, where there was a 13.2% difference between the average experimental cooling time constant and the predicted cooling time constant.

Future work should investigate the impact the channel size has on TCA performance and cooling time, as it may be possible to obtain faster cooling rates with a larger channel.

Chapter 4

Active Cooling of Twisted Coiled Actuators via Fabric Air Channels

This chapter was submitted by A. Lizotte and A.L. Trejos to *Frontiers in Rehabilitation Science*, and it was accepted for publication in November 2022 [102]. It begins by describing the design of the fabric channel in detail, as well as the results obtained from two experiments that tested the channel design. The first experiment investigated the impact that the dimensions of the channel had on TCA performance, followed by a comparison of TCA performance with and without the fabric channel.

Prior to the experimental work presented in this chapter, a pilot study was completed to guide the experimental design. The pilot study and its results are documented in Appendix A. Finally, Appendix B discusses some additional observations made while analyzing the experimental data from the second experiment (Section 4.5) that were not included in the submitted paper.

4.1 Abstract

Twisted coiled actuators (TCAs) are promising artificial muscles for wearable soft robotic devices due to their biomimetic properties, inherent compliance, and slim profile. These artificial muscles are created by super-coiling nylon thread and are thermally actuated. Unfortunately, their slow natural cooling rate limits their feasibility when used in wearable devices for upper limb rehabilitation.

Thus, a novel cooling apparatus for TCAs was specifically designed for implementation in soft robotic devices. The cooling apparatus consists of a flexible fabric channel made from nylon pack cloth. The fabric channel is lightweight and could be sewn onto other garments for assembly into a soft robotic device. The TCA is placed in the channel, and a miniature air pump is used to blow air through it to enable active cooling.

The impact of channel size on TCA performance was assessed by testing nine fabric channel sizes—combinations of three widths (6 mm, 8 mm, and 10 mm) and three heights (4 mm, 6 mm, and 8 mm). Overall, the performance of the TCA improved as the channel dimensions increased, with the combination of a 10 mm width and an 8 mm height resulting in the best balance between cooling time, heating time, and stroke. This channel was utilized in a follow-up experiment to determine the impact of the cooling apparatus on TCA performance. In comparison to passive cooling without a channel, the channel and miniature air pump reduced the TCA cooling time by 42% (21.71 $\pm$ 1.24 s to 12.54 $\pm$ 2.31 s, $p < 0.001$). Unfortunately, there was also a 9% increase in the heating time (3.46 $\pm$ 0.71 s to 3.76 $\pm$ 0.71 s, $p < 0.001$) and a 28% decrease in the stroke (5.40 $\pm$ 0.44 mm to 3.89 $\pm$ 0.77 mm, $p < 0.001$).

This work demonstrates that fabric cooling channels are a viable option for cooling thermally actuated artificial muscles within a soft wearable device. Future work can continue to improve the channel design by experimenting with other configurations and materials.

4.2 Introduction

Each year, approximately 62,000 Canadians suffer a stroke [103]. It is recommended that stroke patients receive at minimum 45 minutes of rehabilitation therapy 5 days per week, which creates

high demands on physiotherapists [104]. High quantities of rehabilitation are important, as it has been shown that increasing the amount of time spent completing physiotherapy exercises improves the ability of the patient to complete activities of daily living independently [105]. One method of increasing access to rehabilitation is to create inexpensive, portable, wearable robotic systems that individuals can use at home and outside of the clinic to complete physiotherapy exercises. Review papers have found that robotic therapy can provide the same benefits as conventional physiotherapy, and that upper limb functions improved when robotic therapy was completed in addition to conventional therapy, especially with chronic stroke patients [20, 21]. Robotic therapy has many advantages such as progress tracking, real-time feedback, and reducing therapist workloads.

These robotic devices are not common due to their high cost and limited portability, which stems in part from using electric motors as the primary actuator [4, 9, 10]. One method to reduce the cost and increase the portability of wearable robotic devices is to use alternative actuators, such as artificial muscles. Artificial muscles have additional advantages of being biomimetic and compliant, which reduces the chance of injury to the user. There are several types of artificial muscles available, such as shape memory alloys (SMAs), pneumatic artificial muscles (PAMs), and twisted coiled actuators (TCAs).

SMAs are thermal actuators that alternate between two states upon heating and cooling. They can be formed into artificial muscles with low voltage requirements and high power-to-mass ratios. Unfortunately, they have large amounts of hysteresis which makes them difficult to control, and their cycle life decreases as the amount they are strained increases [38].

PAMs are fabricated by covering an internal air bladder in a woven mesh such that when the air bladder is inflated, the system contracts [31]. PAMs are advantageous as they are naturally compliant and they have a high power-to-weight ratio when the air compressor is ignored. Their main disadvantage is that they require an air compressor to actuate, which is loud, heavy, and frequently tethers the user to one spot. Recently, these muscles have been embedded into fabric to create a glove to help finger flexion [32, 34].

Finally, TCAs are a promising actuator for wearable robotic devices due to their inherent compliance, low profile, easy and inexpensive fabrication method, and linear actuation [12]. These artificial muscles are created by super-coiling silver-coated nylon thread, and they can carry loads

up to 80 MPa. They will contract up to 21% when electrically heated and extend upon cooling. Unfortunately, their low bandwidth with passive cooling (0.03 Hz) limits their effectiveness in devices designed for rehabilitation purposes [13]. To increase the potential for TCAs to be used in wearable robotic devices, their cooling time needs to be decreased.

Previous work has demonstrated that the cooling time is significantly impacted by the environment that surrounds the TCA. Common solutions have been to coat the TCA in hydrogel, surround it with water, or employ forced air convection [14, 15]. Of these solutions, a hydrogel coating increased the cooling rate the most, although the coating only lasted for 30 actuation cycles. Similar cooling rates have been achieved with forced convection of air and still water, however, when the TCA was surrounded by water it required approximately twice the input power to achieve a stroke of 10%.

Forced air convection has been implemented by running a computer fan near the TCAs or by placing a TCA in a rigid plastic tube and applying compressed air. However, neither of these solutions have been specifically designed for implementation in a soft wearable robotic device [15, 74]. Portable, wearable robotic systems have several design constraints unique to their applications. The systems must be lightweight and have minimal components, as the user must be able to carry the apparatus on their body. Additionally, the system should be flexible, compliant, and minimize any protrusions to ensure user comfort and decrease risk of injury.

Thus, this research presents a novel cooling apparatus for TCAs that is specifically designed for soft wearable robotic devices. It consists of a fabric channel to house the TCA and a miniature air pump to provide forced convection. Previous work performed simulations on this design, however, discrepancies between the simulation and experimental results indicated that additional experimental work would be valuable [87]. In this paper, Section 4.3 outlines the design process and final design for the novel cooling apparatus. Section 4.4 describes the experimental apparatus, methodology, and results obtained for an experiment that investigates the impact of changing the dimensions of the channel on the performance of the TCA (Phase I). Section 4.5 documents a follow-up experiment that was completed to compare the performance of the TCA with and without the novel cooling apparatus (Phase II). Finally, Section 4.6 discusses study limitations, sources of error, and future work.

4.3 Channel Design

The primary purpose of the cooling apparatus is to increase the cooling rate of the TCA, however, it should also facilitate the integration of TCAs into soft wearable robotic devices. To meet these objectives, several design requirements were considered during the development of the channel. First, the cooling apparatus had to be portable and help protect the user from the temperatures reached by the TCAs (up to 120°C). Next, the mass and size of the cooling apparatus needed to be minimized to ensure that the wearable device is as unobtrusive as possible. Ideally, the apparatus will also be durable, flexible, elastic, and breathable, to allow the user to comfortably wear it for extended periods of time. Finally, any negative effects of the cooling apparatus on TCA behavior (e.g., decreased stroke), should be minimized where possible to maintain the capabilities of the TCA.

4.3.1 Cooling Mechanism

While considering the above objectives, the first decision made was how to decrease the cooling time of the TCA. This could have been accomplished by adding a coating to the surface of the TCA to increase its thermal conductivity or by changing the environment in which the TCA resides. Modifying the TCA by adding a coating was disregarded as an initial solution, since coatings increase the manufacturing complexity and cost of the TCA, they do not provide a means of integrating the TCA into a wearable system, nor would they help protect the user against the high temperatures reached by TCAs. Thus, the environment of the TCA was changed by enclosing a TCA in a channel and employing forced convection.

Forced convection could be accomplished with a liquid (e.g., water) or a gas (e.g., air). Water and other liquids have a significantly higher thermal conductivity compared to air, which would drastically reduce the cooling time of the TCA. However, liquid coolants have many disadvantages when considering them for a wearable device. They are denser than air and require additional hardware, such as a reservoir and valves, resulting in a significantly heavier and more complex system. Additionally, there is the risk of leaks, which could decrease user comfort, and nylon TCAs will absorb water over time, degrading their performance [13]. Finally, the higher thermal

conductivity of liquids results in higher power requirements for the heating phase of the TCA [14]. Some of these disadvantages could be alleviated by surrounding the TCA in stagnant water, however this was disregarded as a potential solution as the temperature of the water would gradually increase with prolonged use of the TCA, and similar cooling times can be obtained with forced air convection [14]. The main disadvantage of forced air convection is that air compressors are noisy, however, the advantages of less mass, hardware, and no degradation of TCA performance allow it to meet the requirements better than a liquid system.

There are three main options to circulate air: fans, air pumps, and air compressors. Air compressors were rapidly discarded as potential solutions, as their large size and mass limit their portability. Table 4.1 displays some commercially available miniature air pumps and fans. Air pumps are capable of producing higher air pressures than fans, however, fans have the advantages of being lighter, smaller, and producing more air flow than the pumps. From the options listed in Table 4.1, fans have the additional benefit of producing less noise (between 15–36 dB) when compared to the pumps (around 55 dB). For context, the volume of a normal conversation occurs at around 60 dB [106].

While fans would be the optimal solution due to their advantages, testing with preliminary prototypes using a Sunon Fans MF20100V1-1000U-A99 demonstrated that their low pressure capabilities were unable to force air through the devised solution. Therefore, a pump was selected by maximizing the air flow and pressure capabilities while minimizing the height and mass. From this trade off, the Schwarzer Precision SP 16A RO-DV pump was selected, and is the pump used in all of the experiments described in this paper.

4.3.2 Channel Characteristics

The next step was to devise a method of enclosing the TCA that was flexible, easy to integrate into wearable devices, and could protect the user. It was decided to create a fabric channel, as fabric is flexible and can be sewn onto other materials, including insulation and underlying garments. The fabric for the channel must meet several criteria to ensure the success of the design. It should be flexible, durable, and be able to withstand temperatures above 120°C. Ideally, the material would be able to slightly stretch and be breathable, to ensure user comfort, and be able to hold a shape

Table 4.1: Commercially available miniature air pumps and fans that meet the 20 mm height constraint.

Fan/ Pump	**Company/ Part**	**Maximum Air Flow [cm^3/min]**	**Maximum Pressure [atm]**	**Height [mm]**	**Length [mm]**	**Width [mm]**	**Mass [g]**
Pump	Binaca SX-1	400	0.39	8	32	18	8
	Schwarzer Precision SP 12 RO	650	0.49	12	51	27	23
	Schwarzer Precision SP 16A RO-DV	1500	0.79	16	56	36	38.5
	Binaca CX1	1000	0.69	17	45	27	32
	Schwarzer Precision SP 18A RO-D	2500	0.59	18	62	32	44
Fan	Sunon Fans UB393-700TC	1170	0.00016	9	9	3	0.91
	Nidec Copal Electronics F16FB-05LLC/E	11890	0.00005	16	16	4.5	1.2
	Delta Electronics BSB0205HP-00EFG	16140	0.00098	17	17	5.3	1.81
	Sunon Fans MF20100V1-1000U-A99	53800	0.00071	20	20	10	4.65

without additional supports, to minimize the complexity and cost of fabrication.

Two common durable fabrics are tightly woven nylon and polyester, which are often used in parachutes and windbreakers. While they both have a melting temperature above 220°C, nylon was selected because nylon threads have a lower coefficient of dynamic friction and a similar coefficient of static friction when compared to polyester [107]. The dynamic coefficient of friction of nylon 6 is 7.6–22.2% lower than that of polyester, and the coefficient of static friction ranges between 3.6% smaller, up to 7.9% larger, depending on the circumstances. Tightly woven nylon 6 pack cloth with a thickness of 0.3 mm was sourced from Trident Textiles Corp. The material is 100% nylon with a 0.05 mm coating of ether-based thermoplastic polyurethane (ether TPU) on one side. The channels were created with the ether coating on the outside surface as it seemed to have higher friction, and there were concerns about melting the ether TPU. Ester TPU was selected as an alternative material as it has a melting temperature of approximately 145°C, it can stretch slightly, and it was used in another study to create PAMs embedded in wearable devices [34, 108]. Samples of 0.3 mm ester TPU were obtained from Plastic Film Corporation. Preliminary prototypes proved that both materials were easy to sew and were capable of maintaining their cross-sectional shape. To ensure that they could withstand the temperatures reached by TCAs, a TCA was held on the material at approximately 115°C for 10 minutes. There was no visible deformation to the nylon fabric, however, sections of the ester TPU melted. Thus, the material for the channels was selected to be nylon pack cloth.

After the material was selected, preliminary prototypes were created to determine the cross-sectional shape of the channel. The nylon cloth was sewn into four shapes—a circle, a semi-circle/ellipse, a triangle, and a square (Figure 4.1). The channel must be able to maintain its shape to ensure that there is adequate space for air to flow around the TCA and that no additional friction is caused by contact between the TCA and channel walls. It should also return to shape if deformed to ensure that the performance of the channel does not degrade if the user bumps their limb or folds the fabric. The circle was the easiest channel to manufacture; however, it was easy to flatten and did not return to its shape on its own, which resulted in the TCA being pinched by the fabric on two sides. The triangle was unable to remain open to provide an airway for the TCA. While the square and the semi-circle both had acceptable airways and could quickly return

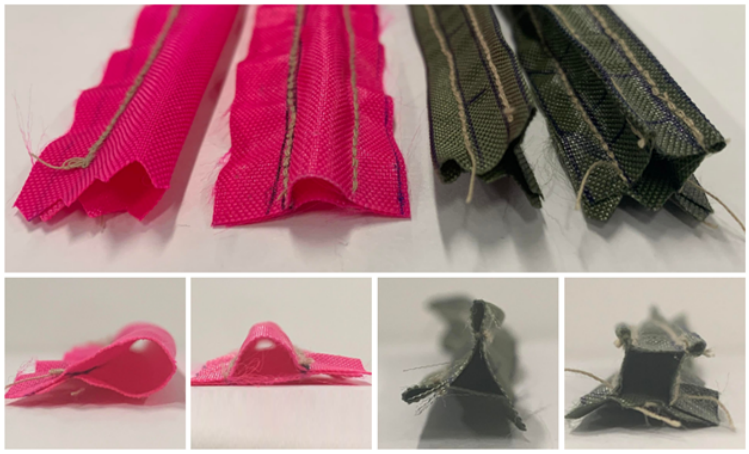

Figure 4.1: The top view (top) and front view (bottom) of the preliminary channel prototypes to test different channel shapes. From left to right the shapes tested include the following: circle, semi-circle, triangle, and square.

to their shapes when flattened, the semi-circle was significantly simpler to manufacture. For the rest of this paper, the channels being designed and tested will be semi-elliptical in shape. The main design parameters will be the width of the channel (the horizontal diameter of the ellipse) and the height of the channel (the vertical radius of the ellipse).

It is desirable to keep the dimensions of the channel as small as possible to reduce both the protrusion from the limb and the space on the device that would not be breathable, as the selected material is air impermeable. Additionally, if either the height or width are much larger than than the other, the ability of the channel to maintain its shape decreases. The minimum height and width were determined by considering the size of the TCA. The diameter of a 4-ply TCA is 1.6 mm, however the crimps used at the ends of the TCAs have a diameter of approximately 3 mm. Some additional space was required for the temperature sensor leads and air inlet. Thus, the smallest channel height and width were 4 mm and 6 mm, respectively.

Since the ideal height and width of the channel were unknown, an experiment (Phase 1) investigated the impact that changing these factors had on the performance of the TCA. Combinations of three heights and three widths were tested to determine if there was an effect from the height, the width, or the overall cross-sectional area (CSA) of the channel. Trial and error in making different sized channels revealed that there is some degree of variance in the size of the channel, even when the same fabrication procedure is followed. Thus, the size step was set to 2 mm to

ensure that the sizes were distinct. The channels will be described as width-by-height, i.e., a 6×4 channel has a width of 6 mm and a height of 4 mm. The final channel sizes that were tested are the following: 6×4, 6×6, 6×8, 8×4, 8×6, 8×8, 10×4, 10×6, 10×8. The channel dimensions were kept as small as possible to minimize how much the channel would protrude, while still ensuring there were distinct differences between the channel sizes.

Prior to beginning the experiment, an inlet piece was designed to connect the channel, air pump, and TCA (Figure 4.2). It is composed of two parts: a small, central piece to attach all of the components, and a cover for the central piece that simplifies changing the size of the inlet to match the size of the channel. At this stage, the inlet was not permanently fixed to the channel to facilitate testing the channels with multiple TCAs. Instead, the inlet was deliberately created 2 mm wider and 0.5 mm taller than the desired dimensions of the channel and it was wedged into the channel inlet. The channel inlet was also created slightly larger than the body of the channel to accommodate the inlet.

The channel fabrication process is outlined in Figure 4.3. To consistently create the channels, templates were designed and printed. Preliminary experimentation revealed that the channels were consistently wider and shorter than the desired dimensions, thus the templates were deliberately created 1 mm narrower and 0.5 mm taller. The channels were made to be 150 mm in length to accommodate TCAs that are 140 mm in length. The length of the channel was set to be approximately 10 mm longer than the loaded length of TCA to ensure that the entire TCA remained covered, as the TCA will creep slightly during use.

Finally, the channel on its own does not have enough insulation to protect the user from the temperatures reached by the TCA (up to 120°C). The pain threshold for hot temperatures has been shown to be between 42°C to 44.6°C [109, 110], thus additional insulation will be required to keep the user comfortable. The primary parameter when selecting insulation is the thermal conductivity, as this will dictate how thick the insulation must be to protect the user. Other properties were considered for the purpose of a wearable device, such as the water absorption (in case the user sweats) and density. Initially the Alpha SmartTemp Liner for prostheses was used, as the material is specifically designed to be comfortable for users when in contact with their skin for extended periods of time. This solution was tested by holding a TCA onto the material at

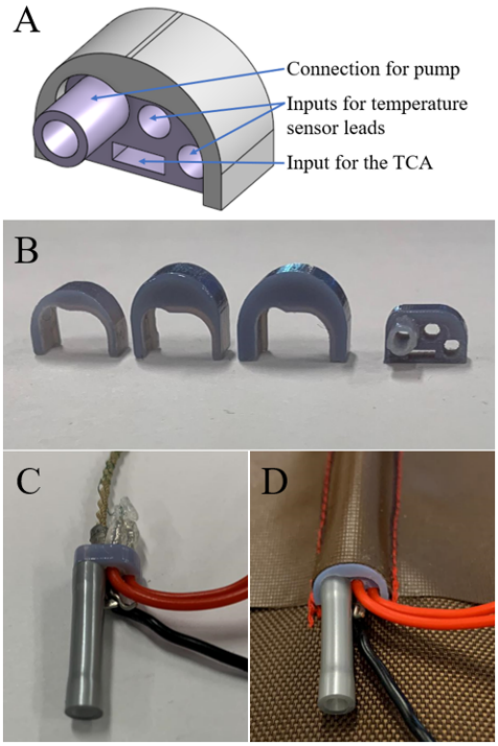

Figure 4.2: Inlet design (A) in CAD, (B) printed with different sized covers, (C) with the components connected, and (D) in a channel.

approximately 110°C for 5 minutes. It was found that two 8 mm layers were required to keep the temperature below 40°C. Thus, alternative options were investigated.

While several types of insulation were considered, mineral wool was selected due to its low thermal conductivity and density. Samples of 3 mm mineral wool with a foil backing were obtained from Insultech Inc. When the foil side of the insulation was placed facing the TCA, the 3 mm insulation was sufficient to protect the user from the temperature of the TCA. For integration in a wearable device, there would have to be an additional layer underneath the insulation, as the insulation will pull apart from itself if left uncovered.

To summarize, the general design for the fabric channels is displayed in Figure 4.4. The channel can be fixed to a wearable device by sewing it to an underlying garment, and the TCA can move freely inside the channel. Thus, the channel can both provide a means of cooling the TCA and a means of assembling it into a system. One end of the TCA was fixed to the channel inlet using the inlet piece described above, and the free end was coupled to its load using a thread as an artificial

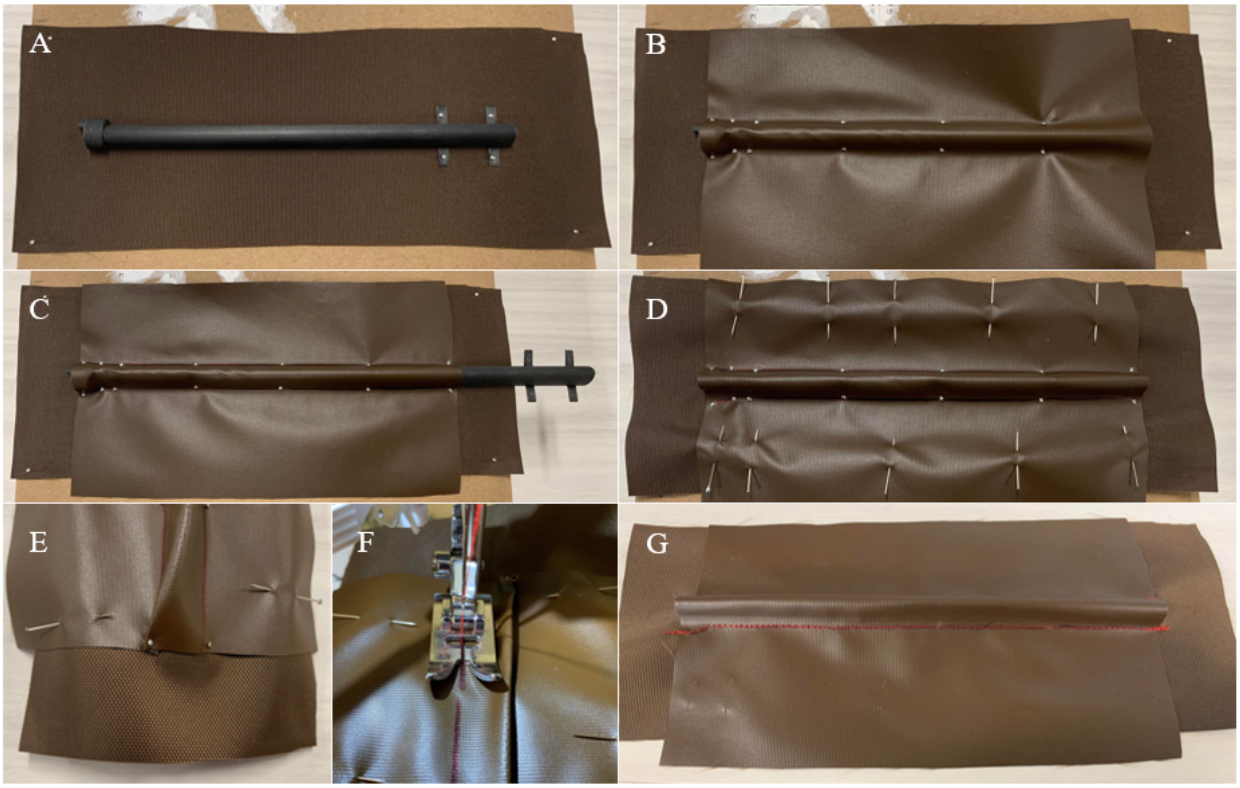

Figure 4.3: The channel fabrication procedure. First, the bottom and top layers are sized such that they are wider than the desired channel size to ensure that there is enough fabric to pin the material. The bottom layer is also sized longer than the desired length to simplify sewing. Then the following steps can be completed to create a channel: (A) The bottom layer and channel template are pinned in place to keep them from moving, and the inlet is placed at the end of the template. For simplicity, this is performed on a cardboard box to allow the pins to be pushed completely through the fabric. (B) The top layer of fabric is placed over the inlet and template, pulled taut, and pinned in place. (C) Before moving the template, the edge of the template is marked with pen as a guiding line for sewing. The template is slightly removed from the channel (to prevent it from getting trapped), and the end of the channel is pinned in place. (D) The two layers of fabric are pinned together to prevent them from slipping, and the channel is removed from the box. (E) To sew the channel, it must be flat along the seam. The fabric can be pulled taut and pinned in place at the outlet to help hold the opposite seam flat while starting to sew. (F) The seam is sewn along the guideline, while keeping the material pushed to the opposite side. (G) The previous two steps are repeated along the other side of the channel to obtain the finished product.

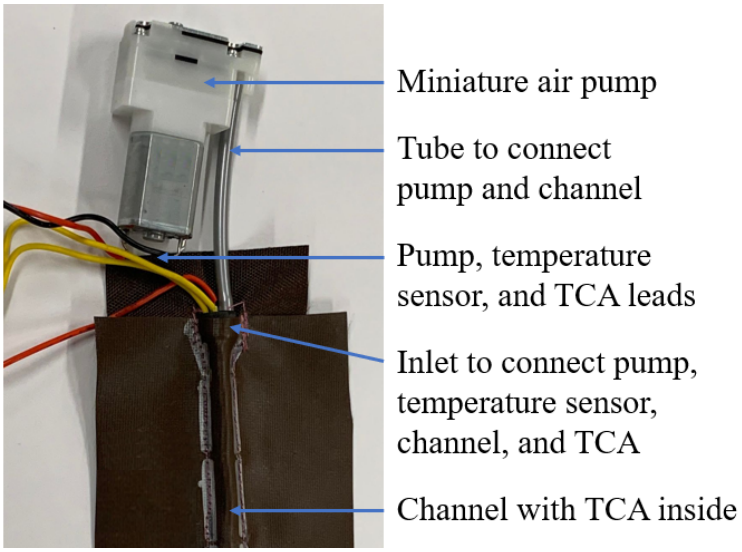

Figure 4.4: Final design of the cooling apparatus. The design consists of a fabric channel to house the TCA with a miniature air pump connected to the channel with a flexible plastic tube.

tendon. A flexible power line was also fixed to the free end of the TCA to allow the TCA to be actuated using Joule heating.

4.4 Phase I: Impact of Channel Height and Width on TCA Performance

4.4.1 Phase I: Methods

After the channel design was finalized, the impact of channel height and width on the performance of the TCA was investigated. This was accomplished by actuating TCAs in the nine channel sizes described above: 6×4, 6×6, 6×8, 8×4, 8×6, 8×8, 10×4, 10×6, and 10×8. TCA performance was assessed by comparing the cooling time, heating time, and stroke of the TCA in each channel, as these metrics are often used when evaluating the performance of thermal actuators [14, 15, 77, 78]. For this experiment, the cooling time was defined as the time it takes the TCA to cool from 100°C to 35°C; the heating time was defined as the time to heat the TCA from 23°C to 100°C; and the stroke was defined as the difference between the maximum displacement of the TCA and its position when it returned to room temperature after the heating–cooling cycle. The cooling time

was stopped at 35°C because preliminary experimentation found that the air output from the pump increases in temperature and can reach up to 30.2°C.

The experimental apparatus used for data collection is displayed in Figure 4.5. Insulation was placed on the platform on which the TCA and the channel rested to mimic the construction of a wearable device. The TCA was attached to a previously developed module that combines pulse width modulation circuitry, a current sensor (ACS70331EESATR-005U3), and a temperature sensor into one circuit board [13]. A resistive temperature sensor detector consisting of a 40 AWG shielded copper wire wrapped around the TCA was used, since the temperature sensor must be able to fit within the channel without easily falling off, or compromising the ability of the TCA to move within the channel [13]. The temperature sensor was located at the fixed end of the TCA to reduce the motion that could dislodge the sensor. The displacement of the TCA was measured using an encoder (AEAT-6012-A06) by fixing a string to the free end of the TCA and wrapping it around a pulley that was attached to the encoder. Set screws were used to prevent slipping between the string, the pulley, and the shaft. A 100 g mass was hung from the other end of the string to keep the TCA in tension.

The TCAs were made using a previously developed methodology [13]. Four-ply silver-coated nylon thread was obtained from VTechnicalTextiles (Part number: 260151023534) and was super-coiled with a load of 165 g. The coiled thread was plyed by folding it in half to prevent untwisting and the ends of the TCA were crimped to prevent the TCA from fraying using standard terminal crimps obtained from McMaster-Carr (Part ID: 69525K47). The untrained TCA length was 85 mm, and it was trained by stretching the artificial muscle 4–5 mm, holding it in position and heating the TCA at approximately 3 W until it reached 140°C. This process was repeated until the TCA was 110 mm (around 30% longer), which resulted in a final, unloaded TCA length of 138 mm, as the crimps add 14 mm on either side of the TCA.

To collect the data, the TCA was centered in a channel, then heated from 23°C to 100°C at an average power of 2 W. The power was regulated to ensure that the heating time could be compared between samples, which was accomplished by controlling the duty cycle of the input voltage (12 V) to account for the change in resistance of the TCA. The resistance of the TCA was computed using $R = V/I$, where R is the electrical resistance of the TCA, V is the average voltage applied

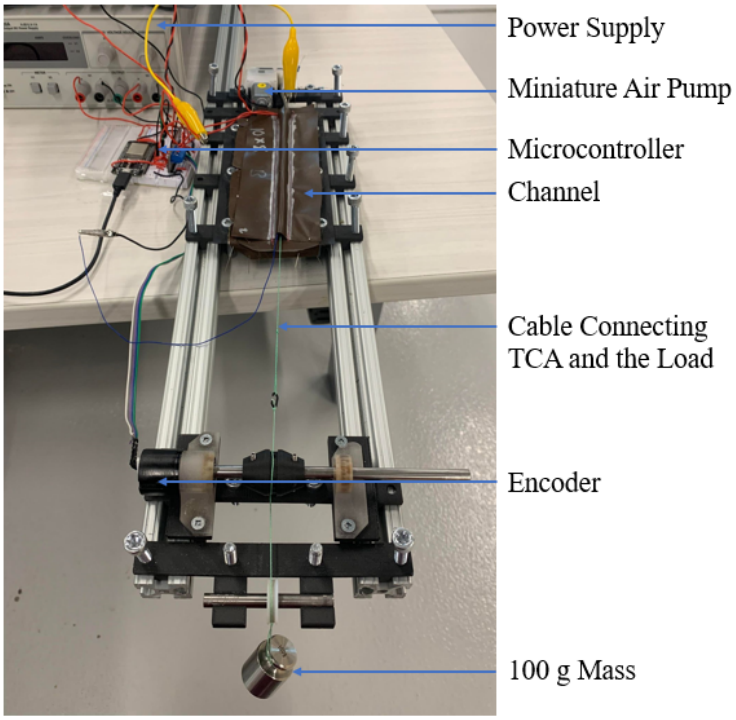

Figure 4.5: The experimental apparatus used to collect data.

to the TCA, and I is the average current through the TCA. Once the temperature of the TCA reached 100°C, the power input to the TCA was stopped, and the miniature air pump was turned on at 12 V. The pump was left on until the TCA reached 35°C, at which point the TCA was left to cool to room temperature passively, and the displacement of the TCA at room temperature was recorded before starting the next trial. This process was repeated three times before changing the channel. In total, 81 data points were collected at each channel size. To account for variability in the fabrication process, these repetitions were split evenly among three channels of the same size and three TCAs. The data collection process was blocked by TCA, i.e., all of the data were collected with TCA 1 before using TCA 2 or TCA 3.

Additionally, a warm-up procedure was completed if the TCA had not been used for more than 10 minutes, as it was noticed that the heating temperature–displacement curve for the heating cycle was significantly different if the TCA had not been used overnight, as seen in Figure 4.6. The warm-up procedure consisted of heating and cooling the TCA between 23°C and 100°C until the difference between the starting and ending positions at 23°C was less than 0.25 mm. This took 2–4 cycles, depending on how long it had been since the TCA was last used.

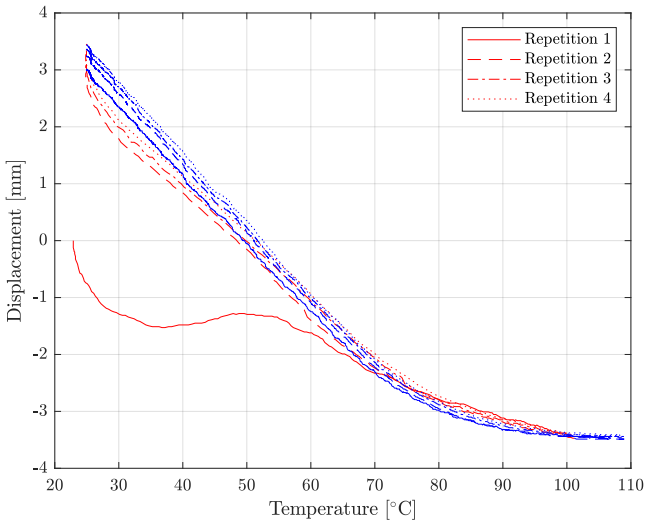

Figure 4.6: Four consecutive cycles of TCA heating from 25°C to 100°C after not being used overnight. The red and blue represent the heating and cooling portions of the cycle, respectively. The heating curve of the first repetition is significantly different from the rest of the trajectories.

4.4.2 Phase I: Results

After the data were collected, a statistical analysis was performed for each of the three parameters (cooling time, heating time, and stroke) to determine if there were differences between the channel sizes. First, the data were assessed to determine if there were outliers by calculating the studentized residuals and determining if any of the residuals were greater than $\pm$ 3. Although the cooling time data had five outliers, it was not possible to remove them from the analysis, as there was no apparent reason for the variation. The heating time data had one outlier, which was removed, because in the immediate trial afterwards, the power line broke, and therefore it is very likely that the power line was already partially broken. The stroke data had no outliers. Then, the normality of the data was assessed using the standardized residuals with the Kolmogorov–Smirnov test, as the sample size was larger than 50. None of the data were normally distributed, thus Friedman tests were performed to determine if differences existed between the channels. The results of the Friedman tests stated that channel size had a significant effect on all three parameters, with $p < 0.001$. *Post hoc* testing was performed using the Wilcoxon test, and a Bonferroni correction factor of 36 was applied to the p values to account for accumulated error from multiple comparisons, as 36

comparisons were performed for each parameter. The correction factor was applied by multiplying the p value by 36, to allow the significance threshold to remain at 0.05. The p values reported are those obtained after the correction factor was applied. The descriptive statistics for each parameter are summarized in Table 4.2, the results of the statistical analysis are shown in Table 4.3, and the p values for all *post hoc* testing are displayed in Table 4.4.

Table 4.2: Descriptive statistics for the parameters that were assessed to compare TCA performance in channels with different dimensions. Channels are ordered from left to right by increasing cross-sectional area.

Channel		6×4	8×4	6×6	10×4	6×8	8×6	10×6	8×8	10×8
Cooling Time [s]	Mean	15.11	14.14	12.16	13.00	14.45	11.98	11.97	12.02	11.42
	Standard Deviation	2.28	2.52	2.10	2.30	3.08	1.93	1.53	1.91	1.33
	Median	15.30	13.70	12.35	12.64	14.46	12.16	12.25	11.87	11.30
Heating Time [s]	Mean	5.36	5.36	5.18	5.39	5.27	5.10	4.98	5.07	4.88
	Standard Deviation	0.50	0.42	0.42	0.43	0.49	0.31	0.45	0.37	0.30
	Median	5.21	5.33	5.18	5.27	5.23	5.09	4.91	5.02	4.89
Stroke [mm]	Mean	7.04	7.53	8.14	7.41	8.29	8.29	8.25	8.42	8.32
	Standard Deviation	0.64	0.76	0.82	0.71	0.86	0.80	0.83	0.80	0.80
	Median	7.11	7.59	8.07	7.43	8.31	8.18	8.37	8.55	8.34

First, the data were analyzed to determine which channel resulted in the best TCA performance. Ideally, one channel would have the lowest cooling and heating times and the highest stroke, however, the best channel is defined as the one that balances these three parameters. The best channel cannot simply be the one with the lowest cooling time if it also greatly increases the heating time or decreases the stroke, as this would have negative implications for a wearable device. Significant increases in heating time indicate that the channel causes the TCA to be less efficient, which would negatively impact the battery lifetime of a wearable device. Likewise, decreases in TCA stroke would negatively impact the performance of the device, as there would either be a

Table 4.3: The Friedman test results and significant differences for the main effects of height and width from Phase I.

Parameter	Factor	Level	Friedman Test	Significant Differences
Cooling Time	Height (4, 6, 8 mm)	6 mm width	$p < 0.001$	4–6, 6–8
		8 mm width	$p < 0.001$	4–6, 4–8
		10 mm width	$p < 0.001$	4–6, 4–8, 6–8
	Width (6, 8, 10 mm)	4 mm height	$p < 0.001$	6–10, 8–10
		6 mm height	$p = 0.391$	—
		8 mm height	$p < 0.001$	6–8, 6–10
Heating Time	Height (4, 6, 8 mm)	6 mm width	$p = 0.177$	—
		8 mm width	$p < 0.001$	4–6, 4–8
		10 mm width	$p < 0.001$	4–6, 4–8
	Width (6, 8, 10 mm)	4 mm height	$p = 0.916$	—
		6 mm height	$p = 0.006$	6–10
		8 mm height	$p < 0.001$	6–8, 6–10, 8–10
Stroke	Height (4, 6, 8 mm)	6 mm width	$p < 0.001$	4–6, 4–8
		8 mm width	$p < 0.001$	4–6, 4–8
		10 mm width	$p < 0.001$	4–6, 4–8
	Width (6, 8, 10 mm)	4 mm height	$p < 0.001$	6–8, 6–10
		6 mm height	$p = 0.01$*	—
		8 mm height	$p = 0.144$	—

*There were no significant differences after the Bonferroni correction factor was applied.

lower achievable range of motion, or a longer TCA would be required to obtain the original stroke.

To illustrate the performance of the TCA in each channel size, Figure 4.7A, C, and E plots the data with respect to increasing cross-sectional area (CSA), with the statistically significant differences for the 10×8 channel marked. It can be seen that for the cooling time, 10×8 is statistically different from all of the channels except 8×8 (11.42 ± 1.33 s vs. 12.02 ± 1.91 s, $p = 0.051$), and for the heating time, 10×8 is significantly different from all of the channels except for 10×6 (4.88 ± 0.3 s vs. 4.98 ± 0.45 s, $p = 1$). Furthermore, there is no statistically significant difference between the stroke for 10×8 and any channel with a height greater than 4 mm. Thus, it can be concluded that for a 4-ply TCA, the best channel out of the sizes present in this experiment is 10×8, as that channel has a good balance between cooling time and heating time, and a comparable stroke to

Table 4.4: Adjusted p values from the *post hoc* testing for Phase I: Evaluating the Impact of Channel Height and Width on TCA Performance. Values below 0.001 are reported as 0 and comparisons that are not statistically significant are marked with †.

	Sheath	6×4	6×6	6×8	8×4	8×6	8×8	10×4	10×6	10×8
Cooling Time	6×4	—	0	0.648†	0.468†	0	0	0	0	0
	6×6	0	—	0	0	1†	1†	0.108†	1†	0.025
	6×8	0.648†	0	—	1†	0	0	0	0	0
	8×4	0.468†	0	1†	—	0	0	0.004	0	0
	8×6	0	1†	0	0	—	1†	0	1†	0
	8×8	0	1†	0	0	1†	—	0	1†	0.051†
	10×4	0	0.108†	0	0.004	0	0	—	0	0
	10×6	0	1†	0	0	1†	1†	0	—	0
	10×8	0	0.025	0	0	0	0.051†	0	0	—
Heating Time	6×4	—	0.424†	1†	1†	0.004	0.002	1†	0	0
	6×6	0.424†	—	1†	0.014	1†	1†	0.005	0.003	0
	6×8	1†	1†	—	1†	0.008	0.006	1†	0	0
	8×4	1†	0.014	1†	—	0	0	1†	0	0
	8×6	0.004	1†	0.008	0	—	1†	0	0.284†	0
	8×8	0.002	1†	0.006	0	1†	—	0	1†	0.002
	10×4	1†	0.005	1†	1†	0	0	—	0	0
	10×6	0	0.003	0	0	0.284†	1†	0	—	1†
	10×8	0	0	0	0	0	0.002	0	1†	—
Stroke	6×4	—	0	0	0	0	0	0	0	0
	6×6	0	—	0.974†	0	0.136†	0	0	0.793†	0.128†
	6×8	0	0.974†	—	0	1†	1†	0	1†	1†
	8×4	0	0	0	—	0	0	1†	0	0
	8×6	0	0.136†	1†	0	—	0.251†	0	0.917†	1†
	8×8	0	0	1†	0	0.251†	—	0	0.068†	1†
	10×4	0	0	0	1†	0	0	—	0	0
	10×6	0	0.793†	1†	0	0.917†	0.068†	0	—	1†
	10×8	0	0.128†	1†	0	1†	1†	0	1†	—

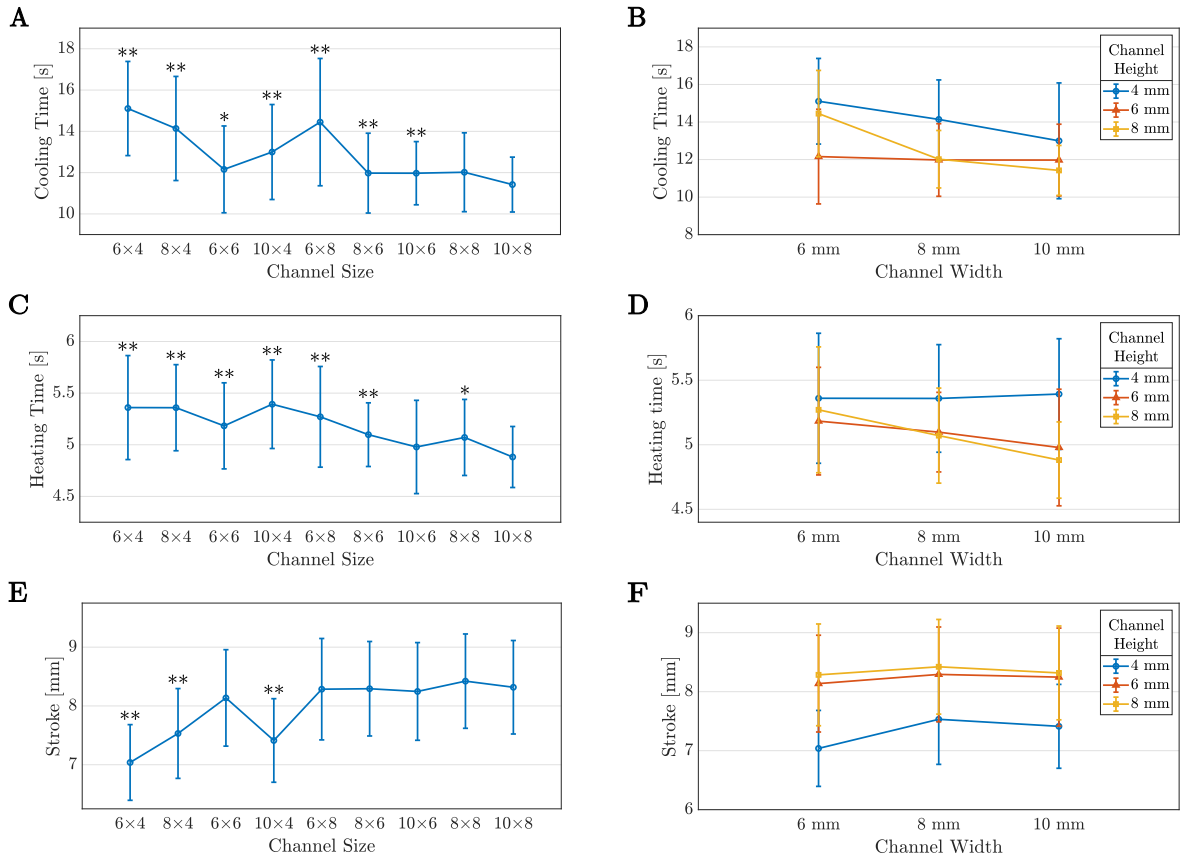

Figure 4.7: The means and standard deviations for the data from Phase I plotted with respect to increasing cross-sectional area (A, C, E) and height and width (B, D, F). In (A), (C), and (E), statistically significant differences with the 10×8 pouch are marked by an $*$ for $p < 0.05$ or $**$ for $p < 0.001$.

the other sizes. While the cooling time for 10×8 is not statistically different from 8×8, 8×8 has a statistically higher heating time. Similarly, the heating time for 10×8 is not different from 10×6, however the cooling time for 10×6 is higher.

Next, the effect of width and height on the TCA performance was examined. To help visualize if there were any trends in the data based on height or width, the data were plotted with respect to these parameters in Figure 4.7B, D, and F.

4.4.2.1 Cooling Time

Figure 4.7B illustrates that the impact of changing the width and height of the channel was different at each level of height and width. These simple main effects were tested using additional Friedman

tests, which stated that height had a significant effect at each width ($p < 0.001$ for all three) and width had a significant effect for heights of 4 mm and 8 mm ($p < 0.001$). The effect of width at a height of 6 mm was not significant ($p = 0.391$).

At all widths, channels with a height of 4 mm (the blue points) had the highest cooling times. When the height was increased to 6 mm (the red points), there was a statistically significant decrease in the cooling time ($p < 0.001$ for all widths). An additional increase in height to 8 mm (the yellow points) resulted in the average cooling time either decreasing further (10 mm width, $p < 0.001$), remaining approximately the same (8 mm width, $p = 1$), or increasing (6 mm width, $p < 0.001$). There was no significant difference between 6×4 and 6×8 ($p = 0.648$).

When analyzing the effect of width on the cooling time, there is a decrease in average cooling time as the width increases at 4 mm and 8 mm heights. At 4 mm (the blue line), the decrease in cooling time is significant when the width increases from 8 mm to 10 mm ($p = 0.004$), however it is not significant between 6 mm and 8 mm widths ($p = 0.468$). The opposite effect is observed at the 8 mm height (the yellow line)—the increase in width is significant between 6 mm and 8 mm ($p < 0.001$), yet it is not significant between 8 mm and 10 mm ($p = 0.051$).

If the data are regarded as average cooling time as a function of CSA, there is a slight downward trend as the CSA increases, with a Pearson correlation coefficient of -0.739 and a slope of -0.071 s/mm^2. Interestingly, the 6×8 and 8×6 channels have the same CSA, hence the stark difference between their mean cooling times (14.45 ± 3.08 s vs. 11.98 ± 1.93 s, $p < 0.001$) highlights that the dimensions of the channel are important, not just the overall CSA.

4.4.2.2 Heating Time

Similarly, the heating time of the TCA slightly decreases as the channel CSA increases with a slope of -0.012 s/mm^2. For this parameter, the Pearson correlation coefficient is -0.884. Again, the difference between the heating times for 6×8 and 8×6 (5.27 ± 0.49 s vs. 5.10 ± 0.31 s, $p = 0.008$) show that the height and width have an impact on the heating time, and these trends are illustrated in Figure 4.7D.

From the simple main effect analysis for heating time, increasing the height of the channel did not have an effect when the width was 6 mm ($p = 0.177$), yet there was an effect at widths of 8

mm and 10 mm ($p < 0.001$ for both). *Post hoc* testing revealed that this effect was only present when the height increased from 4 mm (the blue points) to 6 mm (the red points), with $p < 0.001$. There was no significant difference in the heating time when the height was further increased to 8 mm (the yellow point).

Likewise, the effect of width was not significant at a height of 4 mm ($p = 0.916$), however, increasing the width produced a significant decrease in average heating time at heights of 6 mm ($p = 0.006$) and 8 mm ($p < 0.001$). At a height of 6 mm (the red line), the effect of increasing the width was only significant between 6 mm and 10 mm ($p = 0.003$). However, at a height of 8 mm (the yellow line), the effect of width was significant at both step increases, with $p = 0.006$ for 6 mm to 8 mm and $p = 0.002$ for 8 mm to 10 mm.

4.4.2.3 Stroke

The final parameter that was analyzed was the stroke of the TCA. Again, simple main effects were assessed using the Friedman test and the trends are shown in Figure 4.7F. The effect of height was significant at all three widths ($p < 0.001$ for all three), and the effect of width was significant at a height of 4 mm ($p < 0.001$). *Post hoc* analysis revealed that the effect of height was only significant with the increase from 4 mm (blue points) to 6 mm (red points), with $p < 0.001$ at all three widths. There was no significant effect on the stroke when the height was further increased to 8 mm. Similarly, the effect of width at 4 mm of height (the blue line) was only significant when the width increased from 6 mm to 8 mm ($p < 0.001$). Thus, it appears that the channel dimensions did not significantly affect the stroke of the TCA, provided that the channel height was greater than 4 mm.

4.4.3 Phase I: Discussion

This experiment demonstrated that TCA performance varied as the height and width of the channel changed. As illustrated in Figure 4.7A, there was a slight decrease in mean cooling time as the CSA of the channel increased, however this decrease is influenced by the dimensions of the channel. To decrease the cooling time of the TCA, the thermal resistance between the surface of the TCA and the environment needs to be reduced. The equation of thermal resistance for convective cooling,

R_{conv}, is displayed in Equation 4.1, where h is the convective heat transfer coefficient and A_{TCA} is the surface area of the TCA that is exposed to forced convection [86]. For a given TCA, the surface area would be fixed, thus to decrease the thermal resistance, h must be increased.

$$R_{conv} = \frac{1}{hA_{TCA}} \tag{4.1}$$

The convective heat transfer coefficient depends heavily on the geometry of the hardware. For concentric cylinders, there is a complicated relationship between h and the diameters of the cylinders [86]. It is hypothesized that the relationship between h and the dimensions of the channel would be even more complicated due to the half-elliptical shape and off-center placement of the TCA. However, for concentric cylinders, h is proportional to the input velocity of the fluid. It is assumed a similar relationship occurs with the channels—the cooling time will decrease as the input air velocity increases.

Fluid flow is also heavily dependent on geometry, and for laminar flow in a circular pipe, the flow resistance, R_{flow}, can be predicted using Pousuille's Law, which is shown in Equation 4.2. Here η is the viscosity of the fluid, l is the length of the tube, and r is the radius of the tube [111]. While this equation cannot be directly applied to the channel, the understanding that flow resistance decreases as the pipe radius increases is assumed to be applicable.

$$R_{flow} = \frac{8\eta l}{\pi r^4} \tag{4.2}$$

The flow resistance will directly impact the fluid flow in a pipe, as for a fully developed laminar flow in a horizontal pipe, the flow, Q, is inversely proportional to the flow resistance and directly proportional to the pressure gradient across the pipe, ΔP, as seen in Equation 4.3 [111]. It is also known that for pumps, there is an inverse relationship between the required pressure and the flow rate that the pump can output. Thus, given the limited pressure capabilities of the miniature pump, it is assumed that the cooling time decreased as the channel dimensions increased, because the lower flow resistance allowed the pump to provide a higher flow rate. This relationship was not linear, as the flow resistance, air velocity, and thermal resistance will depend on the specific geometry of the channel. Future work should further investigate and quantify this relationship to

help optimize channel dimensions for variety of applications.

$$Q = \frac{\Delta P}{R_{flow}} \tag{4.3}$$

The effect that the specific height and width of the channel had on the cooling time of the TCA is highlighted by the contrast between the 6×8 and 8×6 channels. Despite the CSA being approximately the same, the cooling time for 6×8 was significantly higher and was the same as 6×4. This could be partially explained by observing the channel itself. The 6×8 channel was the only size where the height was larger than the width, and it was noticed that the sides of the channel had a tenancy to cave in slightly, as shown in Figure 4.8. This would reduce the effective CSA for the channel, increase the air resistance, and could increase the chance of the TCA coming in contact with the channel walls. Thus, it is recommended that the channel height should be the same or less than the channel width.

The geometry of the channel also influenced the heating time of the TCA. Unlike the cooling phase, a higher thermal resistance is better for the heating phase as this would reduce heat loss to the environment and reduce the heating time. As shown in Figure 4.7C, the heating time decreased as the CSA increased, for which a possible explanation is that the additional stagnant air in the larger channels acted as better insulation and allowed less heat loss to the environment. This is consistent with the results found when TCAs were heated in rigid plastic tubes; as the tube diameter increased, the heating time constant decreased [74].

A noticeable exception to this trend are the channels with a 4 mm height—there was no

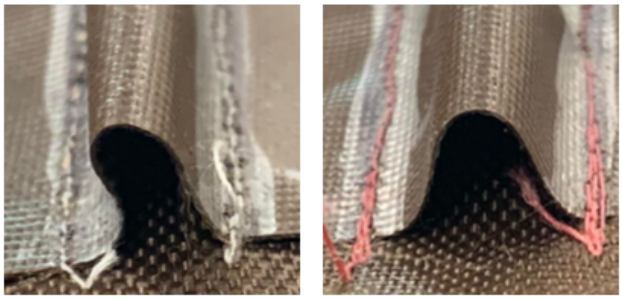

Figure 4.8: The approximate cross-sectional area shape for 6×8 (left) and 10×8 (right) channels. The sides of the 6×8 channel cave in compared to a channel where the width is larger than the height.

difference in the heating times between the 6×4, 8×4, and 10×4 channels. A possible explanation is that due to the low height, the TCA was in contact with the top of the channel, and thus there was heat loss through the channel to the surrounding environment. These channels also had the lowest strokes, which supports the prediction that the TCA was in contact with the channel at the 4 mm height as the stroke could be reduced due to additional friction from increased contact with the channel walls. The 6×4 channel had a lower stroke than 8×4 and 10×4, which is likely due to additional contact with the channel sides.

As illustrated in Figure 4.7F (red and yellow lines), the stroke was the same between the channels with 6 mm and 8 mm heights. This can be explained as once the TCA is no longer in contact with the top of the channel, there would be no additional frictional forces. The only significant difference occurred between 6×6 and 8×8 (8.14 ± 0.64 mm vs. 8.42 ± 0.80 mm, $p < 0.001$). It is unclear why this occurred, as there was no difference between the heating time or cooling time for those two channels.

4.5 Phase II: Effect of Fabric Channel on TCA Performance

4.5.1 Phase II: Methods

As concluded in Phase I, the channel height and width impact the performance of the TCA, and for a 4-ply TCA, the best size out of those tested was the 10×8 channel. An additional evaluation was completed to compare the performance of the TCA with and without the fabric channel to determine the efficacy of the channel in cooling the TCA and its impact on TCA performance. To accomplish this, TCA performance will be compared across the following four cases: 1) active cooling with the channel, 2) active cooling without the channel (current state-of-the-art), 3) passive cooling with the channel, and 4) passive cooling without the channel (basic operation).

This experiment was completed using the same apparatus as Phase I, which is described in Section 4.4.1. The experimental procedure was also very similar to that of Phase I, however two changes were made to be more consistent with how the TCAs and channels would be used in practice. The first change was to reduce the maximum temperature from 100°C to 85°C, as the temperature–displacement curve consistently flattened at around 85°C. This is likely due to the

coils of the TCA coming in contact with one another and preventing further contraction. The second change was to immediately begin the next heating–cooling cycle once the TCA reached 35°C. Thus, the experimental procedure is summarized by the following steps: 1) the TCA was heated to 85°C, without any active cooling; 2) the TCA was cooled to 35°C, with or without active cooling (depending on the case); 3) Steps (1) and (2) were repeated five consecutive times; and 4) the data from the first repetition were discarded as the TCA was heated from room temperature, as opposed to 35°C. For Case 2, active cooling was applied in the same manner as for Case 1—the pump was attached to the channel inlet and air was allowed to flow over the TCA, except that the channel was not present. For each case, 96 repetitions were collected, which were split evenly among four TCAs and, where applicable, among three 10×8 channels (the same ones that were utilized in Phase I), to account for variability in the fabrication procedure. The order of the cases was randomized for each TCA, and the data were blocked such that all of the data were collected on one TCA before moving to the next.

To assess TCA performance, the cooling time, heating time, stroke, and maximum hysteresis were recorded and compared between the cases. For this experiment, the cooling time was defined as the time it takes to cool the TCA from 85°C to 35°C; the heating time was defined as the time to heat the TCA from 35°C to 85°C; the stroke was defined as the difference between the maximum displacement and the position of the TCA at 35°C at the end of the cooling phase; and the maximum hysteresis was defined as the largest difference in TCA position between the heating and cooling curves. The amount of hysteresis was computed by calculating the absolute difference between the position of the TCA at each point on the heating curve and the equivalent point (closest in temperature) on the cooling curve. The largest difference was recorded and was divided by the stroke for that trial, to express the maximum hysteresis as a percent of the stroke. Comparing the hysteresis as a percent of stroke reduces the possibility that a significant difference in the amount of hysteresis between cases exists solely due to a difference in TCA stroke.

4.5.2 Phase II: Results

The descriptive statistics for the four parameters are displayed in Table 4.5. After the data were collected, they were checked for outliers using the studentized residuals. There were no outliers in

Table 4.5: Descriptive data for Phase II.

Case		1. Channel Active Cooling	2. No Channel Active Cooling	3. Channel Passive Cooling	4. No Channel Passive Cooling
Cooling Time [s]	Mean	12.54	8.57	34.92	21.71
	Standard Deviation	2.31	0.71	1.48	1.24
	Median	12.17	8.68	34.90	21.72
Heating Time [s]	Mean	3.76	3.61	3.52	3.46
	Standard Deviation	0.71	0.69	0.66	0.71
	Median	3.50	3.41	3.39	3.32
Stroke [mm]	Mean	3.89	4.66	5.21	5.40
	Standard Deviation	0.77	0.37	0.35	0.44
	Median	4.08	4.66	5.21	5.41
Maximum Hysteresis [%]	Mean	14.06	12.59	11.23	11.60
	Standard Deviation	6.30	3.19	2.38	2.15
	Median	12.02	12.20	11.42	11.56

the cooling time, heating time, or stroke data. There were two outliers present in the hysteresis data, however they were left in the analysis as there was no apparent reason for the variation. Then, the normality of the data were assessed using the Kolmogorov–Smirnov test on the standardized residuals. Once again, the data were not normally distributed, therefore Friedman tests were conducted to determine if a statistically significant difference existed in the data. The Friedman test revealed that there was a significant difference present for each parameter, with $p < 0.001$ for cooling time, heating time, and stroke and $p = 0.041$ for hysteresis. *Post hoc* testing was completed using the Wilcoxon test and a Bonferroni correction factor of 6 was applied to the p values in the same manner as Phase I to account for multiple comparisons. The adjusted p values for all comparisons are presented in Table 4.6.

Table 4.6: Adjusted p values from the *post hoc* testing for Phase II: Comparison of TCA Performance With and Without the Channel. Values below 0.001 are reported as 0 and comparisons that are not statistically significant marked with †.

	Case	1. Sheath Active Cooling	2. No Sheath Active Cooling	3. Sheath Passive Cooling	4. No Sheath Passive Cooling
Cooling Time	1	—	0	0	0
	2	0	—	0	0
	3	0	0	—	0
	4	0	0	0	—
Heating Time	1	—	0	0	0
	2	0	—	0	0
	3	0	0	—	0.013
	4	0	0	0.013	—
Stroke	1	—	0	0	0
	2	0	—	0	0
	3	0	0	—	0.004
	4	0	0	0.004	—
Hysteresis	1	—	$1^{\dagger}$	$0.120^{\dagger}$	$0.180^{\dagger}$
	2	$1^{\dagger}$	—	0.012	0.048
	3	$0.120^{\dagger}$	0.012	—	$0.648^{\dagger}$
	4	$0.180^{\dagger}$	0.048	$0.648^{\dagger}$	—

Figure 4.9 plots the data obtained in this experiment with the statistically significant differences for Case 1 marked. Interestingly, Case 1 is significantly different from all other cases for cooling time, heating time, and stroke, with $p < 0.001$ for all comparisons. Conversely, there is no significant difference between the amount of hysteresis present in Case 1 and the other cases ($p = 1$, $p = 0.120$, and $p = 0.180$, when compared with Case 2, 3, and 4, respectively), however Case 1 has approximately twice the standard deviation.

These data illustrate that the channel successfully reduced the cooling time of the TCA, however this occurred at a cost of increasing the heating time and decreasing the stroke. When the cooling time is compared to basic operation (Case 4, no channel with passive cooling), the cooling

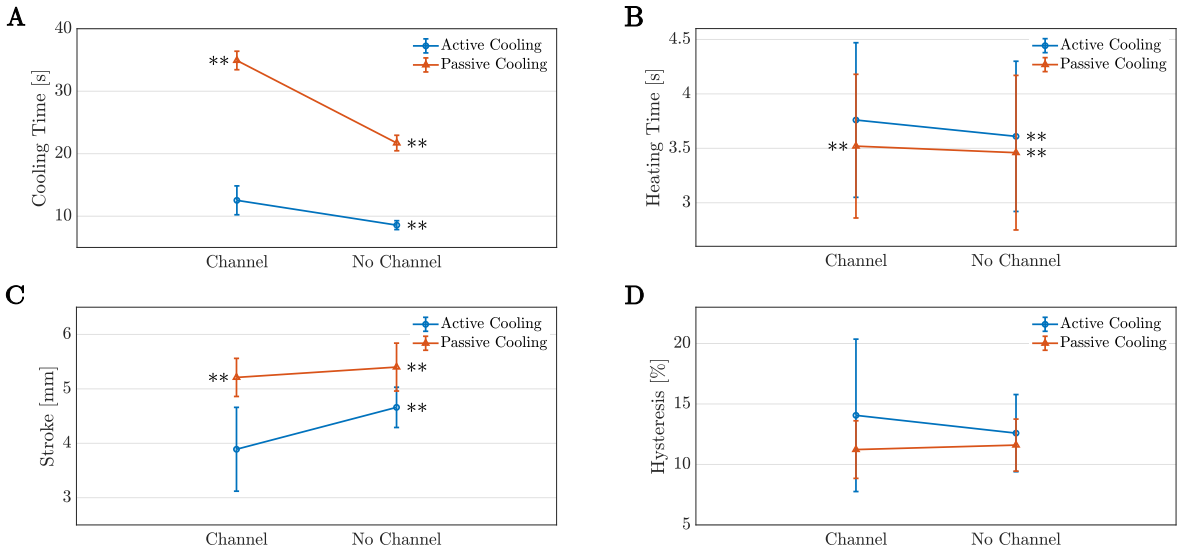

Figure 4.9: The means and standard deviations for the data from Phase II plotted for (A) cooling time, (B) heating time, (C) stroke, (D) and maximum hysteresis as a percent of stroke. The number adjacent to the point marks which case it is and if there is a statistically significant difference with Case 1 (channel, active cooling), it is marked by ** for $p < 0.001$.

apparatus reduced the average cooling time by 42% (21.71 ± 1.24 s vs. 12.54 ± 2.31 s, $p < 0.001$). The cooling time was also compared with the performance in a channel without active cooling (Case 3) to simulate the cooling time in a wearable device if active cooling was not employed. In this instance, the addition of active cooling reduced the cooling time by approximately 64% (34.92 ± 1.48 s vs. 12.54 ± 2.31 s, $p < 0.001$). Finally, to complete the study, the cooling time of the TCA in the channel with active cooling (Case 1) was compared to the current state of the art: active cooling without a channel (Case 2). Unfortunately, the cooling time for Case 1 was larger than the cooling time for Case 2 (12.54 ± 2.31 s vs. 8.57 ± 0.71 s, $p < 0.001$), however Case 2 is not feasible for wearable devices as the exposed TCA could burn the user or become caught on objects in the environment. A cooling time closer to that of Case 2 may be obtainable with further improvements to the channel design.

Ideally, improvements to the channel will also allow the TCA heating time and stroke to be closer to the values obtained without a channel. Surprisingly, the heating time of the TCA increased with the addition of the channel, however this difference was relatively small—approximately 4% between Cases 1 and 2, or 9% between Cases 1 and 4. A larger drawback is the decrease in stroke,

as the addition of the channel caused reduced the stroke by approximately 19% between Case 2 and Case 1 (4.66 ± 0.37 mm vs. 3.76 ± 0.77 mm, $p < 0.001$). Interestingly, the cases with passive cooling obtained higher strokes, even when the channel was present. With passive cooling, the addition of the channel reduced the stroke by 3.5% (5.40 ± 0.44 mm vs. 5.21 ± 0.35 mm, $p = 0.004$).

4.5.3 Phase II: Discussion

Unsurprisingly, the two cases with passive cooling had longer cooling times, and Case 3 (with the channel) had the largest cooling time. In Case 3, there would be minimal air circulation, and the air itself would also have to cool, since it would be warm from the end of the heating phase. Conversely, the other cases had some means of air circulation, whether it be from the pump when active cooling was incorporated in Cases 1 and 2, or natural convection from the hot TCA being exposed to the environment in Cases 2 and 4. It is hypothesized that the cooling time for Case 2 was lower than that of Case 1 due to the lack of channel allowing constant natural convection (especially during the heating phase) in addition to the forced convection from the pump. Natural convection would provide an advantage, as the air that is heated during the heating phase can immediately move away from the TCA, as opposed to being trapped by the channel, reducing the surrounding temperature. Additionally, Case 2 likely has a higher air flow rate than Case 1, as there is no added flow resistance from the channel.

It is also possible that there was additional air flow in Case 2 due to air entrainment. Air entrainment is the phenomenon of air in the environment being pulled (entrained) along the air stream due to the pressure gradient, which increases the total air flow. Air entrainment would be prevented when the channel was used, as the inlet was sized such that the channel was sealed. Thus, future work could investigate improving the channel design by not sealing the inlet of the channel, to allow air entrainment, or by adding small holes in the channel, to allow natural convection.

One of these modifications may be sufficient to reduce the heating time with a channel to what it was without a channel, as the difference was less than 10%. The increase in heating time with the addition of the channel was unexpected, as it was predicted that the stagnant air inside the channel would act as insulation during the heating phase and allow the heating time to be

reduced, as natural convection would not occur to the same extent. However, it is possible that the difference in heating times occurs from the addition of active cooling, not the channel. The difference in mean heating time with and without active cooling is 0.24 s with the channel and 0.15 s without the channel. In contrast, the difference in mean heating times with and without the channel is 0.15 s for active cooling and 0.06 s for passive cooling.

While the difference in heating time with the channel present was small, the addition of the channel and active cooling greatly reduced the stroke of the TCA. This likely stems from a combination of additional friction (when compared to Case 2) and a shorter cooling time (when compared to Case 3). The shorter cooling time would negatively affect the stroke, as preliminary experimentation found that the TCA, when loaded, has a tendency to slowly creep. Thus, the cases with passive cooling achieved higher strokes as the TCA has more time to extend, and it is predicted that this is the reason why the stroke for Case 3 is comparable to that of Case 4, despite the addition of the channel. On the other hand, the stroke for Case 2 is smaller than those of Cases 3 and 4, as the TCA does not have time to creep.

Despite the reduction in stroke, there was no significant difference in the amount of hysteresis present between Cases 1 and 2. There was also no significant difference in the hysteresis between Cases 3 and 4 ($p = 0.648$), indicating that the addition of the channel does not increase the amount of hysteresis present in the system. However, the standard deviation for Case 1 has approximately twice the standard deviation compared to the other cases, suggesting that the behavior of the TCA may be harder to predict and model, as there is more variation. Interestingly, the majority of the samples had the maximum hysteresis occur between 35–40°C, as seen in Figure 4.10. A possible explanation is that when the power is turned on, the sudden increase in temperature causes a quick contraction, however when cooling, the progression over the same positions occurs more gradually. This is likely related to the heat transfer rates, as at the end of the cooling cycle, the reduced temperature differential results in reduced heat transfer.

Finally, a brief comparison between the results for the 10×8 channel with active cooling from Phase I and Phase II was performed. As expected, the average heating time and stroke were higher in Phase I than Phase II (4.88 ± 0.30 s vs. 3.76 ± 0.71 s, and 8.32 ± 0.80 mm vs. 3.89 ± 0.77 mm, respectively), as the temperature range was 23–100°C, compared to 35–85°C. The larger

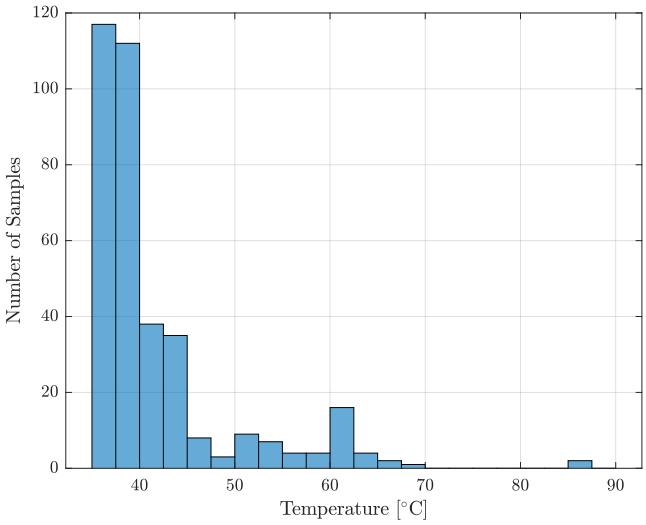

Figure 4.10: The distribution of temperatures at which the maximum hysteresis occurred.

temperature range required additional time to heat the TCA and allowed further contraction of the TCA. Surprisingly, the average cooling time for Phase I was smaller than the average cooling time for Phase II (11.42 ± 1.33 s vs. 12.54 ± 2.31 s), despite the larger temperature range (100–35°C for Phase I and 85–35°C for Phase II). This discrepancy can be accounted for by considering that different TCAs were used for the two different experiments, and each TCA had its own range of cooling times. Specifically, the average cooling times for the three TCAs used in Phase I were 12.79 s, 10.07 s, and 11.4 s, whereas the average cooling times for the four TCAs used in Phase II were 12.00 s, 9.91 s, 12.4 s, and 15.86 s. Since the last TCA used in Phase II has a longer cooling time than the other TCAs, the overall average cooling time for Phase II is longer than that for Phase I. The variations in TCA performance occur due to their fabrication parameters, such as the number of coils added during the twisting phase of fabrication [12, 66], and these variations contribute to the discrepancies seen when comparing experimental results where different TCAs were used. Additionally, Phase I was completed in early spring, and Phase II was completed during the middle of summer, and thus the average ambient temperature and room humidity were higher.

4.6 Sources of Error, Study Limitations, and Future Work

This paper presents the design of a fabric channel to assist with integrating TCAs into soft wearable robotic devices. While there are several advantages to the channel design and cooling apparatus, such as its flexibility and portability, there are a few limitations to the design that should be mentioned.

The primary disadvantage to this design is that air pumps are not silent actuators, and they produce noise during use. Their volume approaches that of conversation, which some users may find difficult to ignore. This is especially a concern for applications in stroke rehabilitation, where many patients are elderly and may be more sensitive to environmental noise. This problem could be overcome by continuing to investigate other means of circulating air. It is possible that a larger fan could overcome the flow resistance of the channel and achieve the same air flow rate with less noise. Alternatively, the pump could be surrounded by acoustic insulation such as rock wool or fiberglass.

Another means of circulating air would also be advantageous if the air pressure or air flow could be increased, without sacrificing the portability of the system. Increasing the air flow would allow the cooling time of the TCA to be further reduced, and increasing the air pressure would ensure that this design could work for longer TCAs that would require longer channels. It is uncertain whether the selected miniature air pump could accommodate longer channels, as it may not be strong enough to overcome the increased air flow resistance. Future work should investigate the relationship between the channel dimensions and air flow to aid with pump selection.

Phase I determined that the best dimensions for a channel, out of those tested, for a 4-ply TCA was 10 mm in width and 8 mm in height (10×8), which was the largest channel. It is possible that increasing the size of the channel more could further improve the performance of the TCA (i.e., reduce the cooling time); however, increasing the height beyond 8 mm would cause the system to protrude too much from the user's limb, and increasing the width more than 10 mm would reduce the maximum number of channels that can be placed in contact with the limb when multiple TCAs are used. It is also likely that the ideal channel size will change depending on the TCA; for example, 2-ply TCAs are considerably smaller than 4-ply TCAs, and the optimal

channel dimensions for them could be a smaller channel size.

There are some sources of error that were present in the Phase I and Phase II experiments. For example, it was more difficult to place the TCAs in some of the channels (especially the ones with the 4 mm height), causing additional downtime between trials. Since it is unknown how quickly the TCA behavior changes when not in use, the amount of variance for the first repetition in each channel changes. This was not a concern for Phase II, since the largest channel was used, making it easy to place the TCA in the channel.

Other sources of variation in the results come from differences in the TCAs and channels due to the fabrication procedure and placement of the TCA in the channel. It was observed that once a TCA was in a channel, the parameters were reasonably consistent. However, if the TCA was removed and put in the same channel, the values for the parameters were noticeably different. This indicated that the placement of the TCA in the channel is critical, and is a source of variation in the results. A limitation of the current channel design is that there is no means to guarantee consistent placement, however, if this design was implemented in a wearable device, the TCA would not be repeatedly removed and replaced in the channel. Future work could devise a method of ensuring the TCA is centered in the channel, such as adding a guide.

Another minor source of error stemmed from the room temperature changing over the course of data collection. The room temperature varied between 21.2–23.5°C (average of 21.8°C) throughout Phase I and 22.2–23.1°C (average of 22.6°C) during Phase II. This impacts the results as the ambient room temperature influences the temperature of the air being blown through the channel and the heat transfer rate between the TCA and the environment.

Finally, when collecting data, it was noticed that the temperature of the TCA continued to increase by 3–7°C over 0.3–0.6 s after the power to the TCA was turned off. Since this effect was not observed when the temperature of the TCA was measured using a thermal camera, a possible explanation is incomplete contact between the temperature sensor and the TCA, resulting in slower heat transfer between them and hence a delay in the temperature sensor reading. This may be rectified by ensuring complete contact between the TCA and the temperature sensor by using a thermal paste, however, future work should perform more validation on the temperature sensor.

4.7 Conclusion

This paper presented the design and fabrication procedure for fabric channels as a means of housing and cooling TCAs on wearable robotic devices. The fabric, nylon pack cloth with a TPU coating, is lightweight and easy to sew. A TCA can be placed in the channel and air can be blown over the TCA using a miniature air pump.

The primary factors in the channel design that would influence the cooling time of the TCA are the channel dimensions. Thus, an experiment was completed to determine the effect that changing the height and width of the channel had on TCA performance. Nine channel sizes were tested with heights of 4, 6, and 8 mm and widths of 6, 8, and 10 mm. Overall, the average cooling time and heating time of the TCA decreased as the channel size increased. The stroke of the TCA was not significantly changed by channel size, provided that the height of the channel was greater than 4 mm. The channels with a height of 4 mm generally performed the worst, and it is hypothesized that this is due to contact between the TCA and the channel walls due to the smaller size. The best channel was the 10×8 channel, as it had a low cooling and heating time, and a comparable stroke to other channels.

The 10×8 channel was utilized in a second experiment where the performance of the TCA in the channel was compared to the performance of the TCA outside of the channel. The best TCA performance occurred with active cooling without the channel, however that is not a practical setup for wearable devices as the exposed TCA could burn the user, get caught on an object, or become damaged. There was a significant decrease (42%) in cooling time between passive cooling without a channel and active cooling in a channel (21.71 ± 1.24 s vs. 12.54 ± 2.31 s).

Future work should investigate means of improving the channel design, such as modifying the inlet, testing other materials, adding holes, or further increasing the dimensions. Additionally, other cross-sectional shapes could be investigated with the addition of rigid supports to ensure that the channel remains open. Future work should also verify the ease of integration of the channel with a wearable device.

Chapter 5

Concluding Remarks

Portable robotic devices have the potential to help improve the quality of life for individuals with musculoskeletal disorders by supporting activities of daily living or by aiding in the rehabilitation process. While some devices are beginning to become commercially available, they have limitations with respect to the number of degrees of freedom, their portability, and their cost. These limitations are in part due to the actuators that are primarily used in these devices—motors and pneumatics. To overcome the limitations of standard actuators, there has been a significant amount of research into alternative actuators for wearable robotic systems. TCAs are one of these actuators, and they have been integrated into wearable devices that actuate either the wrist or the fingers. In comparison to motors and pneumatics, they are lighter, slimmer, and less expensive. However, they present their own challenges for wearable applications, such as high operating temperatures and slow cooling rates.

Therefore, the work presented in this thesis aimed to address these challenges to enable the adoption of TCAs into soft wearable robotic devices. To this end, a flexible fabric channel was designed to help cool the TCA, integrate it with wearable devices, and provide a means for protecting the user. The channel is made from nylon fabric, which enables it to be sewn onto other materials, such as insulation to shield the user from the operating temperatures of the TCA, and other fabrics for assembly into a wearable device. The TCA is fixed at one end of the channel through the use of a custom-designed inlet piece, while the opposite end is free to move in the channel and is attached to the load with a string. To cool the TCA, forced convection was achieved

with a miniature air pump that was also attached to the inlet. The channel was insulated with 3 mm of foil-backed mineral wool from Insultech, with the foil side facing the TCA, to ensure that the user would not be burned by the TCA.

After the channel design was finalized, the smallest feasible dimensions (6 mm width and 4 mm height) were simulated in ANSYS Fluent to establish a relationship between the input air velocity and the cooling time of the TCA. The simulation results were compared with experimental results for an input air speed of 1 m/s, and there was a 13% difference in the cooling time constant for the TCA. Based on the established relationship, it was concluded that the miniature air pumps currently available on the market are insufficient, as they are not capable of cooling the TCA at the required rates for rehabilitation exercises with the current channel design.

Thus, the channel design was revisited to determine if it could be improved. Since heat transfer and fluid flow depend heavily on the geometry of the system, it was decided to investigate the effect that the width and height of the channel had on the cooling time of the TCA. The heating time and stroke of the TCA were also evaluated to obtain a full understanding of the performance of the TCA. The channel geometry was tested experimentally by actuating TCAs in nine channel sizes—6×4, 6×6, 6×8, 8×4, 8×6, 8×8, 10×4, 10×6, and 10×8, where the first dimension is the channel width and the second is the channel height.

These results revealed that, on average, the cooling time of the TCAs decreased as the channel size increased, which is likely due to additional airflow from the lower fluid flow resistance. There was a 3.69 s mean cooling time decrease between the smallest channel, 6×4, and the largest channel, 10×8 (15.11 ± 2.28 s vs. 11.42 ± 1.33 s, $p < 0.001$). Similarly, the heating time decreased as the channel size increased, with an average difference of 0.48 s between the 6×4 channel and the 10×8 channel (5.36 ± 0.50 s vs. 4.88 ± 0.30 s, $p < 0.001$). In contrast to the cooling and heating time, there was no statistically significant difference between the stroke present in the channel, provided that the channel height was above 4 mm. It is believed that there was contact between the TCA and the channel when the height was 4 mm, which resulted in additional frictional forces between the channel and TCA and caused a decrease in stroke. For example, there was an average difference of 1.28 mm between the 6×4 and the 10×8 channel (7.04 ± 0.64 mm vs. 8.32 ± 0.80 mm, $p < 0.001$). Overall, the 10×8 channel had the best combination of cooling time, heating

time, and stroke, and thus it was used in a secondary experiment.

The goal of the second experiment was to determine the impact that the channel had on the performance of the TCA. To accomplish this, the cooling time, heating time, stroke, and temperature–displacement hysteresis were compared between TCAs with and without the channel, and with and without active cooling. When comparing active cooling in the channel to passive cooling without the channel, the cooling apparatus resulted in a 42% decrease in cooling time (21.71 ± 1.24 s vs. 12.54 ± 2.31 s, $p < 0.001$) and a 9% increase in heating time (3.46 ± 0.71 s vs. 3.76 ± 0.71 s, $p < 0.001$). There was a 28% decrease in stroke (5.40 ± 0.44 mm vs. 3.89 ± 0.77 mm, $p < 0.001$), however, this decrease seems to occur primarily due to the addition of active cooling, as discussed in Section 4.5.1. There was no statistically significant difference between the amount of hysteresis present. Interestingly, the cooling time of the TCA decreased further when there was active cooling without a channel present (8.57 ± 0.71 s), however the exposed nature of the TCA in this case is not safe for wearable robotics. Nevertheless, the improved TCA performance indicates directions that could be explored for further improvements to the channel, such as the inclusion of vents.

5.1 Contributions

Overall, the contributions of this work include the following:

1. The major contribution is the development of a novel cooling apparatus for TCAs that was specifically designed for integration into soft wearable robotic devices. The apparatus consists of a fabric cooling channel, made from nylon pack cloth, and a miniature air pump to enable forced convection. The flexibility and low profile of the channel will aid with user comfort, and it can easily be sewn onto other materials for integration into soft robotic devices.

2. The second contribution is the conclusion that commercially available miniature air pumps are not capable of cooling a 2–4 ply nylon TCA in a 6×4 channel quickly enough to support rehabilitation exercises. Thus, future work should investigate alternative means of forced convection.

3. The third contribution is the statistically significant improvement to the channel design by modifying the channel dimensions. Increasing the channel size from 6×4 to 10×8 allowed the TCA performance to improve by decreasing the cooling time and heating time, and increasing the stroke. In general, the TCA performance improved as the channel cross-sectional area increased. This relationship will help guide future improvements to the channel design.

4. The final contribution is the validation that the cooling apparatus successfully reduced the cooling time of the TCA in comparison to passive cooling. However, at the low airflow rates that the miniature air pump produced, the cooling time of the TCA with active cooling was lower without the channel. This knowledge can guide future improvements to the channel, such as the inclusion of vents to enable natural convection.

5.2 Limitations and Future Work

There are some sources of error present in this work. First, during the simulations of the TCA in the channel (Chapter 3), the TCA geometry was simplified, the motion and deformation of the TCA were neglected, and only a portion of the TCA was simulated. Additionally, the only method of heat transfer present in the simulation was forced convection. These simplifications would add to the error present between the simulation results and experimental results, as the simulations do not fully represent the experimental setup. Since the validity of the simulations were only assessed at the lowest input velocity, it is possible that there may be larger discrepancies between the simulation and experimental results at higher input air velocities. Finally, the sensitivity of the simulation results to the TCA and channel dimensions are unknown. The established relationship between the input air velocity and TCA cooling time would change if different TCA configurations, channel dimensions, or simplifying assumptions were used. Therefore, future work should validate the simulation results at higher input air velocities and simulate other TCA and channel configurations to confirm the accuracy of the simulations.

There were also sources of error present in the experimental work (Chapter 4) that resulted in variations in the data. Primarily, there were differences in the TCAs and the channels of the same size due to the fabrication methods used. These differences, coupled with the difficulty of

ensuring that the TCA was centered in the channel, account for a large portion of the variation in the experimental results. Another source of error for the heating time of the TCA is that the input power was not at a consistent 2 W, as the resistance of the TCA was constantly changing. While the resistance of the TCA was estimated using Ohm's law, the non-linear nature of the TCA introduces error into this calculation. Finally, it appeared that there was incomplete contact between the temperature sensor and the TCA, as the temperature of the TCA kept rising by 3–7°C for 0.3–0.6 s after the power to the TCA was turned off.

Despite these errors, the experimental work demonstrated that the cooling apparatus was successful in reducing the cooling time of the TCA, although there are some limitations surrounding the design. The primary limitation is that a miniature air pump cannot provide adequate air flow for rehabilitation or voluntary motion exercises. While the simulations were performed with the 6×4 channel, it is still unlikely that a miniature air pump can provide adequate airflow with the larger channels. Thus, one of the main aspects for future work with this design is to investigate alternative means of forced convection that are capable of producing larger airflows while maintaining portability. Additional airflow could also be achieved by taking advantage of air entrainment—the process where still air is pulled along a moving air stream. This could be achieved by modifying the channel design, to expose the TCA to the environment, such as with the inclusion of vents. Unfortunately, the inclusion of vents in the channel would prevent the channel from fully isolating the TCA, and thus user safety concerns would arise.

Similar to the vents, there are many other aspects to the channel design that could be investigated to improve the cooling time of the TCA. For example, the channel material could be investigated, as an air permeable material may allow better heat transfer between the internal channel and the environment by enabling natural convection, and an elastic material would likely improve the user comfort. Additionally, the channel length must be considered, as the flow resistance will increase relative to the channel length, however, longer TCAs will require longer channels.

Overall, many of the factors that should be tested with the channel design could be incorporated into a detailed thermomechanical model that involves the TCA and the channel. This model could help determine TCA performance (primarily cooling time) based on a variety of channel

design factors (*e.g.*, channel dimensions and material, vent size and placement, input air flow). A detailed model would allow variations on the channel design to be tested without requiring extensive experimental work to test each possible modification. Additionally, if the model adequately considered the parameters of the TCA, it would allow the channel parameters to be optimized for a variety of TCA configurations, such as the ply of the TCA. Therefore, the primary next step in this work would be to develop a detailed model relating channel design parameters to TCA performance. After the channel design has been optimized, it should be incorporated into a wearable device. This would allow the channel to be tested in a realistic setting, where the channel would not be perfectly straight or flat.

5.3 Concluding Statement

The purpose of this work was to develop a solution for the main challenge that currently prevents TCAs from being implemented in wearable robotic devices—increasing their cooling rate in a manner suitable for soft robotics. To address this challenge, a fabric channel was designed to isolate the TCA, enable forced convection, and provide the means for integrating TCAs into soft robotic devices. This design was submitted as a provisional patent in 2022. The channel was made from tightly woven nylon pack cloth and surrounded by mineral wool insulation to protect the user. The channel is flexible for user comfort and easy to sew onto other fabrics. While the experimental work in this thesis was performed with TCAs, the same design could be applied to other thermally actuated muscles, such as SMAs. Overall, this work contributes to the development of soft robotic devices by providing the means to cool thermally actuated artificial muscles and integrate them into the devices. If inexpensive, portable wearable devices can become commercially available, they would be able to assist individuals with rehabilitation and activities of daily living.

References

[1] J. Kopex, J. Cibere, *et al.*, "Descriptive epidemiology of musculoskeletal disorders in canada: Data from the global burden of disease study," *Osteoarthritis and Cartilage*, vol. 27, p. S259, 2019.

[2] R. Macpherson, T. J. Lane, *et al.*, "Age, sex, and the changing disability burden of compensated work-related msds in canada and australia," *BMC Public Health*, vol. 18, no. 758, pp. 1–11, 2018.

[3] Association of Workers' Compensation Boards of Canada, "National work injury, disease and fatality statistics," 2018, accessed 28 July 2020. [Online]. Available: https://awcbc.org/wp-content/uploads/2020/05/National-Work-Injury-Disease-and-Fatality-Statistics-2016-2018.pdf

[4] M. Gandolla, A. Antonietti, *et al.*, "The effectiveness of wearable upper limb assistive devices in degenerative neuromuscular diseases: A systematic review and meta-analysis," *Frontiers in Bioengineering and Biotechnology*, vol. 7, no. 450, 2020.

[5] P. Lum, C. Burgar, *et al.*, "Robot-assisted movement training compared with conventional therapy techniques for the rehabilitation of upper-limb motor function after stroke," *Archives of Physical Medicine and Rehabilitation*, vol. 83, no. 7, pp. 952–959, 2002.

[6] S. Mazzoleni, C. R, *et al.*, "Effects of robot-assisted wrist therapy in chronic stroke patients: A kinematic approach," in *Proceedings of the IEEE RAS and EMBS International Conference on Biomedical Robotics and Biomechatronics (BioRob)*, Roma, Italy, June 24-27, 2012, pp. 1978–1982.

[7] J. Brackenridge, L. Bradnam, *et al.*, "A review of rehabilitation devices to promote upper limb function following stroke," *Neuroscience and Biomedical Engineering*, vol. 4, no. 1, pp. 25–42, 2016.

[8] N. Rehmat, J. Zuo, *et al.*, "Upper limb rehabilitation using robotic exoskeleton systems: A systematic review," *International Journal of Intelligent Robotics and Applications*, vol. 2, pp. 283–295, 2018.

[9] P. Maciejasz, J. Eschweiler, *et al.*, "A survey on robotic devices for upper limb rehabilitation," *Journal of Neuroengineering and Rehabilitation*, vol. 11, no. 3, pp. 1–29, 2014.

[10] T. Desplenter, Y. Zhou, *et al.*, "Rehabilitative and assistive wearable mechatronic upper-limb devices: A review," *Journal of Rehabilitation and Assistive Technologes Engineering*, vol. 7, p. 2055668320917870, 2020.

[11] R. Gopura, D. Bandara, *et al.*, "Developments in hardware systems of active upper-limb exoskeleton robots: A review," *Robotics and Autonomous Systems*, vol. 75, no. B, pp. 203–220, 2016.

[12] C. Haines, M. Lima, *et al.*, "Artificial muscles from fishing line and sewing thread," *Science (New York, N.Y.)*, vol. 343, pp. 868–872, 2014.

[13] B. P. Edmonds, "Feasibility of twisted coiled polymer actuators for use in upper limb wearable rehabilitation devices," Ph.D. dissertation, Western University, 2020.

[14] S. Kianzad, "A treatise on highly twisted artificial muscle: Thermally driven shape memory alloy and coiled nylon actuators," Master's thesis, University of British Columbia, 2015.

[15] M. C. Yip and G. Niemeyer, "On the control and properties of supercoiled polymer artificial muscles," *IEEE Transactions on Robotics*, vol. 33, no. 3, pp. 689–699, 2017.

[16] R. Bogue, "Robotic exoskeletons: A review of recent progress," *Industrial Robot: An International Journal*, vol. 42, pp. 5–10, 2015.

[17] M. Xiloyannis, L. Cappello, *et al.*, "Preliminary design and control of a soft exosuit for assisting elbow movements and hand grasping in activities of daily living," *Journal of Rehabilitation and Assistive Technologies Engineering (RATE)*, pp. 557–561, 2016.

[18] A. Schiele and F. C. T. van der Helm, "Kinematic design to improve ergonomics in human machine interaction," *IEEE Transactions on Neural Systems and Rehabilitation Engineering*, vol. 14, no. 4, pp. 456–469, 2006.

[19] C.-Y. Chu and R. Patterson, "Soft robotic devices for hand rehabilitation and assistance: A narrative review," *Journal of NeuroEngineering and Rehabilitation*, vol. 15, pp. 1–14, 2018.

[20] N. Norouzi-Gheidari, P. Archambault, and J. Fung, "Effects of robot-assisted therapy on stroke rehabilitation in upper limbs: Systematic review and meta-analysis of the literature," *Journal of rehabilitation research and development*, vol. 49, pp. 479–96, 2012.

[21] R. Bertani, C. Melgari, *et al.*, "Effects of robot-assisted upper limb rehabilitation in stroke patients: a systematic review with meta-analysis," *Journal of the Neurological Sciences*, vol. 38, pp. 1561–1569, 2017.

[22] S. S. Xie, *Advanced Robotics for Medical Rehabilitation: Current State of the Art and Recent Advances*. Auckland, New Zealand: Springer Tracts in Advanced Robotics, 2016.

[23] T. Proietti, V. Crocher, *et al.*, "Upper-limb robotic exoskeletons for neurorehabilitation: A review on control strategies," *IEEE Reviews in Biomedical Engineering*, vol. 9, pp. 4–14, 2016.

[24] M. J. Johnson, R. Rai, *et al.*, "Affordable stroke therapy in high-, low-, and middle-income countries: From theradrive to rehab cares, a compact robot gym," *Journal of Rehabiltation adn Assistive Technologies Engineering*, vol. 4, pp. 1–12, 2017.

[25] M. Gull, S. Bai, and T. Bak, "A review on design of upper limb exoskeletons," *Robotics*, vol. 9, no. 1, pp. 16–51, 2020.

[26] B. Sheng, L. Tang, *et al.*, "Alterations in muscle activation patterns during robot-assisted bilateral training: A pilot study," *Proceedings of the Institution of Mechanical Engineers, Part H: Journal of Engineering in Medicine*, vol. 233, pp. 219–231, 2018.

[27] A. Panarese, R. Colombo, *et al.*, "Tracking motor improvement at the subtask level during robot-aided neurorehabilitation of stroke patients," *Neurorehabilitation and neural repair*, vol. 26, pp. 822–33, 2012.

[28] J. Stein, K. Narendran, *et al.*, "Electromyography-controlled exoskeletal upper-limb–powered orthosis for exercise training after stroke," *American journal of Physical Medicine & Rehabilitation*, vol. 86, no. 4, pp. 255–261, 2007.

[29] N. S. K. Ho, K. Y. Tong, *et al.*, "An emg-driven exoskeleton hand robotic training device on chronic stroke subjects: Task training system for stroke rehabilitation," in *2011 IEEE International Conference on Rehabilitation Robotics*, ETH Zurich Science City, Switzerland, June 29–July 1, 2011, pp. 1–5.

[30] H.-J. Yoo, S. Lee, *et al.*, "Development of 3d-printed myoelectric hand orthosis for patients with spinal cord injury," *Journal of NeuroEngineering and Rehabilitation*, vol. 16, pp. 1–14, 2019.

[31] F. Daerden and D. Lefeber, "Pneumatic artificial muscles: actuators for robotics and automation," *European Journal of Mechanical and Environmental Engineering*, vol. 47, pp. 11–21, 2002.

[32] L. Cappello, K. Galloway, *et al.*, "Exploiting textile mechanical anisotropy for fabric-based pneumatic actuators," *Soft Robotics*, vol. 5, pp. 662–674, 2018.

[33] L. Cappello, J. Meyer, *et al.*, "Assisting hand function after spinal cord injury with a fabric-based soft robotic glove," *Journal of NeuroEngineering and Rehabilitation*, vol. 15, pp. 59–68, 2018.

[34] F. Connolly, D. A. Wagner, *et al.*, "Sew-free anisotropic textile composites for rapid design and manufacturing of soft wearable robots," *Extreme Mechanics Letters*, vol. 27, pp. 52–58, 2019.

[35] C. Correia, R. Nuckols, *et al.*, "Improving grasp function after spinal cord injury with a soft robotic glove," *IEEE Transactions on Neural Systems and Rehabilitation Engineering*, vol. P28, pp. 1407–1415, 2020.

[36] A. Borboni, M. Mor, and R. Faglia, "Gloreha-hand robotic rehabilitation: Design, mechanical model, and experiments," *Journal of Dynamic Systems, Measurement, and Control*, vol. 138, pp. 111 003–1–12, 2016.

[37] C. Pylatiuk, A. Kargov, *et al.*, "Design of a flexible fluidic actuation system for a hybrid elbow orthosis," in *IEEE International Conference on Rehabilitation Robotics, ICORR*, Kyoto, Japan, June 23–26, 2009, pp. 167–171.

[38] J. Madden, N. Vandesteeg, *et al.*, "Artificial muscle technology: physical principles and naval prospects," *IEEE Journal of Oceanic Engineering*, vol. 29, no. 3, pp. 706–728, 2004.

[39] L. Miková, S. Medvecká-Beňová, *et al.*, "Application of shape memory alloy (sma) as actuator," *Metalurgija*, vol. 54, pp. 169–172, 2015.

[40] A. Hadi, K. Alipour, *et al.*, "Asr glove: A wearable glove for hand assistance and rehabilitation using shape memory alloys," *Journal of Intelligent Material Systems and Structures*, vol. 29, pp. 1575–1585, 2017.

[41] S.-M. Lee, W.-K. Jung, *et al.*, "Development of a 4d hand gripping aid using a knitted shape memory alloy and evaluation of finger-bending angles in elderly women," *Fashion and Textiles*, vol. 9, p. 11, 2022.

[42] L. Sutton, H. Moein, *et al.*, "Desing of an assistive wrist orthosis using conductive nylon actuators," in *IEEE International Conference on Biomedical Robotics and Biomechatronics (BioRob)*, UTown, Singapore, June 26–29, 2016, pp. 1074–1079.

[43] L. Saharan, M. Andrade, *et al.*, "igrab: Hand orthosis powered by twisted and coiled polymer muscles," *Smart Materials and Structures*, vol. 26, no. 10, p. 105048, 2017.

[44] S. Bahrami and P. Dumond, "Testing of coiled nylon actuators for use in spastic hand exoskeletons," in *IEEE Engineering in Medicine and Biology Society*, vol. 2018, Honolulu, USA, July 17–21, 2018, pp. 1853–1856.

[45] Y. Tadesse, L. Wu, and L. Saharan, "Musculoskeletal system for bio-inspired robotic systems," *Mechanical Engineering*, vol. 138, p. S11, 2016.

[46] L. Wu, M. J. de Andrade, *et al.*, "Compact and low-cost humanoid hand powered by nylon artificial muscles," *Bioinspiration and Biomimetics*, vol. 12, no. 2, p. 026004, 2017.

[47] J. He, J. Li, *et al.*, "Kinematic design of a serial-parallel hybrid finger mechanism actuated by twisted-and-coiled polymer," *Mechanism and Machine Theory*, vol. 152, p. 103951, 2020.

[48] L. Wu, M. Andrade, *et al.*, "Nylon-muscle-actuated robotic finger," in *Proceedings of SPIE: Smart Materials and Materials and Nondestructive Evaluation and Health Monitoring*, San Diego, USA, March 8–12, 2015, pp. 94 310I–1–12.

[49] A. Hamidi, Y. Almubarak, *et al.*, "Poly-saora robotic jellyfish: swimming underwater by twisted and coiled polymer actuators," *Smart Materials and Structures*, vol. 29, no. 4, p. 045039, 2020.

[50] C. Xiang, H. Yang, *et al.*, "The design, hysteresis modeling and control of a novel sma-fishing-line actuator," *Smart Materials and Structures*, vol. 26, no. 3, p. 037004, 2017.

[51] M. Lima, N. Li, *et al.*, "Electrically, chemically, and photonically powered torsional and tensile actuation of hybrid carbon nanotube yarn muscles," *Science (New York, N.Y.)*, vol. 338, pp. 928–32, 2012.

[52] J. A. Lee, N. Li, *et al.*, "Electrochemically powered, energy-conserving carbon nanotube artificial muscles," *Advanced Materials*, vol. 29, p. 1700870, 2017.

[53] J. Huber, N. Fleck, and M. Ashby, "The selection of mechanical actuators based on performance indices," *Proceedings of The Royal Society A: Mathematical, Physical and Engineering Sciences*, vol. 453, pp. 2185–2205, 1997.

[54] S. Nakshatharan, D. Kaliaperumal, and J. Ruth D, "Effect of stress on bandwidth of antagonistic shape memory alloy actuators," *Journal of Intelligent Material Systems and Structures*, vol. 27, pp. 153–165, 2016.

[55] A. Bhardwaj, A. K. Gupta, *et al.*, "Characterization of mechanical and microstructural properties of constrained groove pressed nitinol shape memory alloy for biomedical applications," *Materials Science and Engineering: C*, vol. 102, pp. 730–742, 2019.

[56] I. Hunter and S. Lafontaine, "A comparison of muscle with artificial actuators," in *Technical Digest IEEE Solid-State Sensor and Actuator Workshop*, Head Hilton Island, South Carolina, USA, June 22–25, 1992, pp. 178–185.

[57] S. Mirvakili, A. Ravandi, *et al.*, "Simple and strong: Twisted silver painted nylon artificial muscle actuated by joule heating," in *Proceedings of SPIE: Electroactive Polymer Actuators and Devices (EAPAD)*, vol. 9056, San Diego, USA, August 17–21, 2014, p. 90560I.

[58] S. Kianzad, M. Pandit, *et al.*, "Nylon coil actuator operating temperature range and stiffness," in *Proceedings of SPIE: Electroactive Polymer Actuators and Devices (EAPAD)*, vol. 9430, San Diego, USA, March 9–12, 2015, pp. 459–464.

[59] K. H. Cho, M.-G. Song, *et al.*, "Fabrication and modeling of temperature-controllable artificial muscle actuator," in *2016 6th IEEE International Conference on Biomedical Robotics and Biomechatronics (BioRob)*, University Town, Singapore, June 26–29, 2016, pp. 94–98.

[60] A. Cherubini, G. Moretti, *et al.*, "Experimental characterization of thermally-activated artificial muscles based on coiled nylon fishing lines," *American Institute of Physics (AIP) Advances*, vol. 5, pp. 067 158–1–11, 2015.

[61] C. S. Haines, N. Li, *et al.*, "New twist on artificial muscles," *Proceedings of the National Academy of Sciences*, vol. 113, no. 42, pp. 11 709–11 716, 2016.

[62] L. Saharan and Y. Tadesse, "Fabrication parameters and performance relationship of twisted and coiled polymer muscles," in *ASME International Mechanical Engineering Congress and Exposition (IMECE)*, vol. 50688, Arizona, USA, November 11–17, 2016, pp. 67 314–67 320.

[63] J. Park, J. Yoo, *et al.*, "Electrically controllable twisted-coiled artificial muscle actuators using surface-modified polyester fibers," *Smart Materials and Structures*, vol. 26, p. 035048, 2017.

[64] S. Y. Yang, K. h. Cho, *et al.*, "High performance twisted and coiled soft actuator with spandex fiber for artificial muscles," *Smart Materials and Structures*, vol. 26, p. 105025, 2017.

[65] S. A. Horton and P. Dumond, "Consistent manufacturing device for coiled polymer actuators," *IEEE/ASME Transactions on Mechatronics*, vol. 24, no. 5, pp. 2130–2138, 2019.

[66] K. h. Cho, M. Song, *et al.*, "A robotic finger driven by twisted and coiled polymer actuator," in *Proceedings of SPIE: Smart Structures and Materials and Nondestructive Evaluation and Health Monitoring*, Las Vegas, USA, March 20–24, 2016, p. 97981J.

[67] T. Li, Y. Wang, *et al.*, "Thermal actuation performance modification of coiled artificial muscle by controlling annealing stress," *Journal of Polymer Science Part B: Polymer Physics*, vol. 56, pp. 383–390, 2017.

[68] H. Song and Y. Hori, "Force control of twisted and coiled polymer actuators via active control of electrical heating and forced convective liquid cooling," *Advanced Robotics*, vol. 32, pp. 1–14, 2018.

[69] M. C. Yip and G. Niemeyer, "High-performance robotic muscles from conductive nylon sewing thread," in *2015 IEEE International Conference on Robotics and Automation (ICRA)*, Seattle, USA, May 25–30, 2015, pp. 2313–2318.

[70] B. P. Edmonds and A. L. Trejos, "Computational fluid dynamic study of a soft actuator for use in wearable mechatronic devices," in *7th IEEE International Conference on Biomedical Robotics and Biomechatronics*, Enschede, The Netherlands, August 26–29, 2018, pp. 1333–1338.

[71] D. R. Higueras-Ruiz, H. P. Feigenbaum, and M. W. Shafer, "Moisture's significant impact on twisted polymer actuation," *Smart Materials and Structures*, vol. 29, p. 125009, 2020.

[72] K. Kim, K. h. Cho, *et al.*, "Double helix twisted and coiled soft actuator from spandex and nylon," *Advanced Engineering Materials*, vol. 20, p. 1800563, 2018.

[73] A. Simeonov, T. Henderson, *et al.*, "Bundled super-coiled polymer artificial muscles: Design, characterization, and modeling," *IEEE Robotics and Automation Letters*, vol. PP, pp. 1671–1678, 2018.

[74] B. P. Edmonds and A. L. Trejos, "Design of an active cooling system for thermally activated soft actuators," in *16th IEEE International Conference on Rehabilitation Robotics (ICORR)*, Toronto, Canada, June 24–28, 2019, pp. 368–373.

[75] L. J. Flemming, D. E. Johnson, and S. A. Mascaro, "Optimal control of multi-input sma actuator arrays using graph theory," in *2011 IEEE International Conference on Robotics and Automation (ICRA)*, Shanghai, China, May 9-13, 2011, pp. 6109–6114.

[76] M. D. Pierce and S. A. Mascaro, "A biologically inspired wet shape memory alloy actuated robotic pump," *IEEE/ASME Transactions on Mechatronics*, vol. 18, no. 2, pp. 536–546, 2013.

[77] J. D. Ertel and S. A. Mascaro, "Dynamic Thermomechanical Modeling of a Wet Shape Memory Alloy Actuator," *Journal of Dynamic Systems, Measurement, and Control*, vol. 132, no. 5, p. 051006, 2010.

[78] C. Piao, H. Jang, *et al.*, "Enhanced dynamic performance of twisted and coiled soft actuators using graphene coating," *Composites Part B: Engineering*, vol. 178, p. 107499, 2019.

[79] A. Pathak, J. AuBuchon, *et al.*, "Carbon nanotube (cnt) fins for the enhanced cooling of shape memory alloy wire," *Proceedings of SPIE: The International Society for Optical Engineering*, vol. 6929, pp. 69 291K–69 291K–8, 2008.

[80] S. Oh, R. Tabassian, *et al.*, "Cooling-accelerated nanowire-nitinol hybrid muscle for versatile prosthetic hand and biomimetic retractable claw," *Advanced Functional Materials*, p. 2111145, 2021.

[81] T. Luchetti, A. Zanella, *et al.*, "Electrically actuated antiglare rearview mirror based on a shape memory alloy actuator," *Journal of Materials Engineering and Performance*, vol. 18, pp. 717–724, 2009.

[82] S. Huang, M. Leary, *et al.*, "Optimisation of ni–ti shape memory alloy response time by transient heat transfer analysis," *Materials and Design*, vol. 35, pp. 655–663, 2012.

[83] L. Wu and Y. Tadesse, "Modeling of the electrical resistance of tcp muscle," in *ASME 2017 International Mechanical Engineering Congress and Exposition (IMECE)*, vol. 4A: Dynamics, Vibration, and Control, Tampa, USA, November 3–9, 2017, p. V04AT05A024.

[84] J. van der Weijde, B. Smit, *et al.*, "Self-sensing of displacement, force and temperature for joule-heated twisted and coiled polymer muscles via electrical impedance," *IEEE/ASME Transactions on Mechatronics*, vol. 22, pp. 1268–1275, 2016.

[85] P. Daemi, M. Kamel, *et al.*, "Control of twisted-coiled actuators via multi-dof pid," in *Electroactive Polymer Actuators and Devices (EAPARD) XXIII*, vol. 11587, Online, USA, March 22–26, 2021, pp. 115 780M–1–12.

[86] F. P. Incropera, D. P. Dewitt, *et al.*, *Fundamentals of Heat and Mass Transfer*, 6th ed. John Wiley and Sons, 2007.

[87] A. Lizotte and A. L. Trejos, "Evaluation of a fabric channel cooling apparatus for twisted coiled actuators," in *Canadian Conference on Electrical and Computer Engineering*, Halifax, Canada, September 18–20, 2022, pp. 364–369, © 2022 IEEE. Reprinted, with permission.

[88] B. P. Edmonds and A. L. Trejos, "Frequency response analysis of actively cooled nylon twisted coiled actuators for use in wrist rehabilitation devices," in *8th IEEE RAS/EMBS International Conference for Biomedical Robotics and Biomechatronics (BioRob)*, New York, USA, November 29–December 1, 2020, pp. 434–439.

[89] M. T. Moffroid and R. H. Whipple, "Specificity of speed of exercise," *Physical Therapy*, vol. 50, no. 12, pp. 1692–1700, 1970.

[90] K. A. Mann, F. W. Werner, and A. K. Palmer, "Frequency spectrum analysis of wrist motion for activities of daily living," *Journal of Orthopaedic Research*, vol. 7, no. 2, pp. 304–306, 1989.

[91] M. Tanimoto and N. Ishii, "Effects of low-intensity resistance exercise with slow movement and tonic force generation on muscular function in young men," *Journal of Applied Physiology*, vol. 100, no. 4, pp. 1150–1157, 2006.

[92] SIMSCALE, "K-omega and k-omega sst," 2021, last accessed 12 December 2021. [Online]. Available: https://www.simscale.com/docs/simulation-setup/global-settings/k-omega-sst/

[93] ANSYS, "4.5.2 shear-stress transport (sst) k-ω model," 2009, last accessed 12 December 2021. [Online]. Available: https://www.afs.enea.it/project/neptunius/docs/fluent/html/th/node67.htm

[94] F. M. White, *Fluid Mechanics*, 7th ed. New York: McGraw Hill, 2011.

[95] J. Sun, B. Paulowski, and J. Zhao, "Embedded and controllable shape morphing with twisted-and-coiled actuators," in *International Conference on Intelligent Robots and Systems (IROS)*, Madrid, Spain, October 1–5, 2018, pp. 5912–5917.

[96] ANSYS, "5.2.1 heat transfer theory," 2009, last accessed 20 January 2022. [Online]. Available: https://www.afs.enea.it/project/neptunius/docs/fluent/html/th/node107.htm

[97] ANSYS, "1.2 continuity and momentum equations," 2009, last accessed 20 January 2022. [Online]. Available: https://www.afs.enea.it/project/neptunius/docs/fluent/html/th/node11.htm

[98] ANSYS, "16.5.3 conservation equations," 2009, last accessed 20 January 2022. [Online]. Available: https://www.afs.enea.it/project/neptunius/docs/fluent/html/th/node322.htm

[99] ANSYS, "26.13.1 monitoring residuals," 2009, last accessed 20 January 2022. [Online]. Available: https://www.afs.enea.it/project/neptunius/docs/fluent/html/ug/node812.htm

[100] ANSYS, "18.4.3 pressure-velocity coupling," 2009, last accessed 22 November 2021. [Online]. Available: https://www.afs.enea.it/project/neptunius/docs/fluent/html/th/node373.htm

[101] ANSYS, "26.1 overview of using the solver," 2009, last accessed 22 November 2021. [Online]. Available: https://www.afs.enea.it/project/neptunius/docs/fluent/html/ug/node776.htm

[102] A. Lizotte and A. L. Trejos, "Active cooling of twisted coiled actuators via fabric air channels," *Frontiers in Rehabilitation Sciences*, 2022, accepted: November 9, 2022.

[103] J. Boulanger, M. Lindsay, *et al.*, "Canadian stroke best practice recommendations for acute stroke management: Prehospital, emergency department, and acute inpatient stroke care, 6th edition, update 2018," *International Journal of Stroke*, vol. 13, no. 9, pp. 949–984, 2018.

[104] K. Dworzynski, G. Ritchie, *et al.*, "Rehabilitation after stroke: summary of nice guidance," *BMJ*, vol. 346, p. f3615, 2013.

[105] G. Kwakkel, R. van Peppen, *et al.*, "Effects of augmented exercise therapy after stroke: a meta-analysis," *Stroke*, vol. 35, pp. 2529–2539, 2004.

[106] American Academy of Audiology, "Levels of noise," 2012, last accessed 23 May 2021. [Online]. Available: https://audiology-web.s3.amazonaws.com/migrated/NoiseChart_Poster-%208.5x11.pdf_5399b289427535.32730330.pdf

[107] W. Tsuji, K. Yoshida, and S. Asahara, "The coefficients of friction of various fibers by roeder's method," *Sen'i Gakkaishi*, vol. 41, no. 5, pp. T211–T220, 1985.

[108] T. A. Lin, C.-W. Lou, and J.-H. Lin, "The effects of thermoplastic polyurethane on the structure and mechanical properties of modified polypropylene blends," *Applied Sciences*, vol. 7, no. 12, p. 1254, 2017.

[109] L. C. Greene and J. D. Hardy, "Adaption of thermal pain in the skin," *Journal of Applied Physiology*, vol. 7, no. 4, pp. 693–696, 1962.

[110] R. Defin, M. Shachal-Shiffer, *et al.*, "Quantitative somatosensory testing of warm and heat-pain thresholds: The effect of body region and testing method," *The Clinical Journal of Pain*, vol. 22, no. 2, pp. 130–136, 2006.

[111] P. P. Urone, R. Hinrichs, *et al.*, *College Physics*. OpenStax, 2012. [Online]. Available: http://cnx.org/content/col11406/latest/

[112] Omnexus, "Density of plastics: Technical properties," 2022, last accessed 2 March 2022. [Online]. Available: https://omnexus.specialchem.com/polymer-properties/properties/density

[113] Omnexus, "Polyamide (pa) or nylon: Complete guide (pa6, pa66, pa11, pa12...)," 2022, last accessed 2 March 2022. [Online]. Available: https://omnexus.specialchem.com/selection-guide/polyamide-pa-nylon

[114] Omnexus, "Polyethylene terephthalate (pet): A comprehensive review," 2022, last accessed 2 March 2022. [Online]. Available: https://omnexus.specialchem.com/selection-guide/polyethylene-terephthalate-pet-plastic

[115] Omnexus, "Max continuous service temperature," 2022, last accessed 2 March 2022. [Online]. Available: https://omnexus.specialchem.com/polymer-properties/properties/max-continuous-service-temperature

[116] J. Wojtkowiak, *Lumped Thermal Capacity Model*. Dordrecht: Springer Netherlands, 2014, pp. 2808–2817.

[117] A. Polymeris, P. D. Papapetrou, and G. Katsoulis, "An average body circumference can be a substitute for body mass index in women," *Advances in Medicine*, vol. 2014, 2014.

[118] P. Kadam and S. Bhalerao, "Sample size calculation," *International Journal of Ayurveda Research*, vol. 1, pp. 55–57, 2010.

Appendix A

Pilot Experiment

After the fabric cooling channel was designed, a pilot study was completed to test the experimental procedure and to obtain the standard deviation in the data for a sample size calculation. To complete the pilot study, four channels of each size were fabricated using the method outlined in Figure 4.3. The four channels were evaluated based on their height, width, and consistency of their cross sectional area, and the three best channels were selected for use in the pilot study and future experiments. The channels were tested using the experimental set up shown in Figure 4.5.

To collect the data, a TCA was placed in the channel, heated to 110°C at approximately 6 W, and then cooled to 25°C. The heating–cooling cycle was repeated three times before changing the channel. Each channel was tested once, resulting in nine repetitions for each channel size. In addition, the TCA was tested without the channel or miniature air pump, to ensure that the cooling mechanism had a positive impact on the cooling time. The order of the channels was randomized to help mitigate the effects of TCA performance and variations in the room temperature on the results.

The resulting data are displayed in Table A.1. The data showed that the cooling channel successfully reduced the cooling time of the TCA. Without the channel, the average cooling time was 73.4 s, however with the channel (except for the 6×8 size), the cooling time was 40.1–56.9 s. Despite this decrease, the cooling time with active cooling was larger than expected. Inspecting the data revealed that the cooling rate noticeably decreased when the TCA temperature was below 30°C, and that often the TCA temperature hovered between 25.5–27 for a period of time before

Table A.1: Descriptive statistics for TCA cooling times obtained from the pilot study.

Channel Size	6x4	6×6	6×8	8×4	8×6	8×8	10×4	10×6	10×8	No Channel, Passive Cooling
Average [s]	47.2	53.4	73.5	43.9	40.1	48.1	48.9	56.9	47.1	73.4
Standard Deviation [s]	11.2	6.7	9.5	6.7	2.3	4.7	10.3	15.3	3.9	6.1

reducing to 25°C. This was especially prominent with the 6×8 size, which contributed to its large cooling times. These observations led to investigating the temperature of the air at the pump outlet. It was found that the output air temperature increased the longer the pump ran, with a maximum recorded temperature of 30.2°C. Thus for future experiments, the definition of cooling time was modified to be the time it takes the TCA to cool to 35°C, to maintain a temperature difference between the input air and the TCA.

The results of the pilot study also provide the required information to complete a standard sample size calculation to ensure statistically significant results. Equation A.1 allows the required number of samples (n) for a desired minimally discernible effect size (Δ) to be computed given the standard deviation (s) of the data and the Z-scores for the allowable Type I (Z_α) and Type II (Z_β) errors. The standard acceptable probabilities for Type I and Type II errors are 5% and 20%, respectively, which resulted in a Z_α of 1.96 and a Z_β of 0.80 [118]. The average standard deviation for the TCA cooling time in a channel was 7.7 s and the desired minimal discernible difference for the cooling time was 2.5 s, resulting in 149 required samples. The minimum discernible difference was selected to be 2.5 s, as that is 5% of the average cooling time obtained in the pilot study. As other papers concerning TCAs frequently do not report the sample size, or have less than 5 samples (as seen in Table 2.2), the required sample size was halved to 75 samples to reduce the amount of time the experiment would take. For ease of division between the three channels of the same size and three TCAs, this was increased to 81 samples, and therefore 81 repetitions were completed at each channel size in the Phase I experiment (Chapter 4, Section 4.4).

$$n = \frac{2s^2(Z_\alpha + Z_\beta)^2}{\Delta} \tag{A.1}$$

Appendix B

Additional Analysis with Phase II Data

It is important for the TCA to perform consistently, since if the behavior of the TCA changes significantly over time, it may not be capable of meeting the requirements of a wearable devices after a given number of repetitions. As explained previously in Section 4.5.1, four repetitions were performed consecutively during each trial for Phase II, and 24 trials were performed for each case. The data from these repetitions (Table B.1) were compared within each case, to determine if the TCA performed consistently over each trial.

To perform this analysis, first the data were assessed for outliers by determining if there were any studentized residuals greater than $\pm$ 3. There were two outliers in the heating time data from Case 1 and one outlier in the cooling time data from Case 3, however, as there were no explanations for the outliers present, they were left in the analysis. Next, the normality of the data was evaluated using the Shapiro–Wilk test, as there were less than 50 samples per repetition. If the data from all repetitions were normally distributed, a one-way repeated measures ANOVA was completed to compare the data between repetitions. The sphericity of the data was assessed using Mauchly's Test of Sphericity, and the Greenhouse–Geisser correction was used if the assumption of sphericity was violated. Alternatively, if the data were not normally distributed, a Friedman test was completed to determine if differences existed between the repetitions. Provided the ANOVA

Table B.1: The average cooling times, heating times, strokes, and hysteresis of each repetition.

		Repetition 1	Repetition 2	Repetition 3	Repetition 4
Case 1	Cooling Time [s]	12.03 ± 2.17	12.41 ± 2.31	12.71 ± 2.34	13.00 ± 2.44
	Heating Time [s]	3.65 ± 0.80	3.70 ± 0.70	3.68 ± 0.70	3.67 ± 0.68
	Stroke [mm]	3.96 ± 0.70	3.88 ± 0.77	3.86 ± 0.80	3.87 ± 0.83
	Hysteresis [%]	17.03 ± 9.92	12.51 ± 4.94	12.64 ± 3.99	14.06 ± 3.41
Case 2	Cooling Time [s]	8.53 ± 0.70	8.57 ± 0.72	8.58 ± 0.74	8.61 ± 0.72
	Heating Time [s]	3.59 ± 0.64	3.65 ± 0.73	3.61 ± 0.73	3.59 ± 0.71
	Stroke [mm]	4.71 ± 0.35	4.65 ± 0.38	4.64 ± 0.38	4.65 ± 0.38
	Hysteresis [%]	10.30 ± 3.97	12.66 ± 2.53	13.51 ± 2.50	13.89 ± 2.37
Case 3	Cooling Time [s]	33.79 ± 1.20	34.88 ± 1.30	35.45 ± 1.41	35.54 ± 1.39
	Heating Time [s]	3.52 ± 0.68	3.52 ± 0.68	3.53 ± 0.66	3.50 ± 0.65
	Stroke [mm]	5.21 ± 0.36	5.20 ± 0.36	5.21 ± 0.36	5.20 ± 0.36
	Hysteresis [%]	11.62 ± 2.18	11.06 ± 2.53	10.98 ± 2.21	11.25 ± 2.68
Case 4	Cooling Time [s]	21.31 ± 1.16	21.73 ± 1.16	21.82 ± 1.31	21.99 ± 1.30
	Heating Time [s]	3.51 ± 0.74	3.45 ± 0.69	3.44 ± 0.69	3.43 ± 0.73
	Stroke [mm]	5.41 ± 0.45	5.40 ± 0.44	5.39 ± 0.45	5.39 ± 0.45
	Hysteresis [%]	11.45 ± 2.35	11.36 ± 1.99	11.66 ± 2.09	11.93 ± 2.26

or Friedman test was significant, post hoc testing was completed with either pair-samples t-tests or the Wilcoxon test, depending on whether the data were normally distributed. For all post hoc testing, a Bonferroni correction factor of six was applied to the p values to account for multiple comparisons. The correction factor was applied by multiplying the p values by six to allow the significance level to remain at 0.05. The reported p values are those obtained after the correction factor was applied. The general statistical results from this analysis are summarized in Table B.2.

Beginning with Case 1, Table B.2 indicates that there were statistically significant differences between repetitions for the cooling time, stroke, and hysteresis. Figure B.1 illustrates the post hoc test results, and it can be seen that there are significant differences ($p < 0.001$) between the cooling times of each repetition. A close inspection of the data revealed that the cooling time increased for 99% of the repetitions, with an average increase of 0.32 s per repetition. Unlike the cooling time, there were no significant differences between the heating times in Case 1. For the stroke and hysteresis, there were some significant differences present, as illustrated in Figure B.1C and D. The only significant difference in the stroke was between Repetitions 1 and 3 (3.96 ± 0.70 mm vs.

Table B.2: The ANOVA and Friedman test results for the comparison between adjacent repetitions.

		Number of Outliers	Normally Distributed	ANOVA p value	Friedman p value
Case 1	Cooling Time	0	Yes	< 0.001	—
	Heating Time	2	No	—	0.301
	Stroke	0	Yes	0.013	—
	Hysteresis	0	No	—	0.009
Case 2	Cooling Time	0	No	—	0.002
	Heating Time	0	No	—	0.023*
	Stroke	0	Yes	0.029	—
	Hysteresis	0	No	—	< 0.001
Case 3	Cooling Time	1	No	—	< 0.001
	Heating Time	0	No	—	0.537
	Stroke	0	Yes	0.647	—
	Hysteresis	0	No	—	0.457
Case 4	Cooling Time	0	Yes	< 0.001	—
	Heating Time	0	No	—	0.004
	Stroke	0	Yes	0.432	—
	Hysteresis	0	No	—	0.715

*There were no significant differences between repetitions after the Bonferroni correction factor was applied.

3.86 ± 0.80 mm, $p = 0.041$), which may be a result of the different first repetition phenomenon, as the difference is very slight and there are no other significant differences between the repetitions. The significant differences in the hysteresis occur between Repetitions 1 and 2 ($17.03 \pm 9.92\%$ vs. $12.51 \pm 4.94\%$, $p = 0.023$), and Repetitions 1 and 3 ($17.03 \pm 9.92\%$ vs. $12.64 \pm 3.99\%$, $p = 0.04$).

Overall in Case 1, there is a significant increase in cooling time between repetitions, no change in the heating time, and little change in the stroke and hysteresis. The opposite effect is present in Case 2—there are no significant differences in the cooling time, however there is a slight decrease in stroke after Repetition 1 and an increase in the amount of hysteresis, as illustrated in Figure B.2. It is likely that the difference in stroke only occurs as an effect of the different first repetition, and that additional repetitions would have a constant stroke, as there are no significant differences between Repetitions 2, 3, and 4. However, despite no further changes in the stroke, the amount

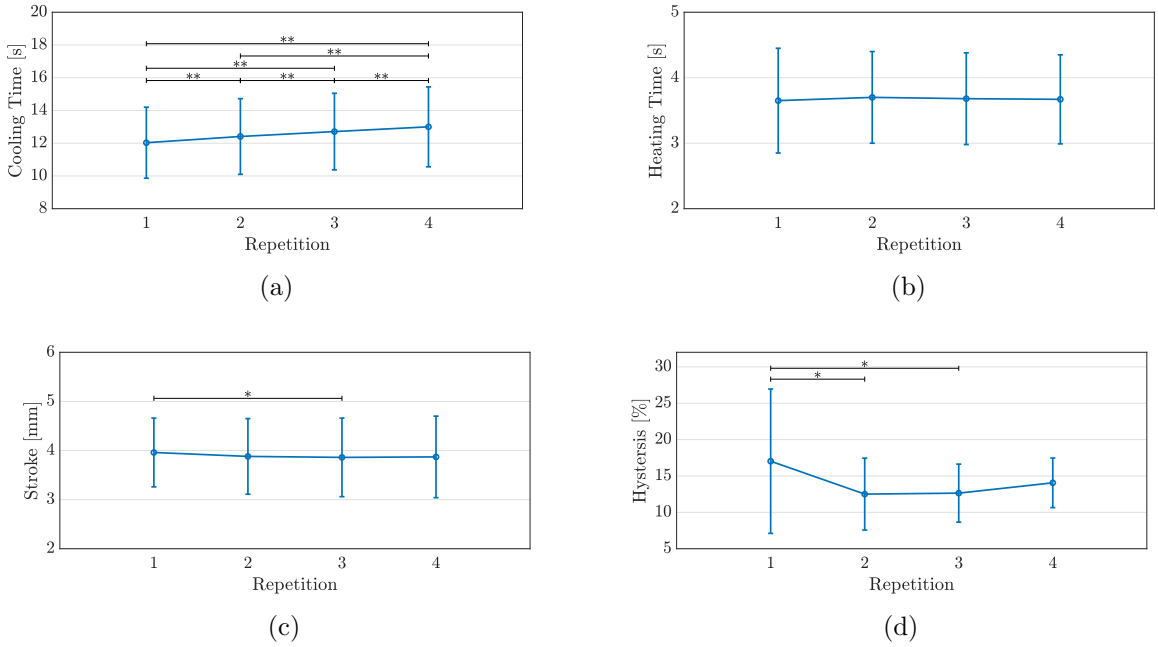

Figure B.1: Comparison of TCA performance between repetitions for Case 1. Statistically significant differences are marked by $*$ for $p < 0.05$ or $**$ for $p < 0.001$.

of hysteresis present continues to increase, as there are significant differences between Repetitions 2 and 4 ($12.66 \pm 2.53\%$ vs. $13.89 \pm 2.37\%$, $p = 0.026$). Unlike the hysteresis, the heating time is approximately consistent, with the only significant difference occuring between Repetition 2 and Repetition 4 (3.65 ± 0.73 s vs. 3.59 ± 0.71 s, $p = 0.019$).

Completely opposite to Case 2, Case 3 (Figure B.3) has significant increases in cooling time, however no significant differences in heating time, stroke, or hysteresis. In Case 3, there are significant increases in the cooling times with $p < 0.001$ between all repetitions except between Repetition 3 and 4, where there was no significant difference. Interestingly, the amount the cooling time changes between repetitions decreased with each subsequent repetition, indicting that the cooling time of the TCA in the channel may stabilize after enough repetitions.

Case 4 (Figure B.4) is similar to Case 3 in that there are no significant differences in the stroke or amount of hysteresis, and the amount the cooling time changes between repetitions decreases with each subsequent repetition. The only difference between Cases 3 and 4 is that Case 4 has a statistically significant decrease in the heating time between Repetition 1 and Repetitions 2, 3, and 4. It is unclear what caused this decrease, as there are no significant differences in the heating

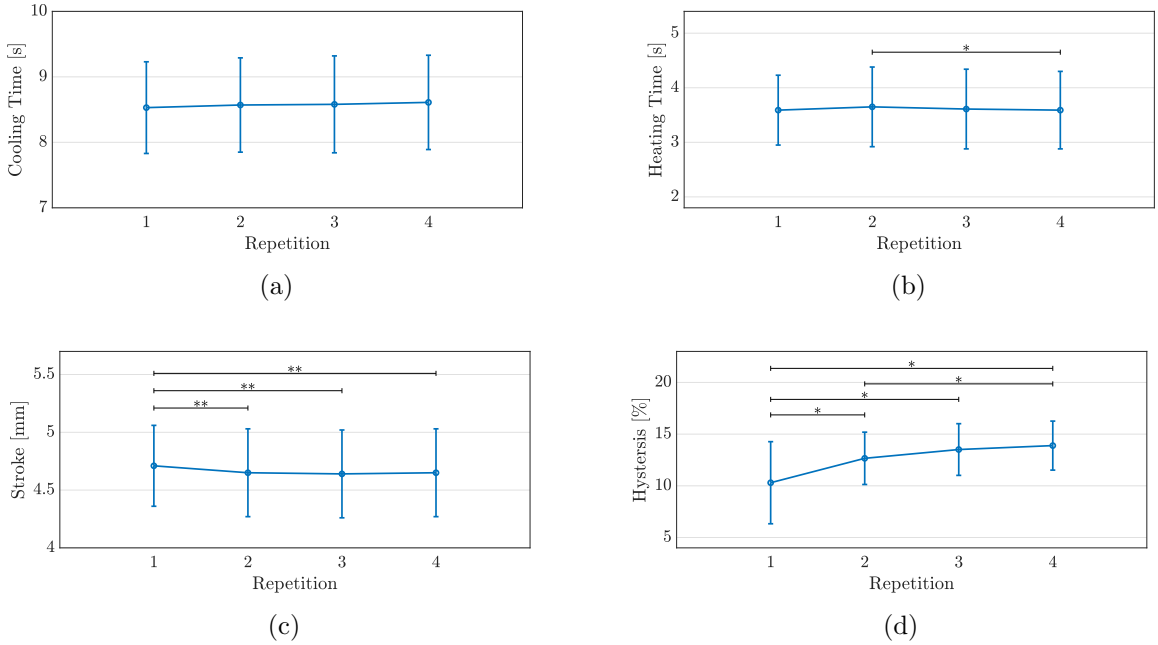

Figure B.2: Comparison of TCA performance between repetitions for Case 2. Statistically significant differences are marked by $*$ for $p < 0.05$ or $**$ for $p < 0.001$.

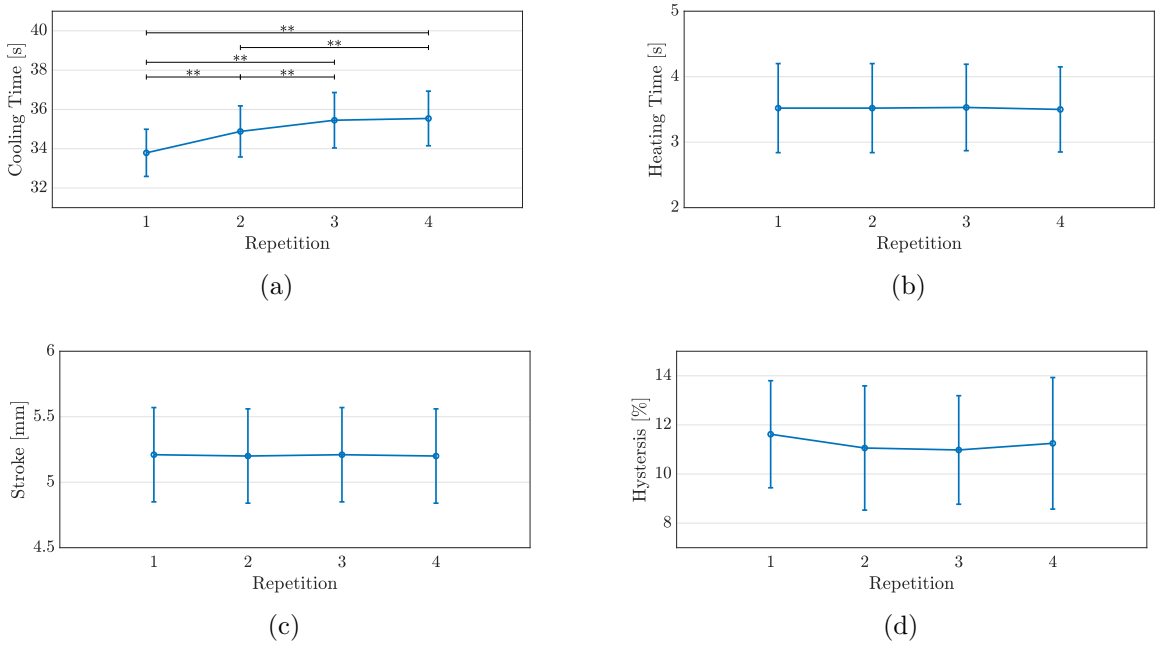

Figure B.3: Comparison of TCA performance between repetitions for Case 3. Statistically significant differences are marked by $*$ for $p < 0.05$ or $**$ for $p < 0.001$.

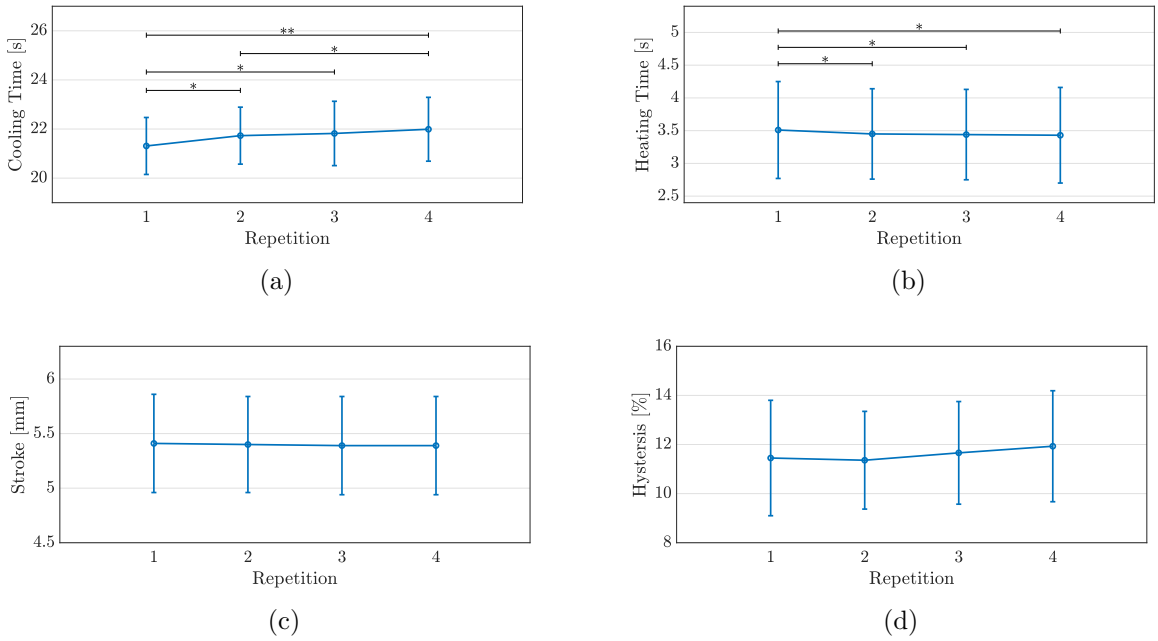

Figure B.4: Comparison of TCA performance between repetitions for Case 4. Statistically significant differences are marked by $*$ for $p < 0.05$ or $**$ for $p < 0.001$.

time between Repetitions 2, 3, and 4.

Overall, with the exception of Case 2, there were significant increases in the cooling time between adjacent repetitions. A possible explanation is that there was heat transfer to the surrounding apparatus (especially the insulation) that decreased the thermal gradient between the TCA and its environment, resulting in slower cooling times. This is not ideal, as if the cooling time continually increases between repetitions, there will reach a point where the device will not be able to meet the speed requirements for a given exercise. This effect does not seem to be caused by the channel, as it was also observed in Case 4, where there was no channel present. It is possible that the cooling time did not increase for Case 2 as there was both natural convection and forced convection, as opposed to only one of those methods. It is possible that the cooling time stabilizes after a few iterations.

Interestingly, there were only significant differences present in the heating time when there was no channel present (Cases 2 and 4). The channel may have helped reduce the variation in the heating time by providing additional insulation.

When considering the stroke and hysteresis, there were significant differences between Repe-

tition 1 and the following repetitions for both Cases 1 and 2. However, there were no significant differences with either Case 3 or 4, indicating that the variation in hysteresis and stroke come from the addition of active cooling.

To conclude, there was a negative effect on the cooling time as the TCA was cycled consecutively. While this effect is not present in the same capacity for the heating time, stroke, or hysteresis, future work should experiment with extended use of the TCA in the channel to fully evaluate the stability of the performance of the TCA.

Appendix C

Copyright Permission

C.1 IEEE

Chapter 3 of this thesis was published with IEEE in 2022. In reference to IEEE copyrighted material which is used with permission in this thesis, the IEEE does not endorse any of Western University's products or services. Internal or personal use of this material is permitted. If interested in reprinting/republishing IEEE copyrighted material for advertising or promotional purposes or for creating new collective works for resale or redistribution, please go to `http://www.ieee.org/publications_standards/publications/rights/rights_link.html` to learn how to obtain a License from RightsLink. If applicable, University Microfilms and/or ProQuest Library, or the Archives of Canada may supply single copies of the dissertation. Additional information about the copyright permission from IEEE can be found at `https://journals.ieeeauthorcenter.ieee.org/choose-a-publishing-agreement/avoid-infringement-upon-ieee-copyright/`.

C.2 Frontiers

Curriculum Vitae

Alex Lizotte

Post-secondary Education and Degrees

BESc Mechatronics Systems Engineering with Professional Internship
Western University, London, Ontario, Canada
2015–2020

MESc Electrical Engineering and Musculoskeletal Health Research
Western University, London, Ontario, Canada
Thesis: Design and Evaluation of Fabric Cooling Channels for Twisted Coiled Actuators
Supervisor: Dr. Ana Luisa Trejos
2020–2022

Publications

A. Lizotte and A.L. Trejos. "Evaluation of a fabric channel cooling apparatus for twisted coiled actuators". *Canadian Conference of Electrical and Computer Engineering (CCECE)*, Halifax, Canada, September 18–20, 2022.

A. Lizotte and A.L. Trejos. "Active cooling of twisted coiled actuators via fabric air channels," *Frontiers in Rehabilitation Sciences*.
Accepted: November 9, 2022.

Provisional Patent

2022. Cooling of Artificial Muscle. 63/373,011, filed August 19, 2022.
Provisional patent.

Honors and Awards

Western University
Christian Lassonde Scholarship
2019

Western University
Konrad and Ruth Plumpe Scholarship in Engineering
2019

The Royal Regiment of Canada Artillery
The Captian General's Diamond Jubilee Bursary
2019

Western University
Dr. E.V. Buchanan Prize
2019

Western University
Mechatronics Systems Engineering
Gold Medal
2020

Natural Science and Engineering Research Council (NSERC)
Canada Graduate Scholarship—Masters
2020–2021

Ontario Graduate Scholarship
2021–2020, Declined
The Royal Regiment of Canada Artillery
Captain G.R.E. Nicholls Memorial Bursary
2021

Bone and Joint Institute
Collaborative Specialization in Musculoskeletal Health Research
Transdisciplinary Research Award
2020–2021

Ontario Graduate Scholarship
2021–2022

Bone and Joint Institute
Collaborative Specialization in Musculoskeletal Health Research
Transdisciplinary Research Award
2021–2022

Canadian MSK Rehab Research Network
Trainee Travel Award
2022

Ontario Graduate Scholarship
2023

Related Work Experience

Teaching Assistant
MSE 4499—Mechatronics Design Project
2020–2022

Advisory Experience

Undergraduate Capstone Project
The students worked on designing, prototyping, and testing a wearable device capable of tracking elbow and shoulder motion for monitoring stroke patient's use of their arm.
2021–2022

Undergraduate Summer Student
The student performed experimental work investigating modifications to the channel design. Additionally, they designed a device to help create TCAs in a more consistent manner.
2022